Concurrent Dual Band Radio-over-Fiber Transmission Using 1-bit Envelope Delta-Sigma Modulation

Lara Juras

A Thesis

in

The Department

of

Electrical and Computer Engineering

Presented in Partial Fulfillment of the Requirements

For the Degree of Master of Applied Science at

Concordia University

Montreal, Quebec, Canada

June, 2018

CONCORDIA UNIVERSITY
SCHOOL OF GRADUATE STUDIES

This is to certify that the thesis prepared

By: Lara Juras

Entitled:
Concurrent Dual Band Radio-over-Fiber Transmission Using 1-bit Envelope Delta-Sigma Modulation

and submitted in partial fulfillment of the requirements for the degree of

Master of Applied Science

Complies with the regulations of this University and meets the accepted standards with respect to originality and quality.

Signed by the final examining committee:

_____ Chair
Dr. R. Raut

_____ Examiner, External
Dr. C. Assi To the Program

_____ Examiner
Dr. G. Cowan

_____ Supervisor
Dr. J. X. Zhang

_____ Examiner
Dr. Y. Shayan

Approved by: _____
Dr. W. E. Lynch, Chair
Department of Electrical and Computer Engineering

_____20_____ _____
Dr. Amir Asif, Dean
Faculty of Engineering and Computer Science

ABSTRACT

Concurrent Dual Band Radio-over-Fiber Transmission Using 1-bit Envelope Delta-Sigma Modulation

Lara Juras

With the growing demand for bandwidth and transmission speed, mobile communication network designs must stay adaptable, efficient and cost-effective. A key integration has been Radio-over-Fiber (RoF) transmission systems that provide a cheaper option and low loss for high frequency signal transfer. For the optical transmitter, delta-sigma modulation (DSM) can be a beneficial addition. The partnership simplifies the Digital-Radio-over-Fiber setup by removing the need for additional converters and prompts adjustments based on system need. Main factors in delta-sigma modulators are the amount of quantization bits and the order of the modulator. Changing quantization bits to a single bit allows the system to use less processing bandwidth and less error experienced from optical transmission. High order structures provide more noise shaping to shift noise away from the band of interest. Still, such setups are prone to linearity problems due to clock jitter from multiple feedback loops.

Different adaptations of delta-sigma modulation have been designed to combat the problems, but a key standout is the implementation of an envelope delta-sigma modulation (EDSM). Envelope delta-sigma modulation's separate processing of envelope and phase delivers time alignment and noise shaping counter the negative implications from high order DSMs. Combining envelope delta-sigma modulation with RoF transmission is an attractive option, but research has yet to delve into carrier aggregation with these setups.

This thesis explores concurrent dual band 64-QAM 20 MHz LTE Radio-over-Fiber using 1-bit envelope delta-sigma modulation. It expands transmitter functionality by concurrent signal integration. Inside the EDSM is a 4^{th} order bandpass delta-sigma modulator custom tailored one of two carrier frequencies. The two frequencies come from two different LTE bands to show

interband compatibility. The carrier frequencies are 2.112 GHz from LTE band 1 and 2.64 GHz from LTE band 7.

Simulation and experimental results confirm the functionality of the proposed envelope delta-sigma modulation RoF system in single and dual band for LTE standards (error vector magnitude < 8%). Experimental results confirm that EDSM is more resilient to RoF transmission than BP-DSM. However, the EVM values for BP-DSM are better for carrier aggregated transmission.

ACKNOWLEDGEMENTS

First, I would like to express my thanks to my parents, Stephen and Mary Ann Juras, who offered more support and encouragement than a child could ask for. My father's assistance and graduate knowledge provided irreplaceable input and insight. My mother's undying commitment to supporting my journey and giving me an outlet at any time was invaluable. Not mention, my brother, Nicholas Juras, helped lower my stress during the graduate life. He always knew how to elevate my mood. Without their presence and experience, this Master's degree would not have been possible.

Next, I would like to thank Professor John Xiupu Zhang for accepting me as a Master's student and providing great supervisory help during the completion of my degree. His expertise and experience taught me a lot about the research journey and how to complete such an endeavour.

I would also like to acknowledge the numerous groupmates who helped me throughout my research. Without the assistance of Hakim Mellah, Weijie Tang, Xiaoran Xie, Piejia Yan, Olivier Cotte and Khan Zeb, I would not have finished my research. A special shout out to Mr. Tang and Mr. Xie who selflessly gave their time to working with me on my simulation and experimental work.

As well, I would like to thank Luis Pessoa for answering my questions regarding his publication. The background information was invaluable to moving forward with my research.

Additionally, I would like to thank Sally Case for providing not only support as a friend, but a critical eye for editing my thesis. Her help gave this thesis an extra polished appearance.

Also, I would like to thank my friends, Taomia Pramiti and Shamma Nikhat, who started this journey with me and gave a certain support only few could comprehend.

Finally, I want to acknowledge those who I missed in my thanks. You were another cog in why I was able to finish my work. I say thank you.

Table of Contents

List of Figures

List of Tables

List of Acronyms

ACLR	Adjacent channel leakage ratio
ACPR	Adjacent Channel Power Ratio
ADC	Analog-to-digital converter
ADT	All digital transmitter
A-RoF	Analog-Radio-over-Fiber
AWG	Arbitrary waveform generator
BB	Baseband
BP	Bandpass
BP-DSM	Bandpass delta-sigma modulation
BPF	Bandpass filter
BS	Base station
BW	Bandwidth
CA	Carrier aggregation
CC	Component carrier
CDMA	Code division multiple access
CORDIC	Coordinate rotation digital calculation
CRFB	Cascade-of-resonators feedback
CS	Control station

D2S	Differential-to-single-ended conversion
DA	Drive amplifier
DAC	Digital-to-analog converter
DC	Direct current
DE	Dual extended
DFB	Distributed feedback laser
DML	Directly modulated laser
DMS	Dual-mode supply
DMSM	Dual mode supply modulator
DPD	Digital predistortion
D-RoF	Digital-Radio-over-Fiber
DS	Delta-sigma
DSM	Delta-sigma modulation
DSP	Digital signal processing
EAM	Electro-absorption modulator
EDSM	Envelope delta-sigma modulation
EML	Electro-absorption modulator integrated laser
EOC	Electric-optic converter
EVM	Error vector magnitude
FFT	Fast Fourier Transform

FIR	Finite Impulse Response
FP	Fabry-Perot
FPGA	Field programmable gate array
GSM	Global System for Mobile Communications
GVD	Group velocity dispersion
HP	High-pass
HP-DSM	High-pass delta-sigma modulation
IEEE	Institute of Electrical and Electronics Engineers
IF	Intermediate frequency
IIR	Infinite Impulse Response
IMD	Intermodal dispersion
IFFT	Inverse Fast Fourier Transform
IQ	Quadrature
LA	Look-ahead
LC	Inductor capacitor
LF	Loop filter
LNA	Low-noise amplifier
LO	Local oscillator
LP-DSM	Lowpass delta-sigma modulation
LPF	Lowpass filter

LTE	Long-Term evolution
MFH	Mobile fronthaul
NTF	Noise transfer function
NRZ	Non Return to Zero
OOK	On-off keying
OEC	Optic-electric converter
OFDM	Orthogonal frequency division modulation
OSR	Oversampling ratio
PA	Power amplifier
PAM4	Pulse amplitude modulation
PAPR	Peak-to-average power ratio
PD	Photodiode
PDSM	Parallel processing delta-sigma modulator
PSD	Power spectral density
PMC	Phase modulated carrier
PWM	Pulse width modulator
QAM	Quadrature amplitude modulation
RAU	Remote access unit
RF	Radio frequency
RoF	Radio-over-Fiber

SA	Successive approximation
SDoF	Sigma-delta over fiber
1-bit DSM	Single bit delta-sigma modulation
SMPA	Switch-mode power amplifier
SNDR	Signal-to-noise and distortion ratio
SNR	Signal-to-Noise ratio
STF	Signal transfer function
TF	Transfer function
TI	Time-interleaved
TI-DSM	Time-interleaved delta-sigma modulation
VCO	Voltage-controlled oscillator
VCSEL	Vertical cavity surface emitting laser
WCDMA	Wideband code division multiple access
WLAN	Wireless local area network

Chapter 1. Introduction

1.1. Introduction to Radio-over-Fiber

Demand for connectivity and huge amounts of data have become common place in the current digital age. These massive data requirements have led towards more developments in signal processing and architecture. One such solution are cloud radio access networks (C-RANs). Such setups employ Radio-over-Fiber (RoF) systems to support their mobile fronthaul networks [1]. They are an attractive option due to their simplification of antenna sites and transparency to mobile communication standards.

Within fronthaul architecture, RoF is the transportation of a radio signal over optical fiber via an optical carrier [2] between a centralized baseband unit (BBU) and remote radio head (RRH) [1]. Figure 1-1 illustrates the basic setup.

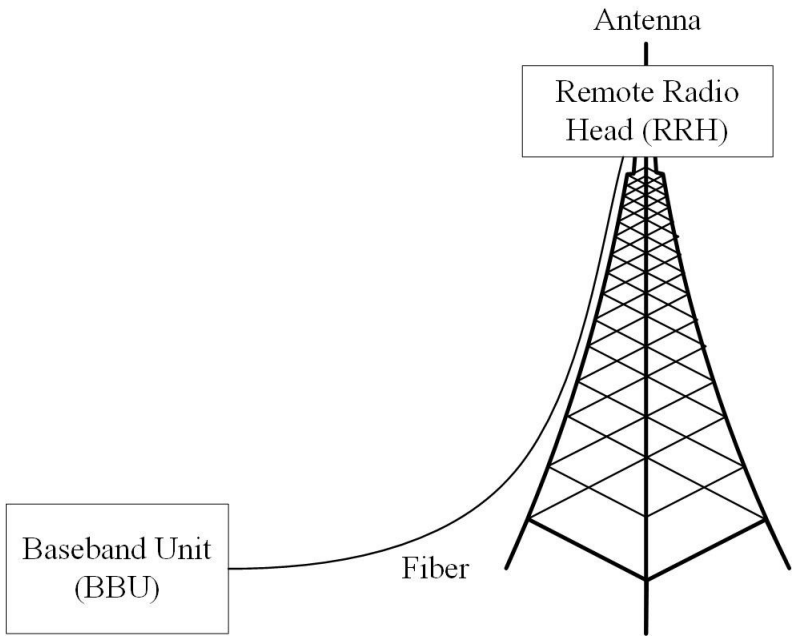

Figure 1-1: Basic fronthaul C-RAN setup (from [3])

In these networks, BBU acts as the main central unit and multiple RRHs can be employed [4]. The baseband unit performs the signal processing and electric-optic conversion while an optic fiber distributes to locations where the data is to be distributed. At the remote radio head, optic-

electric conversion occurs and the signal is transmitted to the user via antenna. The RoF setup allows for low complexity, broad bandwidth and low cost, prompting significant development of RoF systems over the past several decades.

A typical RoF system consists of downlink and uplink transmission. Figure 1-2 shows the block diagram of the system.

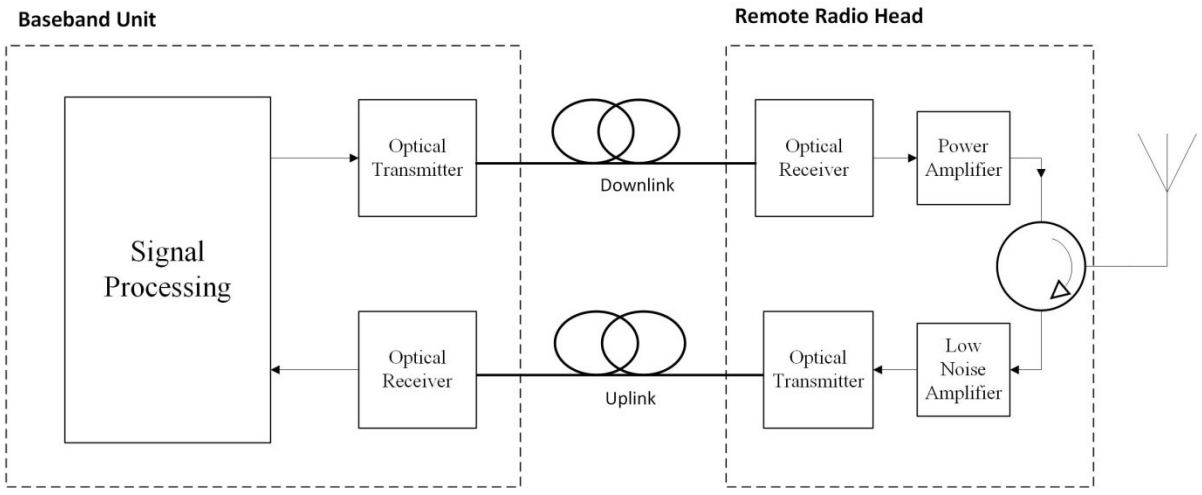

Figure 1-2: RoF Downlink and Uplink system

Downlink is from BBU to RRH. The uplink is the reverse of the downlink. Between the units is a fiber channel specified to the needs of the system. For the signal to transmit successfully, the selection of the optical transmitter is critical [5]. The optical transmitter setup relies on whether direct modulation or external modulation is used. Some commonly implemented lasers for direct modulation are distributed feedback laser (DFB) [6] [7], Fabry-Perot laser (FP) and vertical cavity surface emitting laser (VCSEL) [2] [5]. DFB and FP usually operate at 1310 or 1550nm, but use single and multiple longitudinal modes, respectively [5]. VCSEL are low cost lasers with the ability to support high bitrates [2] at 850nm [5]. Alternatively, optical modulation techniques have been implemented like the electro-absorption modulator (EAM) [8] [9] instead of directly modulated lasers. Regardless of what is chosen, the link performance will depend on the levels of distortion introduced. Link noise and distortion affect the links in different ways. In the downlink, the transmitted wideband noise increases from the additional noise building the channel interference [5]. In the uplink, the base station receiver sensitivity reduces from the link noise [5]. Both links suffer additional interference from distortion [5]. Therefore, the RoF setup must be thought out carefully to maintain link performance.

Three types of Radio-over-Fiber architecture exist: radio frequency (RF), intermediate frequency (IF) transmission and digitized IF transmission [5]. RF transmission has the least complex structure where the RF signal is sent directly over a single mode fiber [2]. IF transmission involves the RF signal being downconverted to an IF signal [5] before being transmitted over a single or multi-mode fiber. At the receiver, the signal is upconverted back to its original RF form. Digitized IF is similar to IF basic transmission, but it applies digitization after down-conversion and before transmission over the fiber [5]. At the receiver, it is changed back to an analog signal and upconverted just like the main IF transmission. Each type can be converted into the other by down-conversion or up-conversion. For example, if the incoming signal is IF, it can be upconverted to an RF signal and vice versa. Of the three, RF is the most common since it has the lowest cost due to its simplicity. Overall, the abovementioned fiber systems are types of RoF systems

Generally, RoF can be classified into two categories: analog or digital. Analog-Radio-over-Fiber (A-RoF) is where the optical carrier is modulated by analog radio signals. In these systems, digital to analog converters (DACs) and analog to digital converters (ADCs) are required at the control station to adapt for the incoming or outgoing signal. This is illustrated in Figure 1-3.

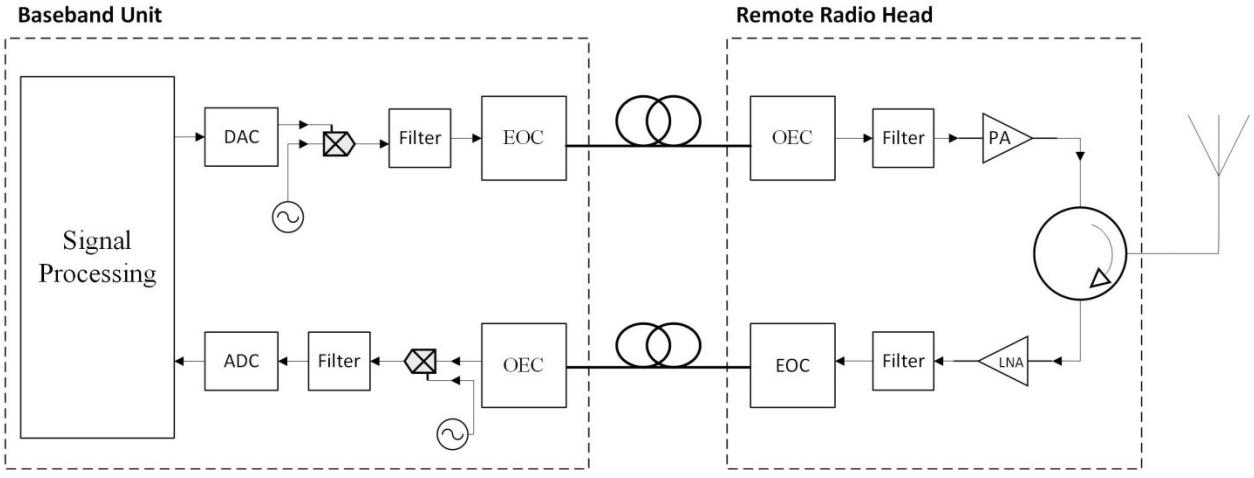

Figure 1-3: Analog RoF (from [2])

First, the signal is created in the digital signal processing (DSP) unit [2]. A DAC converts it to an analog signal that is upconverted with a local oscillator. Afterwards, the signal is filtered before entering an electric-optic converter (EOC). Once it becomes an optical signal, a

fiber curies it to the optic-electric converter (OEC) in the base station. The received signal is filtered again and amplified for wireless transmission by a power amplifier (PA). A circulator sends the boosted signal to an antenna. The reverse of A-RoF downlink path or A-RoF uplink is the inverse with a few changes. Instead of a PA, a low noise amplifier (LNA) is applied and before the DSP unit an ADC is employed.

A-RoF is highly dependent on optical link conditions [10]. A main problem with A-RoF is that intermodulation dispersion (IMD) arises from nonlinearities limiting the overall performance. Various measures have been applied to counter the effects. Modulators have been employed to manipulate the nonlinear components of the signal [2]. Some examples are integrated optical modulators and phase modulators. Another method includes applying clipping and predistortion [7]. This compensation scheme applies "a memory-polynomial-based predistorter and a simple amplitude clipping method" [7]. The predistorter provides power amplifier linearization and the clipping gives peak-to-average power reduction (PAPR) [7].

A key alternative to the A-RoF system is Digital-Radio-over-Fiber (D-RoF). It effectively removes all analog components at the control station and their need for compensation techniques by using digital signal processing and EOCs and OECs only. D-RoF combines "optical and electronic digitization by using high bandwidth ADC and DAC converters at the base station" [2]. This allows IMD to be avoided and the system dynamic range is kept constant. Bandpass sampling is usually kept at the base station to accommodate for wireless standards [2]. Figure 1-4 shows the setup of a D-RoF system.

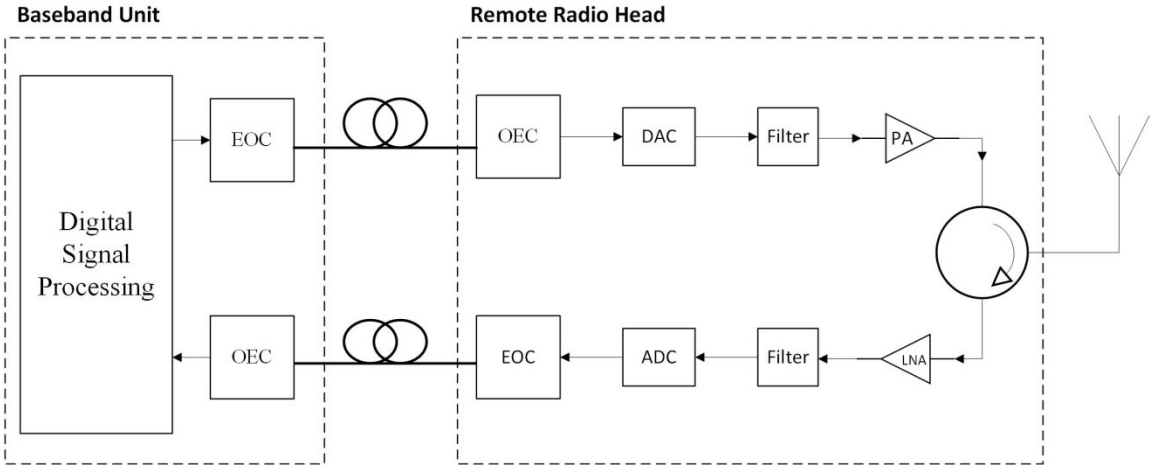

Figure 1-4: Digital RoF (from [2])

Unlike the A-RoF setup, the D-RoF control station is extremely simplified as the upconversion and filtering are performed digitally.

Although D-RoF systems are effective, the additions of the DAC/ADC at the base station cause problems [2]. These include high design costs, large power consumption and compatibility issues. In general, a network consists of many base stations and only one control station, making it very advantageous to avoid converters at the base station. As a result, modulation techniques have been adapted to address base station complexity.

1.2. Introduction to Delta-Sigma Modulation

An emerging method to combat the additional converters in D-RoF systems is the use of delta-sigma modulator (DSM) on the transmitter side of the control station. A DSM is an oversampling and feedback loop filter that consists of an integrator, a quantizer and a DAC [2]. The signal travels through the integrator then a quantizer. Its output is fed back to the input for comparison. Their difference is sent through the feedback loop again. This process is repeated until the difference is zero. Each feedback loop refers to the 'order' of the modulator. Therefore, one loop equals first order and two loops reference second order and so forth. The integrator can be "digitally realized by adders with feed-back around a delay element and filter coefficients" [11]. Finally, the quantizer is comprised of a couple of comparators [11]. Here, the number of quantization bits controls the quantization noise. Quantizers can be multibit to lower the quantization noise or single bit to reduce the bandwidth needed for processing. Once the quantization noise is shaped, the band of interest may achieve a high signal-to-noise ratio (SNR) [2]. After all the processing, the DSM outputs a high speed discrete digital signal or bit stream. A basic diagram of the DSM can be seen in Figure 1-5.

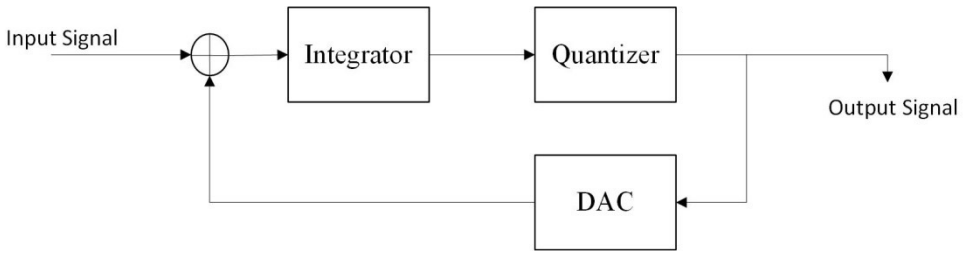

Figure 1-5: Basic delta-sigma modulator block diagram (from [2])

The DSM's main purpose is to oversample the signal and use the feedback loop to lower the band of interest noise [2]. The oversampling ratio (OSR) is determined by the sampling frequency (f_s) and the signal bandwidth (BW). The relationship [2] is highlighted by the equation

$$OSR = \frac{f_S}{2BW} \tag{1}$$

The higher the OSR of the DSM, the more the quantization noise spreads further away from the critical band [2] lowering the noise power. The feedback loop mimics a filter [2] to remove the noise. Increasing the number of loops optimizes the noise shaping [2]. Consequently, the OSR and order of the DSM become attractive optimization options for DSMs.

Every element in the architecture of the DSM can be represented through a series of linear blocks [2] as seen in Figure 1-6. A signal transfer function (STF) and noise transfer function (NTF) [2] help design the linear model. They are created using the desired modulator parameters and elements. The STF is derived using the linear model in Figure 1-6 or Figure 1-7. Based on the linear model in Figure 1-6, the STF [12] is:

$$STF = \frac{Y(z)}{X(z)} = 1 \tag{2}$$

Alternatively, the STF for the Figure 1-7 model can be derived using the loop filter, H(z) [11]. It is written as:

$$STF = \frac{Y(z)}{X(z)} = \frac{H(z)}{1+H(z)} = z^{-1} \tag{3}$$

The NTF is the ratio of the output to the noise, E(z) [11]. It is described as:

$$NTF = \frac{Y(z)}{E(z)} = \frac{1}{z-1} \tag{4}$$

Using the STF and the NTF, the general form of the DSM [11] is:

$$Y(z) = STF(z)X(z) + NTF(z)E(z) \tag{5}$$

The integrator coefficients are acquired from the aforementioned transfer functions. Specifically, the NTF lowers the error at the desired frequency [12]. In the basic setup, the signal energy centered at direct current (DC) frequency has its noise supressed [12].

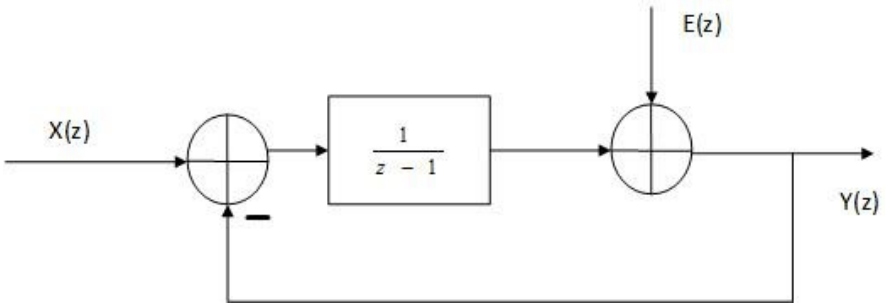

Figure 1-6: First Order DSM Linear Model – Type 1 (from [12])

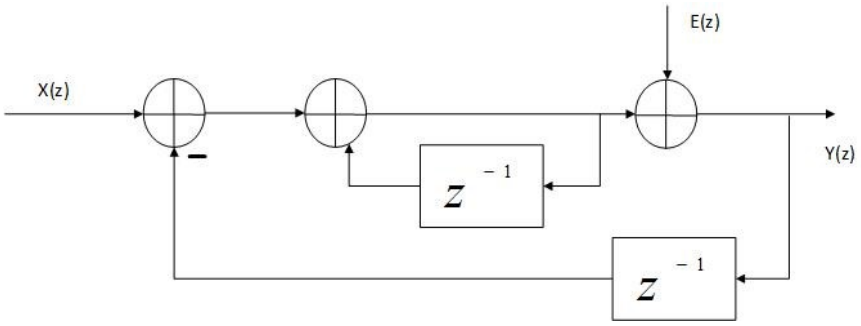

Figure 1-7: First Order DSM Linear Model – Type 2 (from [12])

The first order structure [12] can be mathematically expressed as

$$y(n) = x(n-1) + e(n) - e(n-1) \quad or \quad Y(z) = z^{-1}X(z) + (1 - z^{-1})E(z) \tag{6}$$

Figure 1-7 demonstrates this concept. Alternatively, the STF is represented by 1 or unity and the NTF is represented by $1-z^{-1}$ [2] [12]. This produces $Y(z) = X(z) + (1-z^{-1})E(z)$ as illustrated already in Figure 1-6 [12]. Within the basic equation, the output noise from DSM quantization error can be extracted as $q(n) = e(n) – e(n-1)$ or $Q(z) = (1-z^{-1})E(z)$ [12]. This leads to the definition of the output's power spectral density (PSD) in the frequency domain [12]:

$$PSD(f) = (2\sin(\pi f T_s))^2 PSD_e(f) \quad (7)$$

where $PSD_e(f) = \frac{\Delta^2}{6f_s}$, the quantization error PSD; $T_s = \frac{1}{f_s}$, sampling period [12]. The delta represents the quantizer step size. Additionally, the in-band noise power is determined from integrating the PSD(f) [12]. It can be approximated by:

$$q\_e^2_{rms} = \frac{\pi^2 err^2_{rms}}{3(OSR)^3} \quad (8)$$

where $err_{rms}^2 = \Delta^2/12$; OSR >>1. In equation (8), it can be observed that as the OSR goes up, the noise goes down.

As mentioned, when the DSM order increases, the resolution or noise shaping increases. The second-order structure demonstrates the needed changes to the structure for an order increase. In Figure 1-8, an additional integrator and feedback path [12] are now included. Consequently, the NTF changes to $(1\text{-}z^{-1})^2$ since the model now has two feedback loops. In turn, the linear model equation becomes $Y(z) = z^{-1}X(z) + (1\text{-}z^{-1})^2E(z)$ for Figure 1-8 a) or $Y(z) = X(z) + (1\text{-}z^{-1})^2E(z)$ if STF equals 1 for Figure 1-8 b) [12].

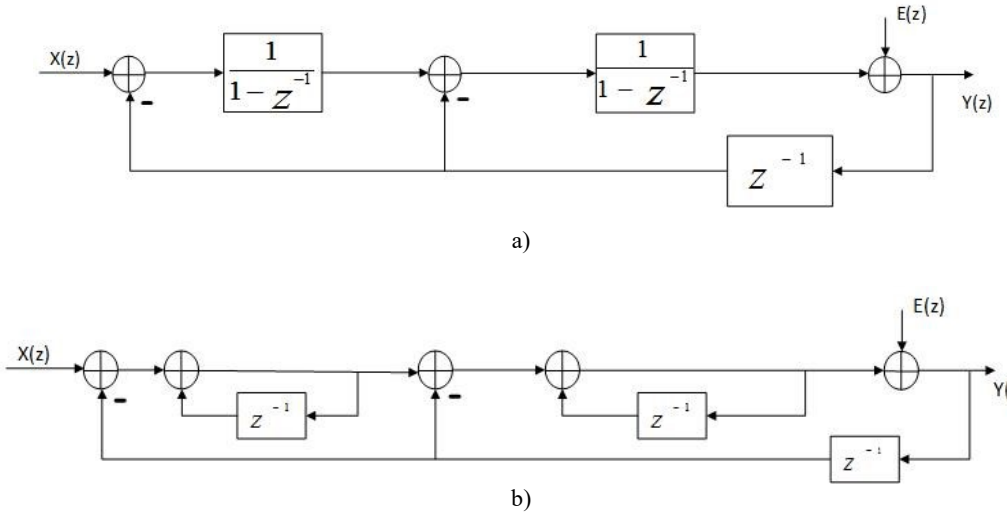

Figure 1-8: Second Order DSM Linear Models: a) Type 1 and b) Type 2 (from [12])

The remaining factors like PSD and in-band noise will change accordingly too. Specifically, for a second order structure the in-band noise is expressed by:

$$q\_e_{rms}^2 = \frac{\pi^4 err_{rms}^2}{5(OSR)^5} \quad (9)$$

where the previous conditions hold true [12]. In general, for orders greater than 1 (M >1), high order equations have been established [12]:

$$NTF(z) = (1 - z^{-1})^M \quad (10)$$

$$Y(z) = z^{-1}X(z) + (1 - z^{-1})^M E(z) \quad (11)$$

$$q\_e_{rms}^2 = \frac{\pi^{2M} err_{rms}^2}{(2M+1)(OSR)^{2M+1}} \quad (12)$$

DSMs have a variety of main topologies. The most basic is lowpass delta sigma modulation (LP-DSM). It acts like a lowpass filter (LPF) at the DC frequency where the maximum signal frequency is much greater than the sampling frequency ($f_{max} << f_s$) [2]. The aforementioned examples of first and second order modulators are examples of LP-DSM since their NTF uses z^{-1}. Like a lowpass filter, LP-DSMs improve the in-band noise by suppressing noise at low frequencies [13]. Figure 1-9 highlights the output power spectra of a LP-DSM.

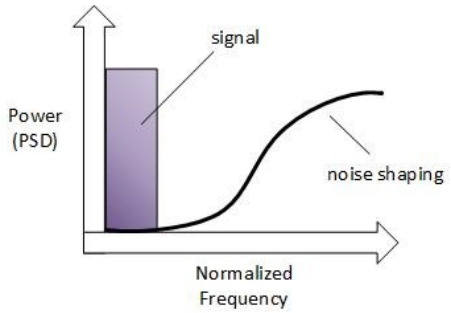

Figure 1-9: Lowpass DSM Power Spectra (from [12])

The noise is moved away from the signal at the low frequencies and shifted to high frequencies. A lowpass filter can be used to extract the signal. Alternatively, the opposite of the LP-DSM exists. It is called high-pass delta sigma modulation (HP-DSM).

HP-DSMs perform the reverse of a LP-DSM where the noise is suppressed at high frequencies. They are easily designed using the NTF of a LP-DSM. As they are the opposite, the z^{-1} just needs to be changed to $-z^{-1}$ to obtain the high-pass (HP) NTF [13]. Since HP-DSM

are used for high frequencies, the input signal should be IF or RF to prevent signal degradation from low frequencies [13]. The HP-DSM power spectra are shown in Figure 1-10.

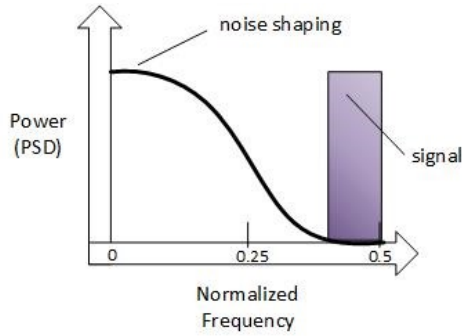

Figure 1-10: High-pass DSM Power Spectra

Here, the noise is filtered away from the high frequencies to the low frequencies. Using a high-pass filter, the shifted noise can be removed. Similarly, bandpass delta-sigma modulation (BP-DSM) is another topology ideal for RF communications [12]. In a BP-DSM, the signal is shifted to a specific center frequency with its narrow BW [12] as seen in Figure 1-11.

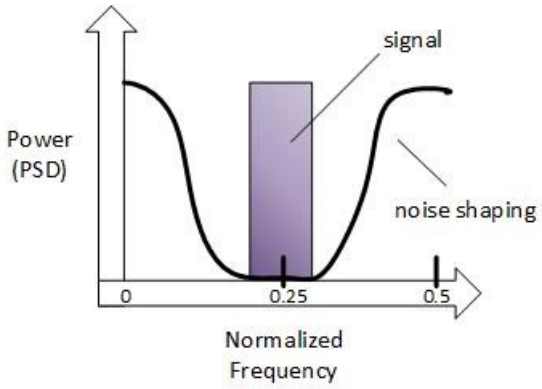

Figure 1-11: Bandpass DSM Power Spectra (from [12])

To accommodate the change, the lowpass or high-pass filter is replaced with a bandpass filter with its zeros shifted from the DC to a new center frequency [2] [12]. These zeros replace the integrator of the LP-DSM [2]. For BP-DSM, the condition $f_{max} / f_s >> 1$ must hold true [2]. The NTF can be easily obtained by performing z mapping on the lowpass NTF that maintains LP stability properties [2]. A 2-path transformation is employed where z is substituted with $-z^{-2}$ [2] [12]. This produces a bandpass (BP) NTF of $(1+z^{-2})$ and its zeros being found at $f_c = f_s/4$ [12]. The closer the center frequency is to $f_s/4$, the higher the SNRs obtained for bandstop noise

shaping [12]. In principle, using the transformation method changes the order of the new modulator [2]. The relationship is stated as M^{th} order LP-DSM = 2*M^{th} order BP-DSM [2].

Using the transformed NTF and Figure 1-8 a), a second order BP-DSM linear model is designed as depicted in Figure 1-12.

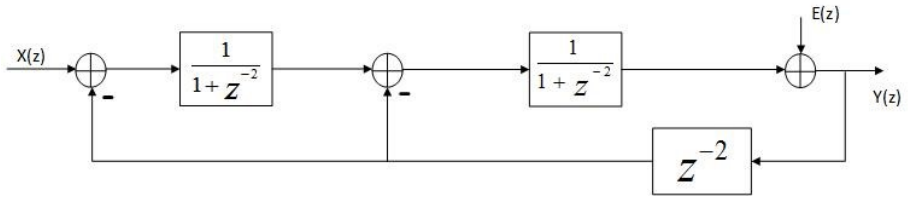

Figure 1-12: BP-DSM Block Diagram (from [12])

This DSM model has z^{-2} and two loops.

Overall, these three designs are the most common topologies within DSM. Many variations of them have been developed and will be further explored in Chapter 2. With the key noise shaping benefits and signal accommodations, DSMs are being integrated into RoF systems to form sigma-delta over fiber (SDoF) systems. Their integration removes the need for the DAC at the base station and replaces it with a filter instead [2]. As a result, only changes need to be made to control station lowering the cost, complexity and power consumption of the base station [2]. Therefore, the inclusion of DSMs is an attractive option for RoF systems.

1.3. Thesis Outline

The thesis will go through the development of the concurrent dual band RoF transmission with 1-bit envelope delta-sigma modulation (EDSM). It shall consist of a literature review, theory, simulation conclusions and laboratory confirmation. The thesis is structured as detailed below:

Chapter 2 examines current models of delta-sigma modulation and envelope delta-sigma modulation (EDSM) and how they have been incorporated into RoF systems. Also, it will highlight how dual-band and multiband have been adapted. This section will present some

background on the previously stated topics and provide an in-depth literature review connecting them.

Chapter 3 dives into the theory of the proposed work. It explains the methodology of the creation of the envelope delta-sigma modulator and its integration into the transmitter design and overall RoF transmission design.

Chapter 4 reveals the simulation results of the modeled DSM and EDSM RoF transmission. It discusses the simulation design and how each simulation case performed.

Chapter 5 exhibits the experimental part of the research. It illustrates the experimental setup and how the proposed concurrent EDSM RoF transmission would operate in a real setting. A comparison of the results is included to showcase the performance.

Chapter 6 states the conclusion of the thesis and provides an analysis of future work for a more effective EDSM setup.

Chapter 2. Background and Literature Review

Delta-sigma modulation provides attractive noise shaping results for communication systems. This chapter takes a look at the implementation of various types of DSM in all digital transmitters (ADTs) and eventually RoF systems. Different DSM adaptations are being made to accommodate the types of signals, address processing time and distortions. One avenue that has garnered high interest is single bit delta-sigma modulation (1-bit DSM) for its simplicity and lower bandwidth use. Specifically, 1-bit DSM architecture will be looked at in depth and related present work will be highlighted. However, like standard DSMs they can suffer from clock jitter and nonlinearities. Envelope delta-sigma modulation is a clear solution to this issue. EDSM will be discussed from the basic setup to current models being used. After establishing the model, the adaptations of DSM and EDSM in RoF transmission systems will be explored. Key focus will be given to the setups that feature concurrent signals in the final section.

2.1. Delta-Sigma Modulation

2.1.1. Current Variants of Delta-Sigma Modulation

Customized DSM models are a prominent feature in DSM literature due to the developing transmitter needs. Solutions are sought for sampling rate reduction, signal compatibility, minimal complexity and low power.

Decreasing the sampling frequency leads to BW improvements and addresses the transmitter BW limitations. Parallel processing techniques integrated with DSMs are a common way to lower the sampling rate. Parallel processing involves computing multiple parts in parallel during one period [14]. Figure 2-1 illustrates how parallel processing works.

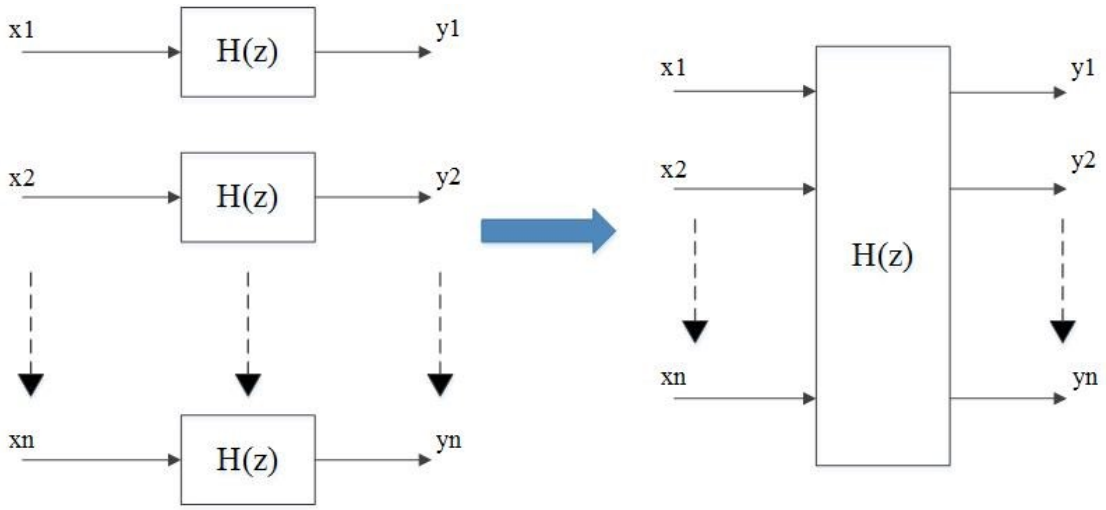

Figure 2-1: Parallel processing general setup (from [14])

In the parallel processing shown in Figure 2-1, n inputs are transformed by the same function and n outputs are produced. The number of inputs per clock cycle equates the parallel processing level, L [14]. Increasing the number of these simultaneous processes effectively lowers the computation time.

Time-interleaved delta-sigma modulation (TI-DSM) is a commonly used parallel processing method in ADTs [15] [16] [17]. A TI-DSM uses polyphase decomposition where one transfer function (TF) becomes transfer function matrices [15]. Block filtering is the main approach to acquiring the TF matrices [15]. Figure 2-2 provides a general layout of block filtering structure.

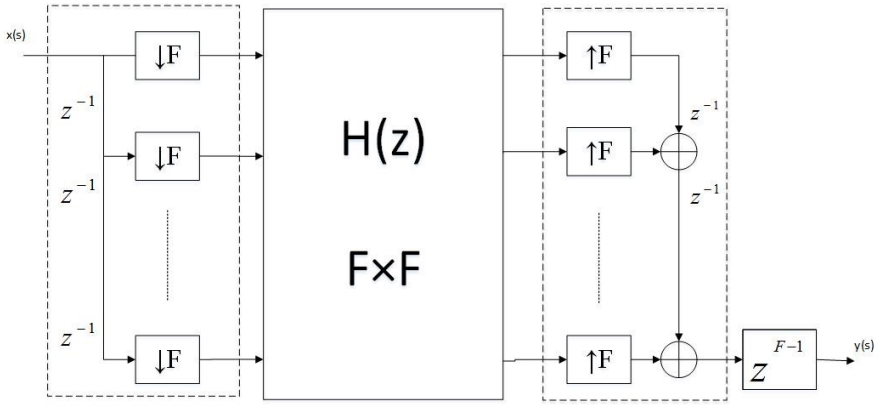

Figure 2-2: Block Filtering Diagram (from [15])

A single-input single-output transfer function, H(z), creates Figure 2-2 [15]. The input signal is divided into F number of delayed versions. Each delayed instance corresponds to a channel.

The sampling rate f_s will be downsampled based on the number of channels or F times. Each channel is processed individually before being upsampled and recombined back to the original f_s [15]. Using this model, the DSM is integrated into the transfer function portion.

One implementation, in particular, showed successful field programmable gate array (FPGA) employment of an ADT with 28 GHz TI-DSM. Look-ahead (LA) time-interleaved (TI) architecture is used for lower clock rate and no channel limitations [16]. Additionally, the system achieved multiple standards by using a reconfigurable digital circuit [16]. Their work was able to meet the Institute of Electrical and Electronic Engineers (IEEE) 802.11a wireless local area network (WLAN) standard in the 5.2 GHz band [16].

TI-DSMs have also been applied to create a reconfigurable cross-coupled DSM [17]. The flexibility in the architecture allows the modulator to be compatible with various wireless applications like Global System for Mobile Communications (GSM), Wideband code division multiple access (WCDMA), WLAN, etc. [17]. The paths of the DSM and the quantizer are readjusted based on the standard [17]. The dual extended (DE) noise shaping provides seamless switching between DSM orders [17]. Overall, the two path DS modulator had minimal complexity, low sampling rate and low power while providing support across an array of wideband standards [17].

Parallel processing of multiple DSM cores and high speed logic [18] is another implementation besides TI-DSM. It involves the independent operation of several DSM cores in parallel branches [18]. Unlike other parallel setups, the phases are kept separate [18]. This allows for linear scaling improvements of the transmitter's sampling frequency and in turn, bandwidth enhancements [18]. Applying such a method worked for BWs less than 20 MHz and up to 122 MHz and achieves a SNR always above 30dB [18].

Another way to lower the sampling rate is through techniques like borrow-save arithmetic, non-exact quantization and differential dynamic logic [19]. The DSM is adapted into borrow-save notation to reduce delay and uses non-exact quantization to maintain the benefits introduced by borrow-save [19]. Differential dynamic logic lowers the operation time, but must have the reset signal synchronized with the clocks to avoid acute sensitivity [19]. Frappé et al. were able

to reduce the sampling rate to twice the center frequency or 3.9 GS/s [19]. All three techniques can be used in high order modulators for sampling rate improvements [19].

Another way to allow for signal agility and reconfigurability is designing a tunable DSM [20]. Using the basis of an error-feedback structure, the DSM applies a gain value in the NTF based on when the frequency response is equal to zero [20]. This DSM can be good for the single or dual carrier ADTs [20]. Dinis et al.'s model was able to keep the error vector magnitude (EVM) below 4.5% while maintaining a low hardware complexity [20]. Their final design could use a dual-band configuration up to 2.5 GHz of carrier frequency [20].

Finally, Ding et al. demonstrated a different take with DSMs by addressing distortion effects. They model DSM/PWM based transmitters using a newly derived baseband Volterra model with a focus on nonlinearity [21]. Their accurate models of transmitter nonlinear behaviours and nonlinearity compensation allowed them to achieve the best output power and efficiency [21]. Using the proposed model, digital predistortion (DPD) was capable of linearizing a digital transmitter with an adjacent channel power ratio (ACPR) improvement of 5 dB for a 10 MHz Long-Term evolution (LTE) signal [21].

Through parallel processing methods, tunable setups and nonlinearity compensation coupled with DSM, transmitter limitations can be addressed. Delta-sigma modulators with parallel processing and/or digital logic, improve the sampling frequency, minimize complexity and provide signal reconfigurability. Similarly, tunable DSM primarily focuses on reducing the hardware, but maintaining signal compatibility. Alternatively, distortion and nonlinearities can be addressed with pairing DPD and DSM based transmitters. Although these adaptations are viable independently, combining them with 1-bit DSM adds further benefits.

2.1.2. 1-bit Delta-Sigma Modulation Models

Multibit quantizers lower the quantization noise by increasing the numbers of quantization levels [22]. Nonetheless, they use a larger bandwidth for processing. In effort to reduce the network bandwidth, 1-bit quantization has become a popular option. Using one quantization bit for processing allows for an easier design, more precision and lower cost [23].

Unlike multibit DSMs, a single bit implementation removes the need for comparison operations [11]. Not to mention, 1-bit DSM save network bandwidth by using less quantization bits per sample [24]. This leads to the structure needing less area, low power and staying linear [11].

1-bit delta-sigma modulators have quantizers with a single bit. This refers to the quantizer possessing two levels or outputs. The quantizer produces a digital bit stream of 1 or 0. The minimal amount of bits per sample allows low bandwidth use for the transmitter. Any DSM structure can implement a 1-bit quantizer. For instance, a high order 1-bit BP-DSM allows for easier design, better efficiency and higher oversampling [2]. The generated signal passes through a single bit sigma-delta modulator to create 1-bit streaming data. Digital streams are able to directly modulate electro-optic converters (EOCs) [2]. Currently, many researchers have enhanced the 1-bit DSM structure for additional benefits.

Single-bit architecture has been integrated with semi-parallel processing [25]. A parallel processing delta-sigma modulator (PDSM) used "simplified processing steps for n sequential clocks of a regular LP-DSM" [25]. The model has a trade-off between high-frequency processing and low oversampling ratios (OSR) [25]. Keeping the band limit of the signal, the OSR can be lowered [25]. The sampling frequency will decrease according to equation (1). When used in software defined ratio (SDR) transmitters, the signal quality was maintained and BW was increased up to four times before changing the sampling frequency [25].

1-bit DSMs can also be combined with tuning techniques. For a continuous-time filter, Kuang and Wight used an unstable DSM that detects stability to create 1-bit digital tuning signal [26]. This DSM had a very sensitive stability to loop filter tuning and will have high output amplitudes from quanitzer saturation [26]. The proposed architecture was simple and free of multi-bit DSP [26]. Through their scheme, 2% tuning accuracy was achieved [26].

With DSM integration, time waveform mismatches have been shown to cause distortion. Maehata et al. explain that the asymmetric component of the waveform was the key culprit and that digital predistortion cannot control it well. Therefore, they presented a new feedforward distortion compensation method for BP-DSM to combat this distortion [27]. Their scheme used the main signal and a distortion compensation signal as 1-bit digital pulsed trains [27]. The distortion compensation signal was a copy of the BP-DSM output that undergoes decomposition

then unity based on a series of elements [27]. These parts included BPF, negative gain, BP-DSM, pulse generator and attenuator [27]. Once the two signals were added, the distortion of both canceled each other out leaving a clean signal [27]. When tested with a 5 MHz LTE signal at 1.2288 Gb/s, the new 1-bit technique improved the ACLR by 4 dB [27].

Another adaptation of single-bit DSM can be found in the proposed architecture of Reyhani and Hashemipour [28]. Their work employed a single-bit DSM and a successive approximation (SA) algorithm [28]. The DSM kept linearity like a single-bit DAC and no longer required a high slew rate operational amplifier [28].

One way to reduce the complexity in the digital filter designs of FPGAs are 1-bit DSMs [29]. Memon et al. improved the filtering operations by using the DSM to lower the input and filter coefficients word length [29]. Through various tests, the authors concluded that 1-bit ternary finite impulse response (FIR) like filters performed the best over the multibit versions when staying at low orders [29].

Nevertheless, delta-sigma modulation is not without its problems. High order structures are susceptible to linearity issues. This prevents the improvements from more noise shaping. Also, 1-bit DSMs can suffer from being less efficient at noise shaping from timing jitter and consequently require a high OSR to compensate [11]. This compensation can lead to an increased demand for bandwidth negating a key benefit. One main way to combat the instability introduced with high level DSMs and 1-bit DSMs is employing envelope delta sigma modulators.

2.2. Envelope Delta-Sigma Modulation

When sending the envelope of a signal through the delta sigma modulator, the combination is called envelope delta sigma modulation (EDSM). Two main types of EDSM exist: one based on the modified Kahn-technique and the other using polar methodology.

One of the first instances of the modified Kahn-technique was first introduced by Wang in 2003 [30]. He proposed a transmitter based on Kahn technique for RF amplifiers [30]. This involved dividing the signal into the envelope and carrier for individual modifications and

powering an amplifier. The first difference Wang made from the Kahn method was the application of the DSM on the envelope rather than a pulse width modulator (PWM). The envelope was extracted by an envelope detector like the Hilbert transform [30]. Once the envelope was obtained, a DSM processed it for efficient noise shaping [30]. Figure 2-3 illustrates the original Kahn structure and the modified model.

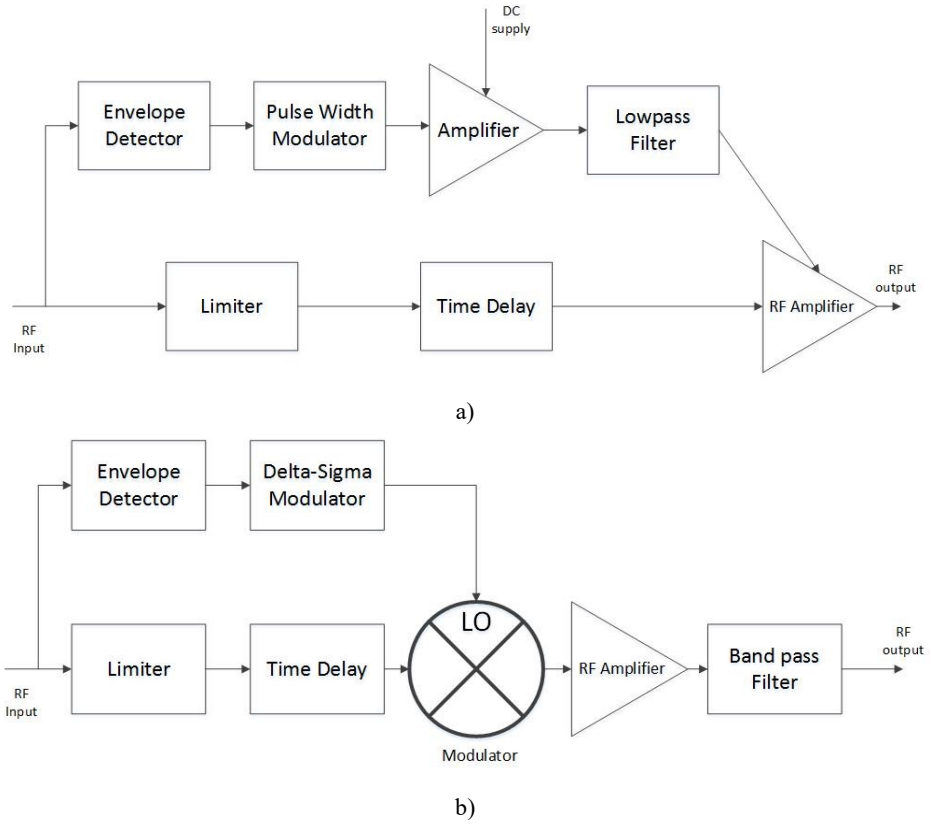

Figure 2-3: a) Original Kahn Structure and b) Modified Kahn Structure (from [30])

While one path modified the envelope of the signal (amplitude) in Figure 2-3 a) and b), the other changed the carrier signal [30]. The carrier signal consists of the constant envelope RF carrier containing phase information [30]. Along this path, the carrier signal passed through a limiter [30]. Afterwards, it was subjected to a time delay to compensate for the processing of the envelope along the other path.

When both paths have finished their modifications, the divided signals were combined via a local oscillator (LO) modulator as in Figure 2-3 b). This changed the envelope back to the original phase-modulated carrier [30]. Lastly, Wang removed the LP filter after the PWM and

added a BP filter after the power amplifier (PA) [30]. The restored signal passed through an amplifier and a bandpass filter (BPF) to obtain the original RF output. This technique allows the signal to enter a switching mode amplifier without adding any in-band distortion [2]. Consequently, the newly developed architecture improved the high power efficiency significantly from the traditional Kahn.

Expanding from the modified Khan technique, Dupuy and Wang developed a model that operated with a Class-E power amplifier [31]. The structure did not change from Figure 2-3 b) except for the PA changing from a Class-S to Class-E amplifier [31]. This alteration was implemented due to the high efficiency introduced while working in a particular switching mode [31]. With this change, they successfully demonstrated how the partnering of an EDSM and switch-mode power amplifier (SMPA) produces high linearity and efficiency [31].

Similarly, in polar transmitters, the signal is divided into the envelope and phase signal from the original complex signal. Like the modified Kahn-technique, a DSM processes the envelope. Yet, the phase is modulated by a local oscillator at the desired center frequency as shown in Figure 2-4.

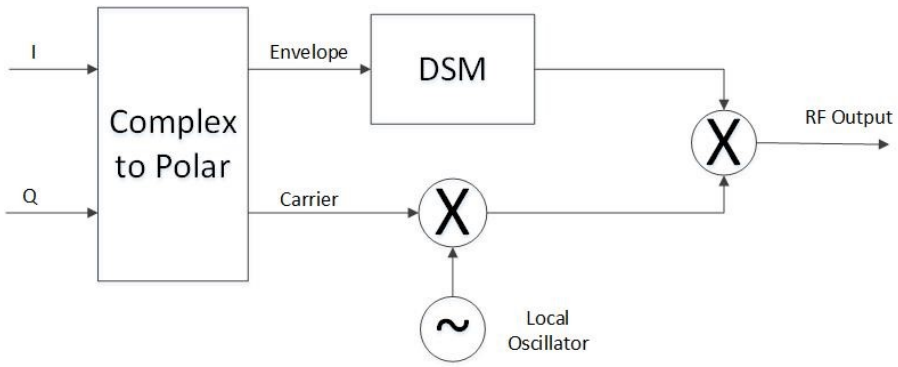

Figure 2-4: Polar Structure

The signals are subsequently multiplied back together after they have been processed in Figure 2-4. The RF output may proceed to a RF amplifier and BPF. The latter method is much simpler to construct and has been favoured in various work.

A complex polar transmitter with key modifications was proposed by Zhou et al. [32]. The envelope path consists of a digital IF pulse width modulator (PWM) based power switch,

driver buffer and inductor capacitor (LC) filter [32]. The pulse signal was subjected to a differential 1-bit delta-sigma modulator and a voltage-controlled oscillator (VCO) [32]. The VCO provides high tuning linearity and RF modulation to obtain the phase [32]. After each path was processed, the envelope and the phase were united using a power amplifier [32]. Through this setup, the developed EDSM achieved time alignment of both polar signals with low power.

A key design factor for EDSM is the quantizer level. As previously discussed in Chapter 2.1.2, the DSM can be single bit or multi-bit. To configure 1-bit EDSMs, two-level quantization is used. This can be represented as 1 and 0 outputs in the DSM for the envelope signal as it will keep the signal positive [33]. Alternatively, ±1 quantization can be employed as well to simplify the combination of the envelope signal and the phase signal [33]. However, this causes a disadvantage due to the negative values produced that will incur more noise [33].

Single bit quantization is employed in a digital DSM polar RF transmitter for code division multiple access (CDMA) IS-95A signals [33]. The constant envelope modulator used a 2^{nd} order LP-DSM with a sampling frequency of 80 MHz and OSR of 32. The envelope output turned the SMPA on and off [33]. The phase signal was upconverted and rejoins the envelope in the SMPA [33]. Their transmitter structure featured the basic features of polar transmitters for power amplifiers. This included signal conversion via coordinate rotation digital calculation (CORDIC), envelope modulated by DSM, phase upconversion and a power supply [33]. The 1-bit EDSM proved capable of effectively controlling the PA and amplifying the signal while satisfying the CDMA standard [33].

In contrast, multi-level DSM structures are investigated with EDSM structures [22]. One specific model used an envelope/phase component decomposer to split the signal and simplify the processing of each branch [22]. The envelope only experiences delta sigma modulation and the phase goes through a delay [22]. Afterwards, the two signal pieces are combined via a LO. Three levels in the DSM were found to be the maximum amount for improving overall transmission efficiency [22].

An alternative study into multilevel DSM versus EDSM transmitters was demonstrated in Singh et al [34]. Unlike the previously mentioned EDSM, the upconversion happens after the phase signal is recombined with the envelope [34]. Their EDSM used a 2^{nd} order LP-DSM when

comparing the quantizer levels [34]. The tests were conducted with a LTE signal and a WCMDA signal, but both reacted similarly to the modulation schemes [34]. The work concluded that with high level polar DSM, improvements to the coding efficiency and signal-to-noise and distortion ratio (SNDR) were achieved [34].

Keeping with the theme of multi-level quantizers, tri-level envelope encoding in transmitters has been shown to improve the sampling frequency and coding efficiency [35]. Using the premise of polar modulation like the previous example, a 522.24 MHz second order DSM converted the envelope to a tri-level signal using three levels of encoding [35]. Alternatively, a quadrature (IQ) modulator was used to process the phase signal. Both signals undergo delay correction to fix the mismatch [35]. After each signal is processed, a wideband mixer rejoined the polar parts and a differential-to-single-ended conversion (D2S) and drive amplifier (DA) prepare the tri-state RF signal [35]. This output drove the PA along with the dual mode supply modulator (DMSM) output. Using a DMSM, the PA operated at maximum leading to high efficiency despite suffering degradation from tri-level encoding [35].

Alternatively, alignment may be fixed through the phase modulated carrier (PMC) clocking the DSM [36]. Specifically, the DS modulated envelope was multiplied with the PMC to realize a 1-bit pulse train. This allowed the phase information to remain an analog signal, free from quantization noise introduced in the DSM [36]. The pulse train was submitted to a switching power amplifier before being sent for transmission. Inside the EDSM, a 1-bit low pass DSM was used due to the nature of the PMC architecture [36]. The modulator supported LTE 5 MHz bands up to 3GHz and 2.4 GHz ISM band [36].

Similarly, wideband and multiband transmitters employ EDSM. Like the modulator above, Cho et al. designed a transmitter covering LTE bands from 960 MHz to 3 GHz [37]. For a non-constant envelope, their DSM setup featured a second-order loop filter (LF) and 1.5-bit quantizer while operating at 800 MHz [37]. This paper expanded tri-level encoding through the additions of a dual-mode supply (DMS) and broadband PA [37]. The signal and the DMS drove the power amplifier. The work achieved high efficiency by using a second-order single op-amp resonator to suppress the phase shift introduced by the DSM and simplify the architecture [37].

EDSM architecture is a growing avenue for transmitter architecture. Whether it has single bit or multibit quantization, it has proven to be an attractive option for running PAs and transmitting a variety of mobile communication standards. Unlike standalone BP-DSMs, EDSMs provide a higher coding efficiency and lower sampling rate due to the envelope only containing quantization noise while the phase remains un-discretized [8][33]. They provide an answer to the problems encountered with certain DSM structures like clock jitter and linearity. Combining these benefits with the DSM BW improvements makes them suited to being integrated with RoF.

2.3. Delta-Sigma Modulation / Envelope Delta-Sigma Modulation in Radio-over-Fiber Systems

Modifying the signal at the transmitter to aid its journey across communication networks has sparked different types of RoF systems in today's research. To improve input stability, Mateo et al. proposed adding orthogonal basis modeling and DPD to a LTE-RoF system [6]. The new technique was created using Zernike polynomials [6]. It allowed perfect matching of complex input signals [6]. DPD efficiently canceled intermodulation while being a simple and low cost solution [6]. Clipping could also be combined in succession with DPD for high distorted OFDM-RoF systems [7]. The signal's peak-to-average power ratio (PAPR) consequently decreased and the linearity improves [7].

To improve RF signal power and suppress IMD3 for RoF, a cost-effective linearization technique has been developed [9]. Zhu et al. employed optical subcarrier modulation through the use of a directly modulated laser (DML) and an electro-absorption modulator integrated laser (EML) [9]. By adjusting the EML bias voltage, the IMD3 of each laser was suppressed [9]. IMD3 antiphase was created from the DML while the IMD3 inphase evolved from the EML. These phases effectively canceled each other out as the outputs were coupled [9].

Despite these RoF setups being viable options, one key type of D-ROF system called SDoF is emerging (see Figure 2-5). Many adaptations have been developed to create highly efficient communication networks.

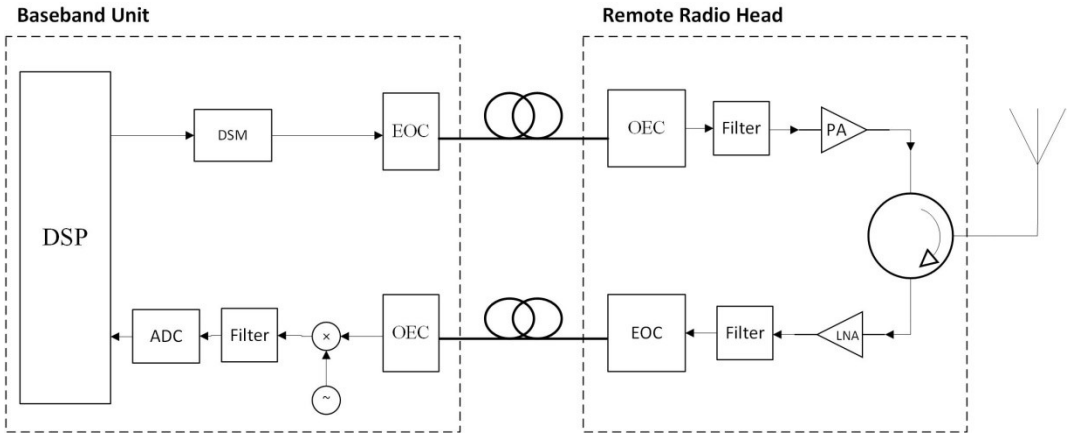

Figure 2-5: Delta-Sigma Modulation RoF block diagram (from [2])

Figure 2-5 is based on Figure 1-3 where many of the same parts are used. Here, the digital signal is created and undergoes DSM where a square waveform is produced. It directly modulates the EOC and travels along a fiber to the base station. The OEC, usually a PD, changes the signal back to its electrical form. A filter recovers the signal before amplification for the wireless transmission. The uplink section is identical to the A-RoF setup in Figure 1-3. The analog components are included since the filtering in the BS acts like a DAC.

In the first known merging of a DSM and a RoF system, a 4th order BP-DSM was the only component on the control station (CS) transmitter excluding the digital signal processing (DSP) unit [2]. The fourth order structure used a four compounded delay loops and fed directly into a VCSEL to transform the signal to the optical domain [2]. The signal travels down a single mode fiber and is received and transformed it back to the electrical domain via a photodiode (PD) [2]. Using the DSM to create into a Non Return to Zero (NRZ) bit stream [2], high frequency replicas of the incoming signal were created. This prevented the need of upconversion as the carrier frequencies could be recovered at the receiver [2]. The SDoF system also had the added benefit of being a lower cost structure than its D-RoF counterpart [2].

EDSM can also be implemented in a downlink D-RoF system. Currently, only one documented work has shown such a combination [8]. The instance exhibited how using a 1-bit DSM in an EDSM is more effective than just a BP-DSM and how EDSM was a strong option for RoF [8]. Using an EDSM, the phase modulated carrier lowered the 1-bit modulation switching rate and in turn, improved the jitter tolerance at high carrier frequencies [8]. The SNR and adjacent channel leakage ratio (ACLR) were main indicators of the improvements. Specifically,

the case covered 3GPP LTE bands greater than 2 GHz and IEEE 802.11 WLAN without serious degrading.

The inclusion of 1-bit modulation provides benefits to RoF systems. First, a 1-bit digital stream will incur lower degradation when being transmitted over an optical fiber for long distances [38]. Next, 1-bit transmission is able to cover a large frequency range [38]. This is possible as the output can be a carrier frequency identical to the harmonic frequency [38]. Finally, the 1-bit signal can be used to control RF amplifiers in the RRH.

Despite covering the major bands with 5 MHz bandwidth, the known EDSM RoF case does not exhibit a multi-band transmitter structure that can simultaneously transmit two or more frequency bands. Carrier aggregation is becoming necessary in multiband transmitters with high demands for transmitting signals concurrently.

2.4. Concurrent Dual-band and Multi-band Systems

Dual-band and multi-band RoF systems have been well documented. Yet, few have examined the integration of concurrent bands with DSM, EDSM or SDoF systems. Concurrent bands or better known as carrier aggregation (CA) is becoming an important feature in wireless communications. As a main feature of LTE-Advanced or 4G, CA involves aggregating up to 32 component carriers (CCs) for greater transmission bandwidth [39][40]. CCs follow the same bandwidth standards as LTE signals.

Three categories of CA arrangements exist. The first deployment type is the intra-band contiguous model. This involves contiguous CCs from the same LTE band being aggregated [41]. It is the easiest scenario, but not always practical. Intra-band non-contiguous allocation is preferred where CCs are more fragmented [41]. In this setup, as shown in Figure 2-7, the CCs have gaps between them [40]. Although, sometimes intra-band can be a limiting factor itself. This has prompted inter-band deployments where the carriers come from different LTE bands. Despite being a more complex setup, inter-band non-contiguous allows more options for aggregation. All three setups are depicted in Figure 2-6 through Figure 2-8.

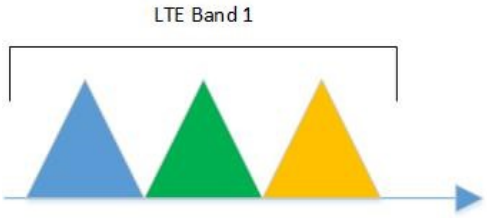

Figure 2-6: Intraband Contiguous (from [41])

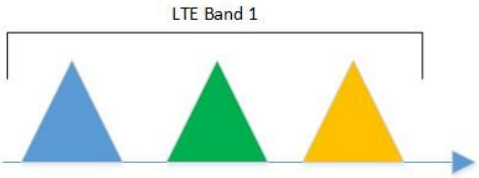

Figure 2-7: Intraband Non-Contiguous (from [41])

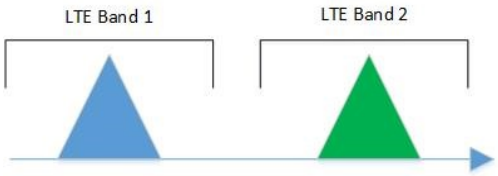

Figure 2-8: Interband Non-Contiguous (from [41])

With its added benefits, CA is being integrated into DSM designs. Rahman proposed a transmitter design implementing concurrent dual band DSM using noise shaping notches [42]. Applying the principles of BP-DSM, the architecture shaped the noise to specific frequency bands and created nulls where the alternate frequency could be fit [42]. This method prevented the out-of-band-noise from degrading the other carrier(s).

A similar dual-band solution using 1-bit DSMs to transmit separate frequency bands using carrier aggregation (CA) exists. The DSM was designed using noise shaping notches to match the selected carrier frequencies. By creating custom NTFs based on the center frequencies, the same structure could be employed. After each signal was processed through the 4^{th} order DSM, a multiplexer upconverted the signal to the specified frequency the DSM was based on [43]. This combination allowed the signals to be placed at the desired notch location and avoid the noise. Once upconverted, the signals were combined together [43]. Three different cases of dual-band were compared: LP-BP, BP-BP where $f_1 = f_2/2$ and BP-BP where $f_1 \neq f_2/2$ [43]. The combination of notches and CA setup allowed clean noise shaping.

An alternative concurrent dual-band transmitter involves two BP-DSMs sharing part of the feedback loop [44]. The sharing instance allowed the two stop-bands to subdue the quantization noise [44]. Consequently, the transmitter architecture was stable, less complex and able to independently configure to two carriers. The model used a 1-bit DSM, but only a 6^{th} order capacitor resistor feedback (CRFB) BP-DSMs [44]. The transmitter achieved high ACLR for each frequency by using two 5 MHz LTE signals at 3.9 Gb/s [44].

The same model was expanded from concurrent dual-band work to concurrent multiband in 2017. Here, the same idea of sharing feedback loops of multiple DSMs was used, but now parallel BPFs were included [45]. 2^{nd} order parallel infinite impulse response (IIR) filters suppressed the quantization noise for each carrier frequency and maintain stability [45]. Based on the number of bands, the architecture adapted the BPFs and the RF signal bandwidth determines the level of complexity [45]. For testing this structure, two or three 40 MHz LTE signals with intra-band and inter-band CA were transmitted at 10 Gb/s [45]. The dual-band case produced a high ALCR of -49 dBc and more than -45 dBc for three bands. Therefore, 1-bit BP-DSMs were good for wideband signals and 1-bit data streams are capable of multiplexing multiple RF signals [45].

In a different approach, digital mobile fronthaul (MFH) architecture has been adapted with DSM and CA. Single bit and double bit DSM were used in partnership with on-off keying (OOK) or pulse amplitude modulation (PAM4) optical intensity modulation-direct detection (IM-DD) transmission [46]. The structure was tested with 32 LTE CCs and purposely sent them over a 25 km single wavelength 10-Gbaud OOK/PAM4 link [46] for support. The customized CA setup permitted four times the fronthaul capacity. Error vector magnitudes (EVMs) resulted in less than 5% or 2.1% meeting the LTE standards for 256 QAM or 1024 QAM [46]. The research showed how partnering DSM with current MFH provides resilience against noise and nonlinear effects [46].

CA integration is still fairly new to DSM partnerships and current work shows how researchers are adapting such features. Still, this concept remains uncommon, revealing the key need for more investigation into concurrent DSM RoF transmission.

2.5. Motivation and Contribution

Delta-sigma modulation can be a beneficial addition to any transmitter or RoF transmission system. However, due to the ever expanding and demanding nature for bandwidth in this digital age, mobile communication systems need to be even more adaptable, efficient and low cost. Different adaptations of DSMs have been discussed that provide further positive implications. A key standout is the implementation of an EDSM instead of a DSM to combat jitter noise from using high order structures. The individual processing of the envelope and phase provides time alignment and allows the noise shaping benefits. Additionally, using a single bit quantizer in the EDSM structure keeps BW transmitter improvements. Another main area of motivation was implementing a system to understand the impact of optical components in conjunction with EDSM transmitters. Finally, an area hardly addressed in literature is the implementation of concurrent dual-band or multi-band RoF systems with DSM or EDSM. Many papers express the compatibility of multiple communication standards, but do not look at transmitting them all together. As many new band standards are being designed and used, carrier aggregation (CA) is becoming an important reality. CA involves transmitting two or more carriers from the same band or different band. By integrating concurrent signals into the transmitter, the functionality increases.

In this thesis, a concurrent dual band 64-quadrature amplitude modulation (64-QAM) 20 MHz LTE Radio-over-Fiber system using EDSM is proposed. The transmitter side of the RoF transmission accepts two LTE signals and individually applies 1-bit envelope delta sigma modulation before combining the two via carrier aggregation. The DSM in the EDSM is custom tailored for the center frequency and uses 4^{th} order BP-DSM design. This transmitter setup is compared with using the 1-bit BP-DSM setup with the same design as the one in the EDSM setup. After either modulation is applied, the new signal is sent over the optical link. Once received, it is subjected to a recovery process. This work demonstrates the advantages and disadvantages in a concurrent dual-band system RoF system with EDSM. The system is able to satisfy the EVM LTE standards while using a high order BP-DSM and maintain them with RoF transmission.

Chapter 3. Theory of Concurrent Dual Band Envelope Delta-Sigma Modulation

The theory of the proposed concurrent dual band Radio-over-Fiber system using 1-bit EDSM is explained in this chapter. The system is broken down from the DSM of the EDSM. The architecture of the DSM is critical to the noise shaping efforts for the signal. Next, the EDSM setup is reviewed looking at how the DSM is used. Afterwards, the EDSM's integration into the transmitter is laid out. Finally, once the transmitter is established, the inclusion of it and the remaining RoF components are presented.

3.1. Implemented Delta-Sigma Modulation

A 4^{th} order BP-DSM is employed in the overall design. The general structure is a high order DSM with a single quantizer as shown in Figure 3-1.

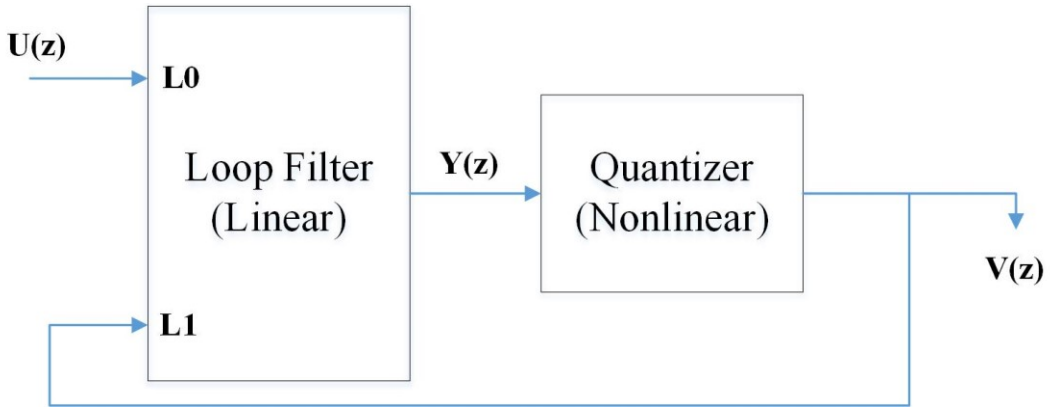

Figure 3-1: General Structure for High Order and single quantizer DSM (from [12])

The modulator consists of a linear and nonlinear part [12]. Linearity depends if memory elements are used or not [12]. The loop filter accepts the input U(z) and output V(z) and outputs Y(z). To describe the filter's function, the equation (5) for the DSM can be altered to

$$Y(z) = L_0(z)U(z) + L_1(z)V(z) \tag{13}$$

where $L_0(z) = \frac{STF(z)}{NTF(z)}$ and $L_1(z) = 1 - \frac{1}{NTF(z)}$ [12].

The quantizer of the model accepts the output of the loop filter, Y, and adds error, E(z) [12]. Equation (14) shows the relationship.

$$V(z) = Y(z) + E(z) \tag{14}$$

Using the above equations [12], it can be modified to

$$V(z) = STF(z)U(z) + NTF(z)E(z) \tag{15}$$

STF, NTF and the quantizer properties are only factors determining the loop filter characteristics [12]. Consequently, the structure of the loop filter does not factor in the ideal behaviour of the modulator [12].

Since the model is 4th order, the DSM model contains four feedback loops to its improved noise shaping efforts. Extending the BP-DSM structure previously shown in Figure 1-12, the implemented DSM is created. The architecture uses a series of integrators and coefficients and a quantizer as seen in Figure 3-2.

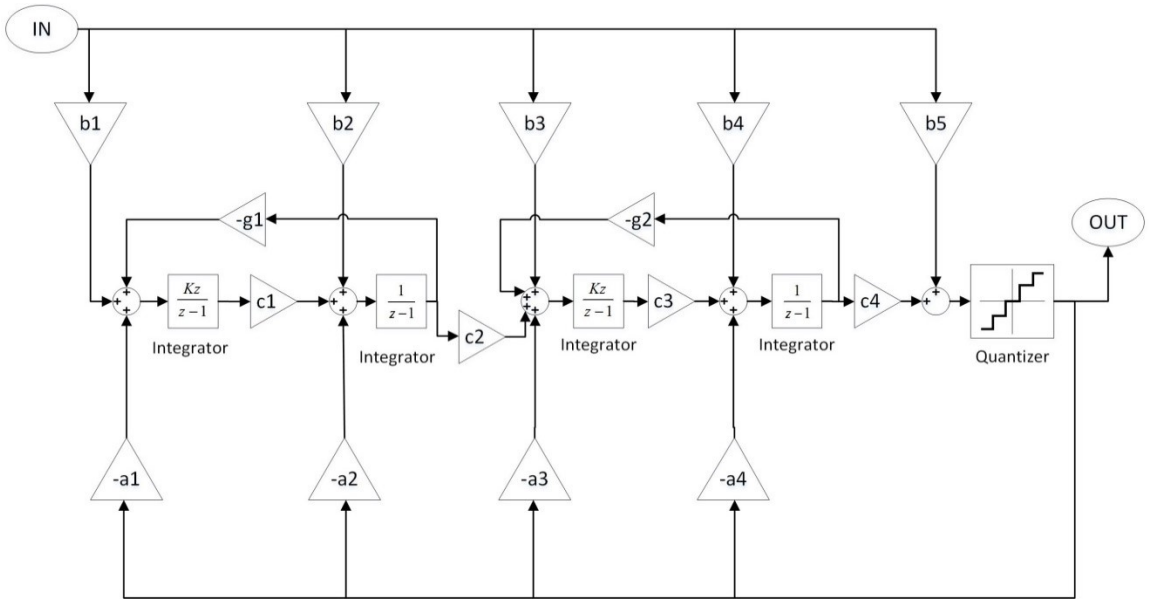

Figure 3-2: 4th order CRFB BP-DSM structure (from [12])

This layout is called cascade-of-resonators with distributed feedback (CRFB) where linear loop filters are employed [12]. Due to its flexibility and common use, the layout was employed. On the unit circle, CRFB has the zeros located at non-zero frequencies [12]. Two conjugate complex pairs are used to determine the four NTF zeros [12]. The first two integrators and feedback path represent a resonator. This produces two complex poles using the formula $z^2 - (2 - g_1)z + 1$ that can be found on the unit circle at frequencies $\pm\omega_1$ [12]. The second resonator, created by the next two integrators and feedback path, produces the next two poles at frequencies $\pm\omega_2$ [12]. The frequency can be calculated as $cos(\omega_n) = 1 - \frac{g_n}{2}$ or an approximation for the normalized pole frequency can be determined by $\omega_n \ll 1, \omega_n \approx \sqrt{g_n}$ [12]. For the poles to remain on the unit circle, one integrator must be delay free.

The transfer function for the first resonator can be represented as $H_1(z) = \frac{a_1 z + a_2(z-1)}{z^2-(2-g_1)z+1}$ [12].

Similarly, the second resonator has a similar transfer function $H_2(z) = \frac{a_3 z + a_4(z-1)}{z^2-(2-g_2)z+1}$ [12].

Using these transfer functions, the loop inputs $L_0(z)$ and $L_1(z)$ [12] can be formulated as

$$L_0(z) = -\frac{b_1 z + b_2(z-1)\cdot z + \left[z^2-(2-g_1)z+1\right]\cdot b_3 z + b_4(z-1)}{[z^2-(2-g_1)z+1]\cdot[z^2-(2-g_2)z+1]} + b_5 \quad (16)$$

$$L_1(z) = \frac{a_1 z + a_2(z-1)\cdot z + [z^2-(2-g_1)z+1]\cdot a_3 z + a_4(z-1)}{[z^2-(2-g_1)z+1]\cdot[z^2-(2-g_2)z+1]} \quad (17)$$

When the order is even, the number of resonators is equal to the order divided by 2. In the uncommon case when the order is odd, subtract one from the order and divide by 2 to find the number of resonators [12]. Additionally, when odd, the loop filter must contain a plain integrator [12]. Since this is a 4th order model, 2 resonators are implemented.

The parameters of the BP-DSM are customized for the input signal. The signal bandwidth is 20MHz as a 20MHz LTE signal is used. The carrier frequencies selected are from LTE band 1 and band 7. Using the LTE standards [47], the following calculations were made to find the correct carrier frequency:

$$Band\ 1:\ 2110 + 0.1(20 - 0) = 2112\ MHz$$
$$Band\ 7:\ 2620 + 0.1(2950 - 2750) = 2640\ MHz$$

The sampling rate of 6 GHz is applied due to these center frequencies of 2.112GHz and 2.64GHz. Using formula (1) in Chapter 1.2, the OSR is 150 due to the high sampling rate.

For the DSM transfer functions, the STF is kept to unity or 1. The BP-DSM NTF and coefficients are determined using the MATLAB DSM toolbox. To get the specific NTF, the function 'synthesizeNTF' is used. The input variables are order, OSR, optimization (opt), maximum out-of-band gain and normalized center frequency as summarized in Table 3-1.

Table 3-1: NTF Parameters

Order	4
OSR	150
Opt	1
Maximum out-of-band NTF gain	1.5
Center frequency ratio	fc/fs

The optimization '1' corresponds to using the high-OSR limit to optimize the zeros. The function bases the NTF on Lee's rule [12] where for a stable DSM the maximum out-of-band gain must be less than 2. In this case, the default value of 1.5 is applied. The normalized center frequency is tailored to the input signal. Since the sampling frequency of the signal is 6 GHz and the selected bands are 2.112 GHz and 2.64 GHz, the center frequency ratios are 0.352 and 0.44, respectively. With this information, the NTF for 2.112 GHz is

$$\frac{(z^2 + 1.218z + 1)(z^2 + 1.173z + 1)}{(z^2 + 1.168z + 0.6296)(z^2 + 0.7279z + 0.7055)}$$

and the NTF for 2.64 GHz is

$$\frac{(z^2 + 1.87z + 1)(z^2 + 1.849z + 1)}{(z^2 + 1.474z + 0.5823)(z^2 + 1.486z + 0.7631)}$$

Using the two NTFs, the following plots are produced in Figure 3-3 and Figure 3-4.

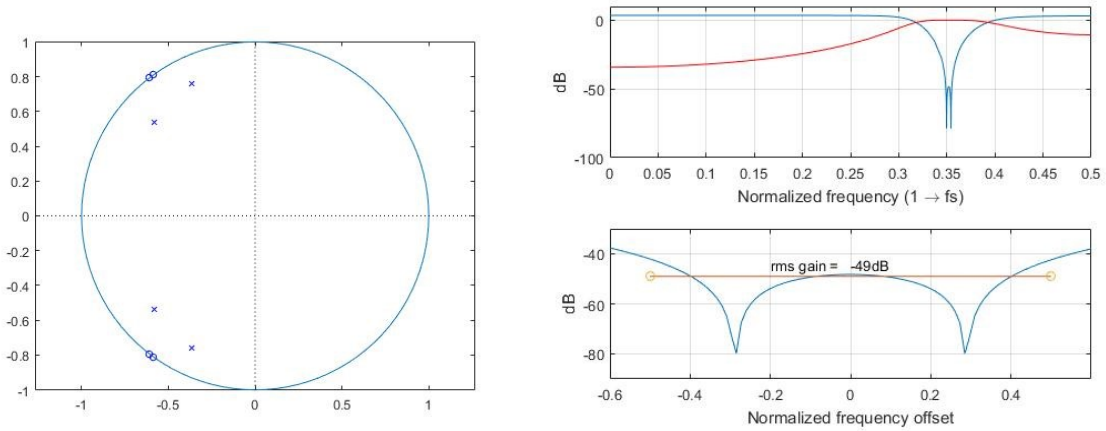

a) b)

Figure 3-3: 2.112 GHz a) Zero/poles and b) Frequency response plots

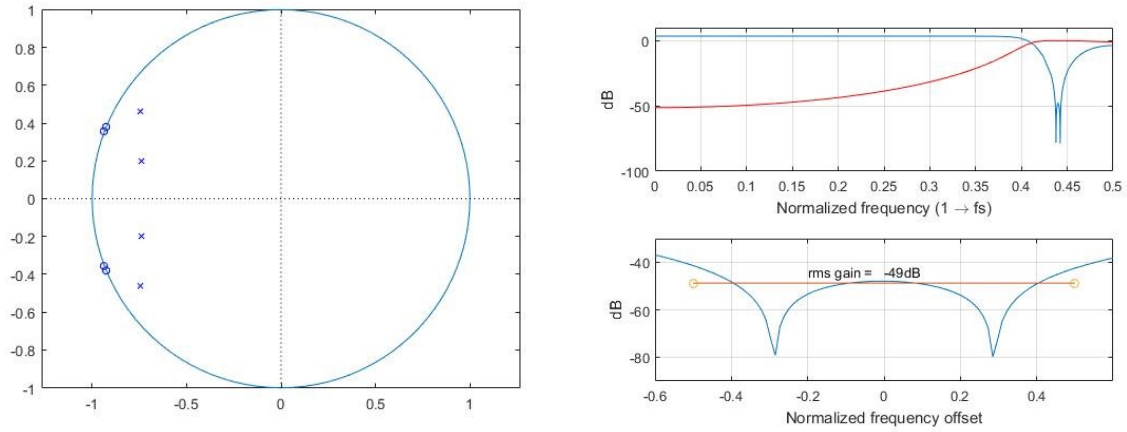

a) b)

Figure 3-4: 2.64 GHz a) Zero/poles and b) frequency response plots

Figure 3-3 a) shows the zero/pole plot for 2.112 GHz DSM. The circles represent the 4 zeros on the unit circle and the crosses are the 4 poles inside the unit circle. The corresponding frequency response in Figure 3-3 b) shows the normalized frequency filtering of the noise transfer function for 2.112 GHz. Similarly, Figure 3-4 a) depicts the zero/pole plot for 2.64 GHz DSM. The circles and crosses change positions based on the NTF. The normalized frequency plot in Figure 3-4 b) has its center at 0.44. The offset plots for both center frequencies show the same rms gain at -49dB.

The adjusted NTFs allow the noise shaping to happen at the desired RF carrier frequencies. Once the NTF is obtained, another function 'realizeNTF' is run to obtain the

coefficients a_i, b_i, c_i and g_n for the model in Figure 3-2. Using the two loop input equations (L_0 and L_1) made from the CRFB transfer functions and their relation to the NTF and STF, the coefficients are calculated. The output is the feedback/feedforward coefficients, resonator coefficients, feed-in coefficients and integrator inter-stage coefficients. Using these coefficients the above model in Figure 3-2 is populated [12].

The quantizer used in both DSMs is a 1-bit quantizer. The levels of the quantization correspond to 2^B where B is the number of bits. Therefore, in this case, the quantizer has 2 levels. The quantizer has a specific step value represented by delta, Δ, according the levels. Equation (18) uses the number of bits desired and the dynamic range of the signal amplitude.

$$\Delta = \frac{|Max\ Amplitude| + |Min\ Amplitude|}{2^B} \tag{18}$$

3.2. Proposed Envelope Delta-Sigma Modulation

For the proposed EDSM model, the basis of a polar transmitter setup is used. The architecture is based on a polar transmitter model, but does not include specific clock matching. Figure 3-5 shows the implemented schematic.

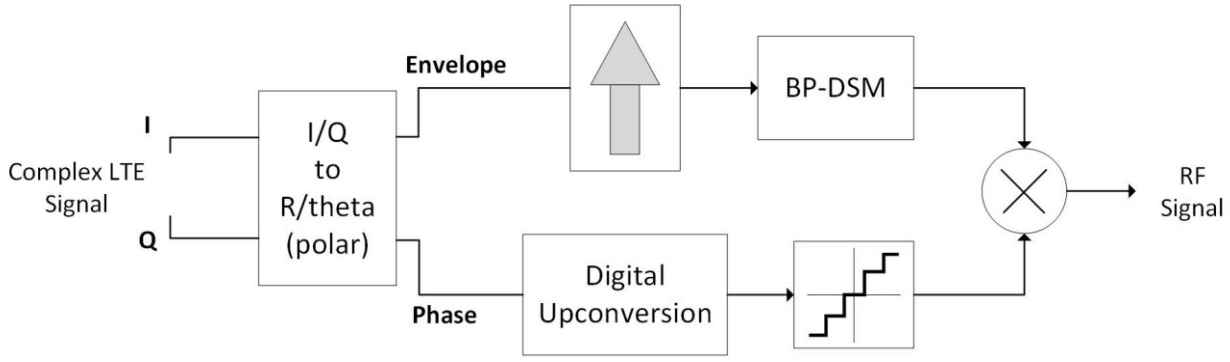

Figure 3-5: EDSM setup

First, the complex LTE baseband signal, v(t), is transformed into its polar coordinates the envelope and phase, a(t) and θ(t), respectively.

$$v(t) = i\,(t) + q(t)i \quad \xrightarrow{transform} \quad v(t) = a(t)e^{-i\theta(t)} \tag{19}$$

Afterwards, the envelope is upsampled from 30.72MHz to 6GHz. The output signal from the upsampler undergoes delta-sigma modulation. The DS modulator integrated into the EDSM model is the BP-DSM described in Chapter 3.1. The center frequency, f_c, of the BP-DSM matches the value used in the phase upconversion. The EDSM is tunable for the center frequency as long as it satisfies Nyquist's rule. It explains that the sampling frequency must be greater than twice the center frequency. Therefore, since the sampling frequency is 6 GHz, the center frequency must be less than 3 GHz. In the other path, the phase is digitally upconverted to the center frequency and then the values are quantized. For the quantizer of the phase path, this work employs the use of 1 and -1 for simplicity. The modified envelope and phase are recombined again to form the desired RF signal.

3.3. Transmitter Design

The transmitter of the dual band 64-QAM 20MHz LTE Radio-over-Fiber system is kept simple. Two LTE signals are created and undergo EDSM matched to their carrier frequencies. This allows for optical noise shaping. The setup is illustrated in Figure 3-6.

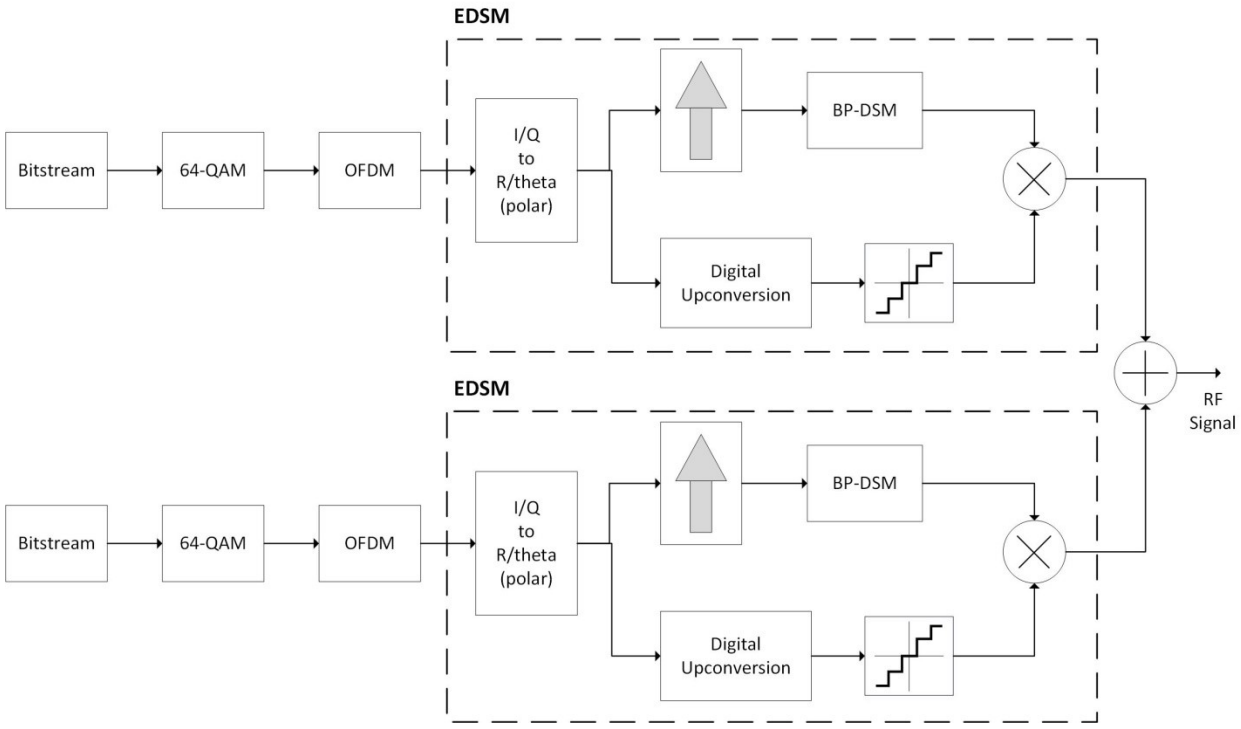

Figure 3-6: Block Diagram of Proposed Transmitter

The general structure consists of the LTE block components and two 1-bit envelope delta-sigma modulators. Two baseband (BB) LTE signals with 64 QAM are designed. For each signal, a bit stream first undergoes QAM modulation where the bits are organized into constellations. Specifically, grey coding is implemented. Next, orthogonal frequency division modulation (OFDM) maps the QAM symbols onto orthogonal subcarriers using Fast Fourier Transforms (FFTs) [48]. Afterwards, Inverse Fast Fourier Transform (IFFT) transforms the subcarriers back into the time domain [48].

Once the BB LTE signal is acquired, the signal undergoes EDSM. As discussed in Chapter 3.3, the signal is changed from its complex coordinates to its polar coordinates. An upsampler changes the envelope sampling frequency from 30.72 MHz to 6 GHz. The upsampled signal undergoes BP-DSM according to the specified carrier frequency. The DSM will spread the quantization noise away from the band of interest in preparation for the phase. The phase of the LTE signal is digitally upconverted to the same carrier frequency as the corresponding DSM. Post upconversion, a quantizer changes the phase signal to 1 and -1.

After both the envelope and phase finish their individual processing, a multiplier rejoins the two parts and outputs an RF LTE signal centered a the specified center frequency. The second LTE signal follows the same process, but for a different frequency.

The two carrier frequencies are selected from two different LTE bands. This indicates that the interband CA arrangement will be applied. The two component carriers are combined into one concurrent instance using an adding block. Now, the signal is ready for transmission.

3.4. Radio-over-Fiber Design

The Radio-over-Fiber elements are easily combined with the transmitter setup. In the control station, the transmitter design in Chapter 3.3 is combined with an optical transmitter. At the base station, an optical receiver processes the signal and feeds to electrical components. An optical fiber connects the two stations. Figure 3-7 depicts the RoF transmission design.

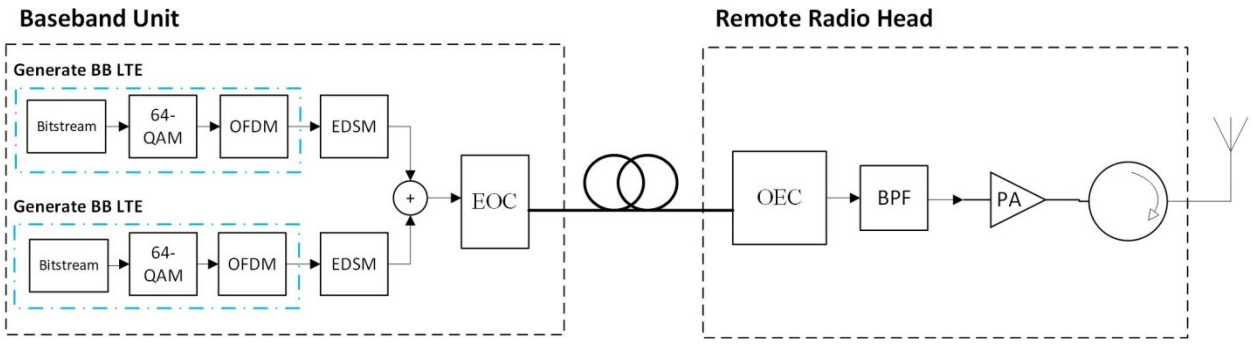

Figure 3-7: RoF setup with EDSM integration

After the concurrent RF signal is produced, an electro-optic converter transforms it to the optical domain. In the EOC, the signal directly modulates the laser. The newly developed optical signal is transmitted along a single mode fiber. At the receiver, the optic-electro converter accepts the optical signal and transforms it back into an electrical signal. A photodiode performs this function. The reacquired electrical signal is demodulated and recovered by a digital signal processing unit if being examined. However, for full transmission, the signal would be filtered by a bandpass filter (BPF) recovering the analog component and amplified by a PA for wireless transmission. A circulator would send the signal to an antenna.

Chapter 4. Simulation of Concurrent Dual Band Envelope Delta-Sigma Modulation Radio-over-Fiber

In co-simulation, MATLAB, Simulink and VPIphotonics create the simulation designs and results to demonstrate the controlled functionality of the proposed system. The signal, modulation and recovery are performed with MATLAB and Simulink. The RoF design and optical tests are completed with VPIphotonics. The design uses a single and dual band 64-QAM 20MHz LTE signal for the various parts. When testing concurrent dual band compatibility, the carrier frequencies tested are 2.112 GHz from LTE band 1 and 2.64 GHz from LTE band 7. The results are evaluated using the constellation diagrams and corresponding EVMs. When evaluating the system, EVM readings are taken after the BP-DSM/EDSM (before the laser) and after the transmission.

4.1. Simulation Design

For the simulation, the general process is outlined in the flowchart below.

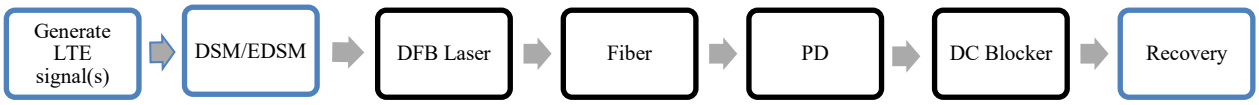

Figure 4-1: Simulation setup flowchart

The blue portion of the flowchart represents the DSP module. Here, the creation and the modulation of the signal are performed. With MATLAB, the LTE signal is designed by creating a bit stream. Using the QAM example on the MathWorks website [49] as a guide, the bit stream is mapped into binary groups and changed from binary to integers. The built-in QAM modulation function processes these integers by mapping with gray coding according to the constellation size, M. This creates an M-QAM signal where M = 64 or 6 bits per symbol. After QAM modulation, the array is applied to the built-in orthogonal frequency-division multiplexing (OFDM) modulator. Figure 4-2 shows the stages of the BB LTE generation.

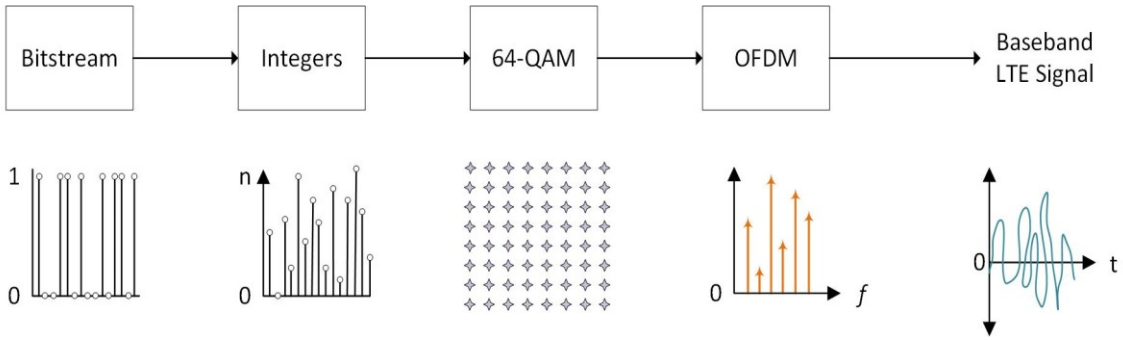

Figure 4-2: Generation of the Baseband LTE signal in MATLAB (from [48])

In OFDM, the signal carriers are transformed to being orthogonal via Fast Fourier Transforms (FFTs). OFDM allows for no cross-talk due to orthogonal properties of the carriers and consequently, the carrier separation can be small. The signal is split into N low rate signals where the channel delay is smaller than the symbol duration [50]. Three type of OFDM subcarriers exist: data, pilot and null [50]. Since this is a 20MHz signal, LTE standards need to be followed for OFDM application. The number of occupied subcarriers is 1200 plus a DC subcarrier and they are spaced at 15 kHz in a 2048 sized FFT [47][51]. Table 4-1 summarizes the LTE standards implemented.

Table 4-1: Summarization of LTE Standards for 20 MHz BW (from [47])

LTE Standards	
Channel BW	20 MHz
FFT/IFFT size	2048
Number of Resource Blocks	100
Number of Occupied Subcarriers	1200
Sample Rate	30.72 MHz
Subcarrier Spacing	15 kHz

Pulse shaping is performed in the OFDM via a square root-raised cosine filter. Additionally, a cyclic prefix of 14 is added to the newly transformed signal. Afterwards, the inverse fast Fourier transform (IFFT) changes the 2048 FFT vector to a time domain signal for sending through the channel. Through these steps, an OFDM signal is designed.

In order to be a proper and usable LTE signal, the OFDM signal must be upconverted to become a radio frequency (RF) signal. The upconversion will depend on the method of DSM applied. Two different scenarios are used: BP-DSM and EDSM.

For a basic BP-DSM, the signal is directly upconverted after OFDM. Digital upconversion involves the BB LTE signal being inserted into a zero filled array at the array index representing the center frequency. The process is performed in the frequency domain where the BB LTE signal is called the FFT vector. The stages are represented in Figure 4-3 to Figure 4-5.

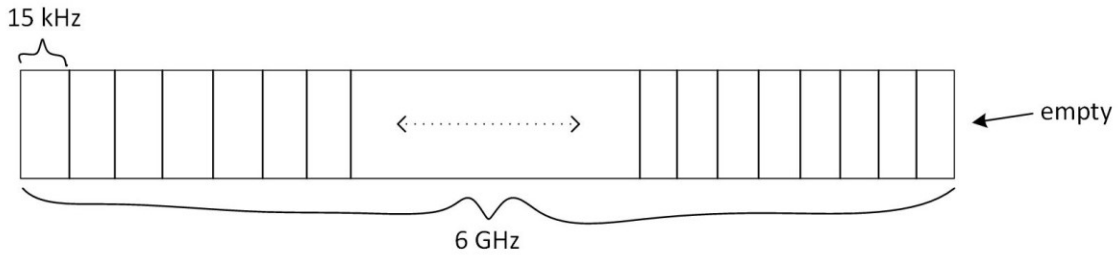

Figure 4-3: Empty RF vector

The RF vector begins as a zero filled array representing a 6 GHz signal. Figure 4-3 illustrates how the array is divided into 15 kHz subcarriers. Based on the desired center frequency, the starting subcarrier in the RF vector for the BB LTE signal is:

$$starting\ subcarrier = \frac{f_c}{15e3} - \frac{NFFT}{2} \tag{20}$$

where NFFT is the size of the FFT. With this known subcarrier, the FFT vector can be inserted into the RF vector as illustrated in Figure 4-4.

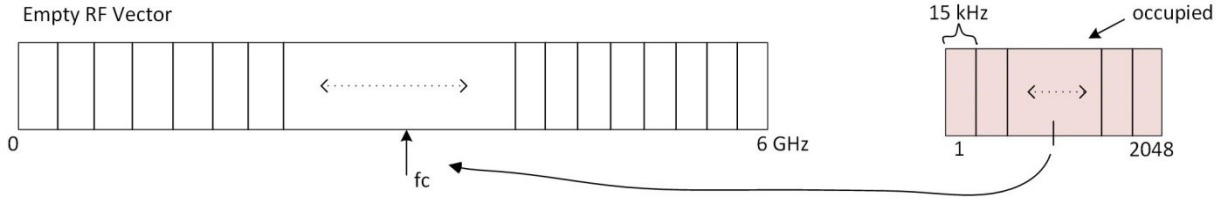

Figure 4-4: Empty RF Vector with fc point marked and FFT vector

Figure 4-4 shows the empty RF vector with the carrier frequency marked and the setup of the FFT vector. As shown in Table 4-1 and in Figure 4-4, the 20 MHz LTE signal has FFT of

2048 where each subcarrier is 15 kHz. Once the starting point has determined, the FFT vector is placed into the RF vector, subcarrier by subcarrier. Figure 4-5 shows the finished RF vector.

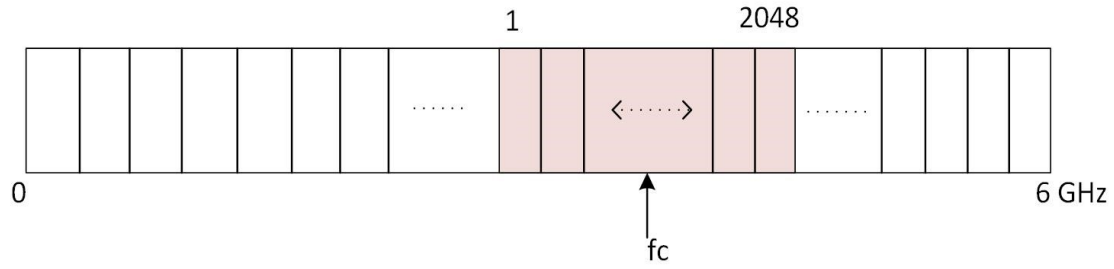

Figure 4-5: Complete RF Vector - FFT vector inserted into RF vector

As seen in Figure 4-5, the remaining RF subcarriers remain zero. After the points are inserted, the RF array is changed back to the time domain via inverse fast Fourier transform. Now, the RF signal is ready for BP-DSM.

The BP-DSM accepts the RF signal from the MATLAB code and processes it in Simulink. Figure 4-6 shows the block diagram of the signal processing.

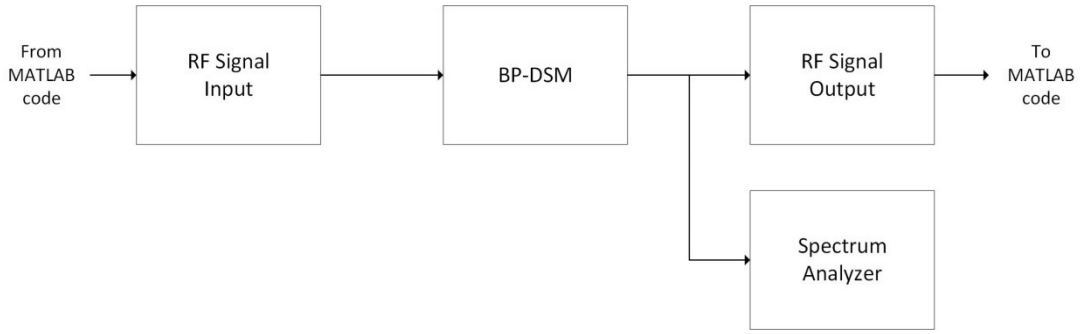

Figure 4-6: Simulink layout of signal processing

The BP-DSM model is setup as a single bit 4^{th} order CRFB. The DSM toolbox for MATLAB calculates the coefficients for the layout. The quantizer step size is determined using equation (18) in Chapter 3.1. The amplitude max and min values of the input signal are 0.03459 and -0.00117. This produces an interval value of 0.01788 for the implemented quantizer. Figure 3-2 in Chapter 3.1 shows the DSM layout and discusses how the model is setup. The signal leaves the BP-DSM and returns to the MATLAB code ready for transmission. Figure 4-7 a) and b) show an example of the RF signal before BP-DSM and after.

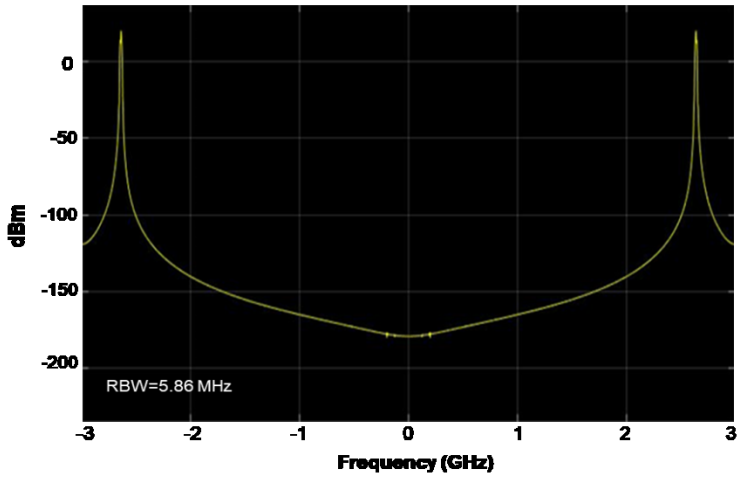

a)

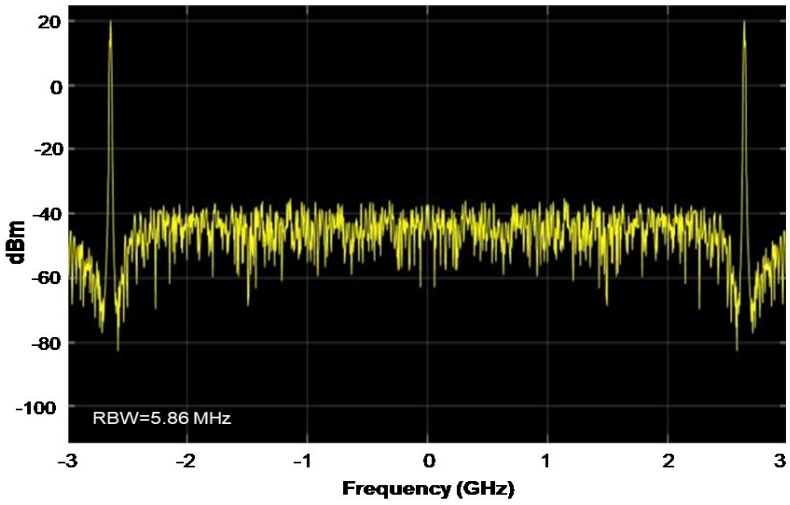

b)

Figure 4-7: RF signal in frequency domain – a) Before BP-DSM and b) After BP-DSM

The main difference in the two figures is the addition of the quantization noise and noise shaping at the center frequency. Figure 4-7 b) will be the signal used for direct modulation.

For the EDSM case, the upconversion only happens to the phase part of the signal. As discussed in Chapter 3.2, the BB LTE signal is converted from its in-phase and quadrature components to the polar coordinates. Next, the envelope is upsampled from 30.72 MHz to 6 GHz to match the upconversion of the phase. Once upsampled, the envelope is sent to the Simulink setup as in Figure 4-6, but this time the signal is baseband. Figure 4-8 a) and b) show the differences compared to Figure 4-7 a) and b).

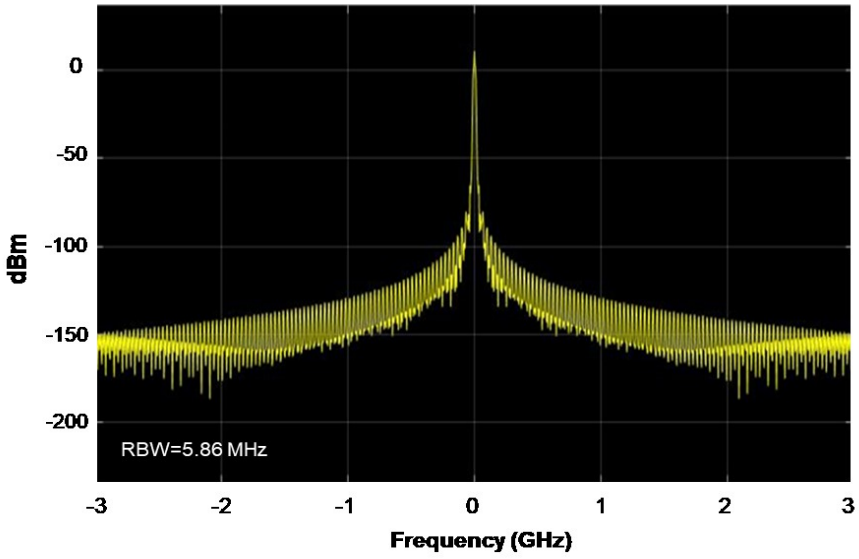

a)

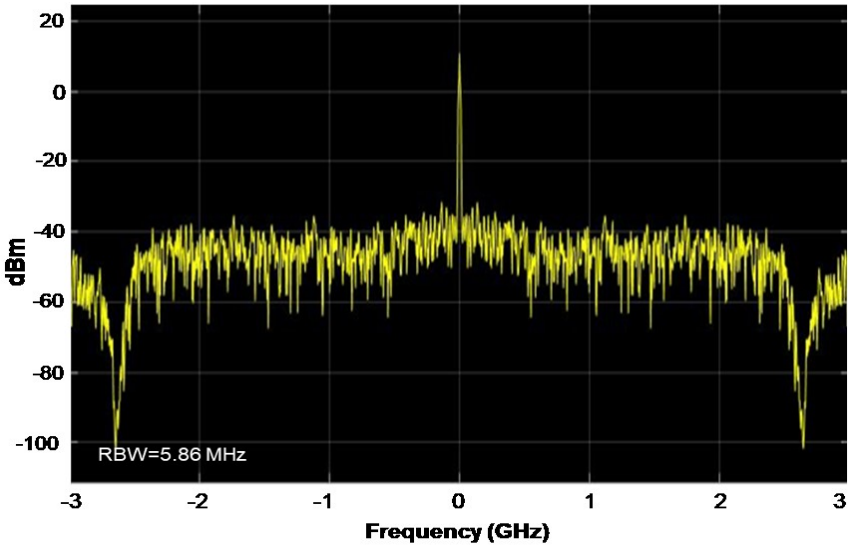

b)

Figure 4-8: Envelope of BB LTE Signal – a) Before BP-DSM and b) After BP-DSM

The frequency notches from the BP-DSM are visible in Figure 4-8 b). Unlike Figure 4-7 a) and b), the DC is still at 0 and not shifted. Meanwhile, the phase undergoes digital upconversion by inserting the phase into a RF vector. At first, it follows the same steps from Figure 4-3 through Figure 4-5 except the FFT vector is the phase instead of the whole signal. Once the RF vector is designed, a quantizer quantizes the upconverted phase to values of 1 or -1. The quantized value is joined with the output from the BP-DSM to create the RF signal for transmission. Figure 4-9 exhibits the EDSM output in the frequency domain.

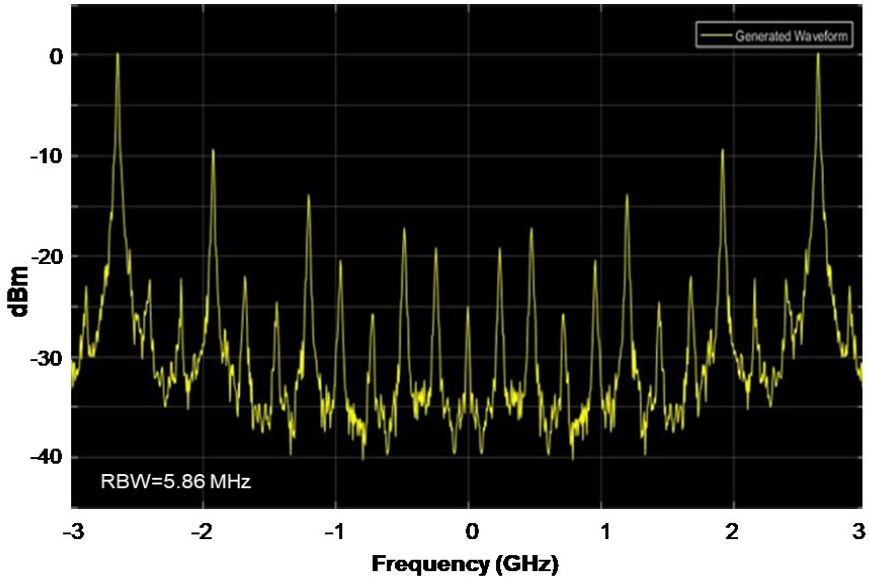

Figure 4-9: EDSM output in frequency domain

The EDSM output differs from the BP-DSM output from the additional copies of the center frequency. The copies are a result of the quantization of the phase. Unlike Figure 4-7 b), the noise shaping in Figure 4-9 is not as defined at the center frequency.

After the signal is prepared from either BP-DSM or EDSM, it is sent to VPIphotonics for the RoF portion of the system. VPIphotonics is simulation software that allows modeling of electrical, photonic and optical transmission design. Pre-built photonic elements are arranged together to create the RoF transmission. Figure 4-10 shows the VPIphotonics schematic used.

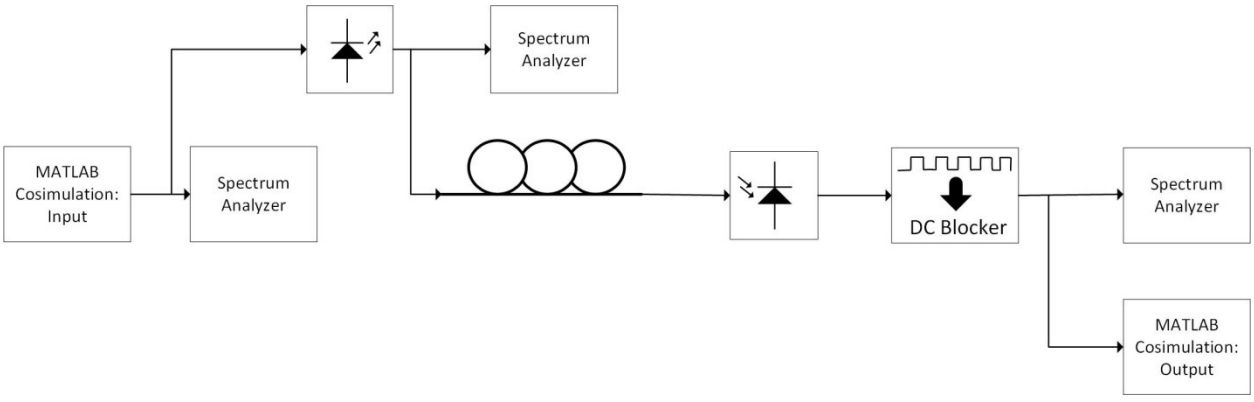

Figure 4-10: VPI RoF block diagram

In the VPIphotonics simulation environment, co-simulation blocks are implemented to run MATLAB. For the co-simulation to work, the signal prepared via MATLAB code must be packaged in a structure unit for VPI. The structure uses the following parameters in Table 4-2.

Table 4-2: Parameters for VPI Electrical Signal

Electrical Signal VPI Parameters	
Sample Rate	6 GHz
Time Grid Spacing	$\frac{1}{6 \times 10^9}$
Frequency Grid Spacing	$\frac{1}{15 \times 10^3}$
Signal Duration (in terms of grid points)	400000
Bandwidth (in terms of grid points)	400000

The electrical parameters are selected using the original signal parameters. The grid point amounts are the same size as the signal being sent from MATLAB to VPI. Specifically, the input co-simulation block opens MATLAB and runs the code to setup the RF signal for transmission. The incoming electrical signal is directly sent to the laser and becomes an optical signal. A rate equation laser is used in the model and Table 4-3 displays its main parameters.

Table 4-3: VPI Laser Parameters

Laser Rate Equation Parameters	
Emission Frequency	193.55 THz
Sample Rate	6 GHz
Power Norm	6 mW
Bias to Threshold	4
Modulation to Threshold	1.3

The sampling rate from Table 4-3 is kept the same across the entire RoF VPI setup. Power Norm is the laser's output power from a single source. The bias to threshold is the ratio of bias current to threshold current. Different ratios of bias to threshold are tested. A ratio of 4 is found to produce the best output. Finally, the modulation to threshold is the ratio of the current modulation amplitude and threshold current. The default value is implemented.

The optical signal proceeds over a standard 2 km single mode fiber (SMF). The fiber uses the pre-set values in VPI. Table 4-4 shows the parameters.

Table 4-4: VPI Fiber Parameters

Single Mode Fiber VPI Parameters	
Length	2 km
Attenuation	0.2×10^{-3} dB/m
Dispersion	17×10^{-6} s/m^2
Dispersion Slope	0.08×10^{3} s/m^3
Non-Linear Index	2.6×10^{-20} m^2/W

After the fiber, a photodiode block receives the optical signal to convert back to an electrical signal. A general PIN photodiode is applied with responsivity of 1 A/W. Next, the electrical signal goes through a DC blocker to remove the DC content. The output signal is displayed on an oscilloscope and sent back to MATLAB through a co-simulation block for recovery. Figure 4-11 a) shows an example of the signal before the laser and Figure 4-11 b) shows it after the DC blocker.

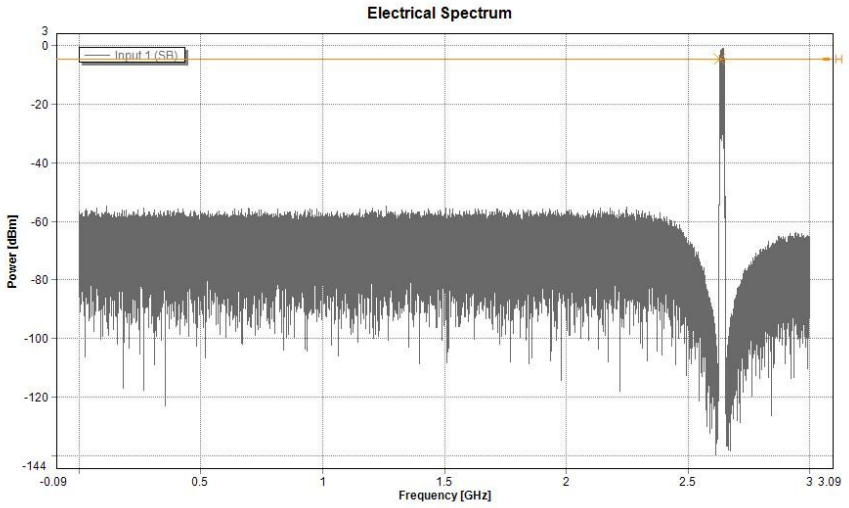

a)

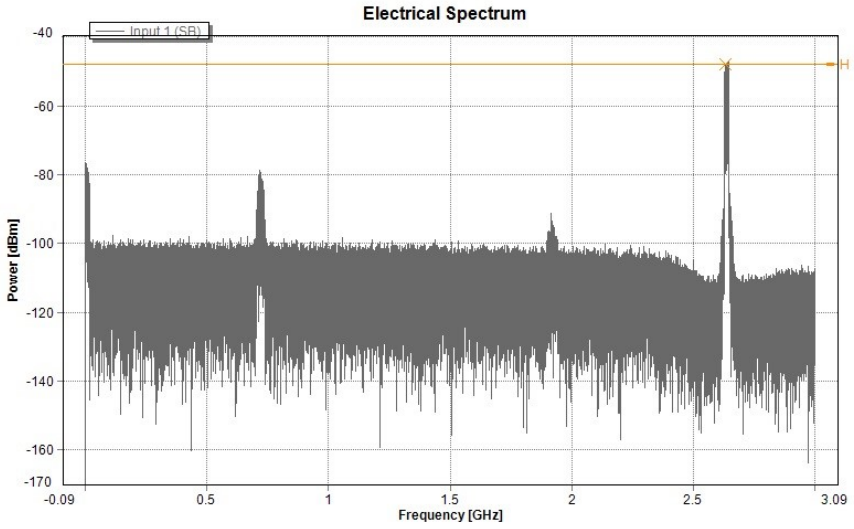

b)

Figure 4-11: a) Signal from MATLAB before laser and b) Signal after DC blocker in VPI

The signal before transmission in Figure 4-11 a) shows a clean single sided output. It matches one half of the MATLAB DSM output (Figure 4-7 b)). Although, the power is different from the two plots due to the VPI settings. After transmission, the signal suffers a considerable power loss. However, the recovery of the signal in MATLAB can accommodate the change.

Once the RF signal has returned to MATLAB, the transmitter steps are reversed. If a BP-DSM was applied, the signal is filtered based on knowing the transmitted center frequency. The received RF vector has the FFT vector extracted using the known positions from insertion. After obtaining the LTE signal, phase correction is applied. The phase correction is for fixing the rotation from the phase delay experienced.

Alternatively, for EDSM, the signal needs to be converted to its polar coordinates for recovery. The envelope is desampled from 6 GHz back to 30.72 MHz while the phase is downconverted. The phase FFT vector is filtered using the known center frequency. Once obtained, the envelope and phase are changed back to their Cartesian coordinates. The same method of phase correction is applied as the BP-DSM scenario.

Next, the recovered LTE signal undergoes OFDM demodulation using the built-in MATLAB function. The demodulator is created using the original OFDM modulator. The resulting signal is the recovered version of the 64-QAM signal. With the recovered 64-QAM

signal, the EVM is calculated. The EVM is a measure of error between the original signal and an altered version. Additionally, constellation diagrams are constructed using the two QAM signals. The diagram provides a visual representation of the constellation before and after transmission.

In the following result sections, the EVM and constellation diagrams are the main source of evaluation for the performance of the proposed setup.

4.2. Optimal Delta-Sigma Modulation Order

In order to understand the effects of the DSM order on the EDSM results, three orders of BP-DSM are simulated. The orders were 2^{nd}, 4^{th} and 6^{th}. As previously stated, as the order increases, the stability will suffer in basic scenarios. Although, with the setup of the EDSM, the input will degrades less. The fourth order BP-DSM model is presented in Chapter 3.1 and its layout is shown in Figure 3-2. The other CRFB models are designed in Simulink. Figure 4-12 shows the 2^{nd} order model implemented.

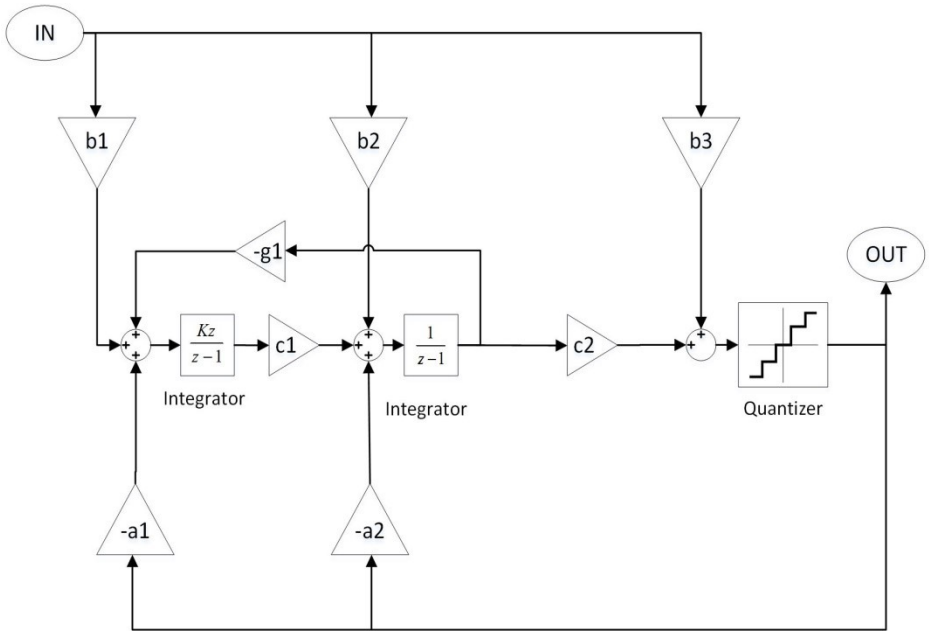

Figure 4-12: 2^{nd} order CRFB BP-DSM structure (from [12])

The second order model in Figure 4-12 is a basic BP-DSM with the coefficients determined using the MATALB DSM toolbox in the same way as the 4^{th}. Unlike the fourth, the

2^{nd} order model has one resonator built with two integrators and a feedback path. Additionally, the model contains 2 feedback loops performing the least amount of noise shaping among the tested models.

In contrast, the sixth order BP-DSM performs the most noise shaping with 6 feedback loops. Figure 4-13 shows the entire layout of the 6^{th} order model.

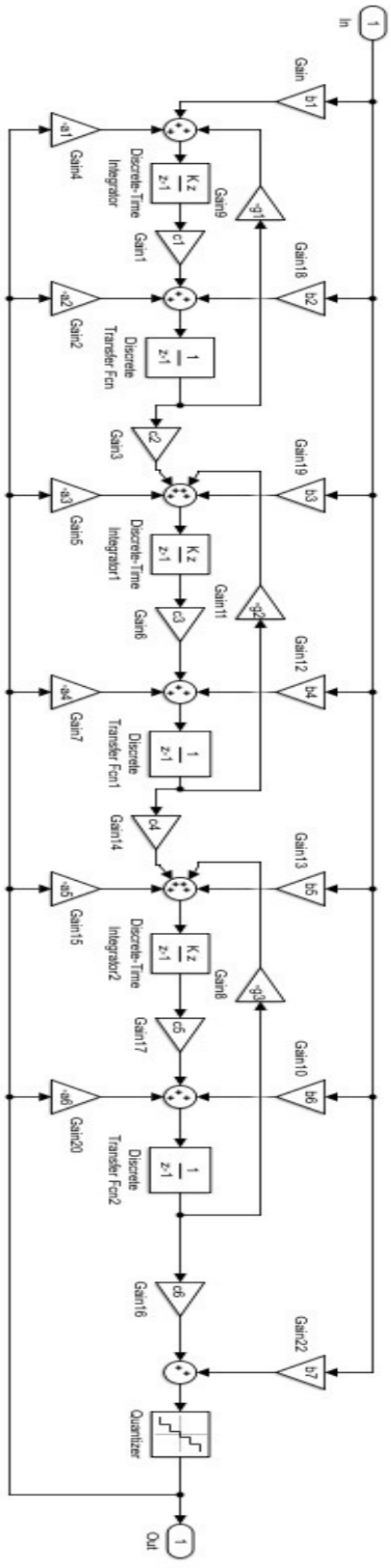

Figure 4-13: 6th order CRFB BP-DSM structure (from [12])

Like the other BP-DSM models, the coefficients for Figure 4-13 are created with the MATLAB DSM toolbox [12]. Since it is sixth order, the design contains 3 resonators where each has 2 integrators and 1 feedback loop. Despite having the most noise shaping, the 6th order model is the most susceptible to linearity issues.

The three BP-DSM models were implemented into EDSM setups and combined with the VPI schematic. Figure 4-14 shows the different BP-DSM order integration.

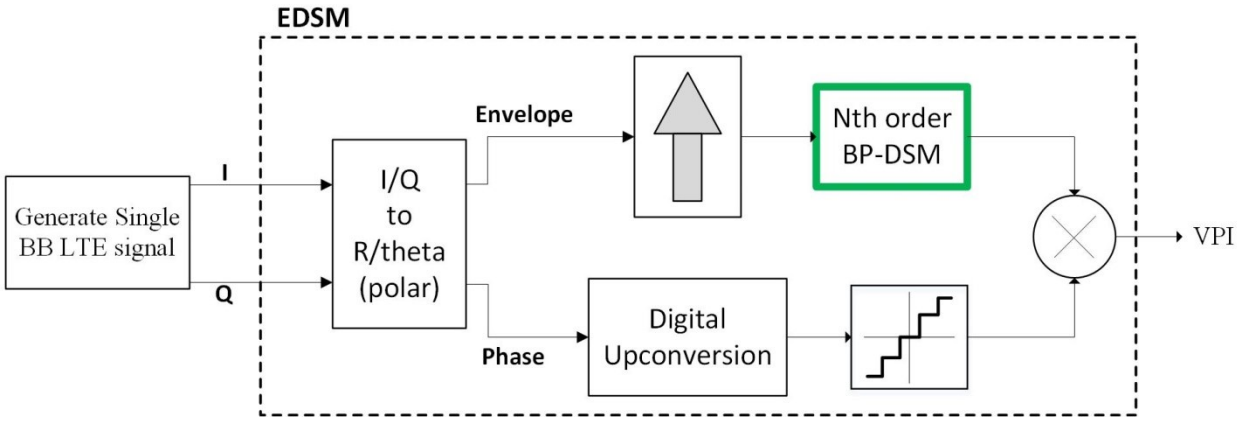

Figure 4-14: Order of EDSM test setup

The bolded green BP-DSM in Figure 4-14 represents the changing structure for the order tests. A variety of input LTE signals with 64-QAM modulation are evaluated. First, a single carrier LTE signal at 2.112 GHz is used. The EVM is measured at two points: after the EDSM and after transmission. Table 4-5 summarizes the EVMs for each order.

Table 4-5: EVM Results for 2.112 GHz LTE signal with EDSM

Order	EVM after EDSM	EVM after transmission
2	3.8791	4.0301
4	3.5543	3.5545
6	3.5353	3.6488

As the order increases, the EVM decreases except in one scenario. The change between the fourth and sixth order is very minimal after the EDSM while the change between the two after the transmission is larger and in reverse. The EVM results are illustrated using

constellation diagrams. The original 64-QAM spread is compared with the recovered QAM signal. The diagrams for the 2nd order EDSM are presented in Figure 4-15 a) and b).

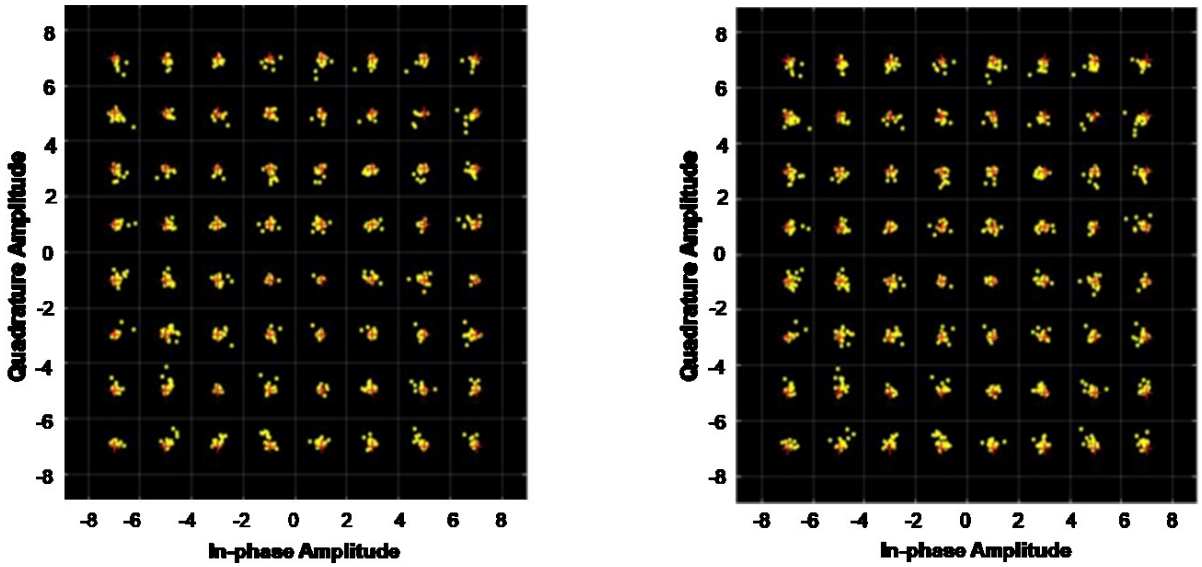

a) b)

Figure 4-15: Constellation diagram plots for 2nd order EDSM with 2.112 GHz LTE signal – a) after EDSM and b) after transmission

Examining the plots in Figure 4-15, the error change from a) to b) is subtle. According to the EVMs, the difference is 0.105%. In the fourth order plots, the change in EVM before and after the optical components is almost zero. The exact value is 0.0002%. As a result, Figure 4-16 a) and b) are almost identical.

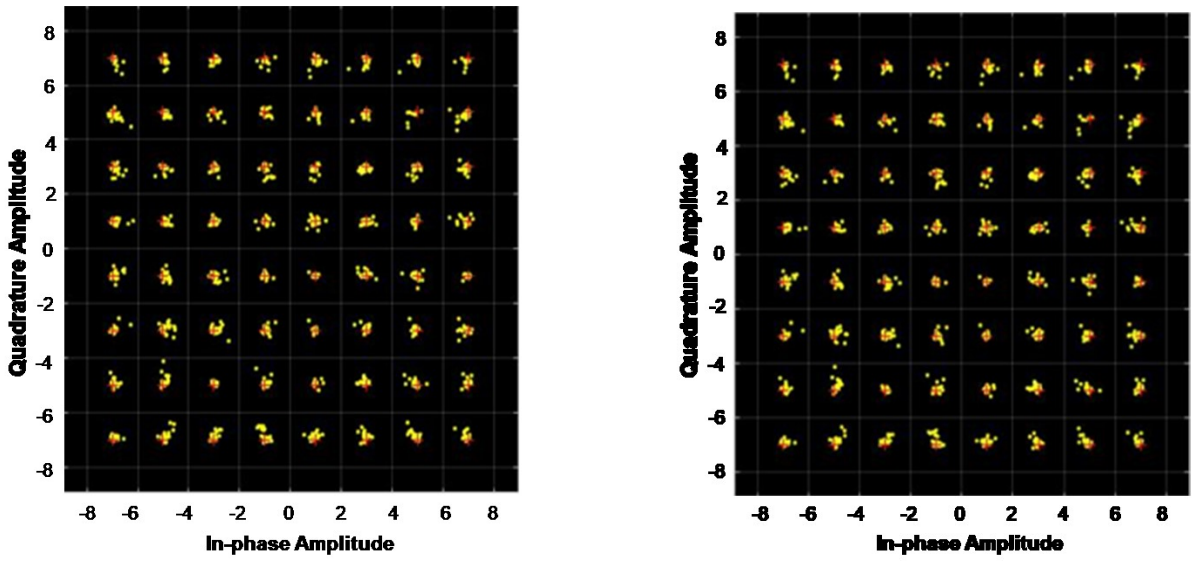

a) b)

Figure 4-16: Constellation Diagram plots for 4th order EDSM with 2.112 GHz LTE signal – a) after EDSM and b) after transmission

Despite the similar EVMs before and after transmission, a slight change should have been observed in Figure 4-16 b) due to error from the optical components. The expected pattern returns for the 6th order scenario in Figure 4-17 a) and b).

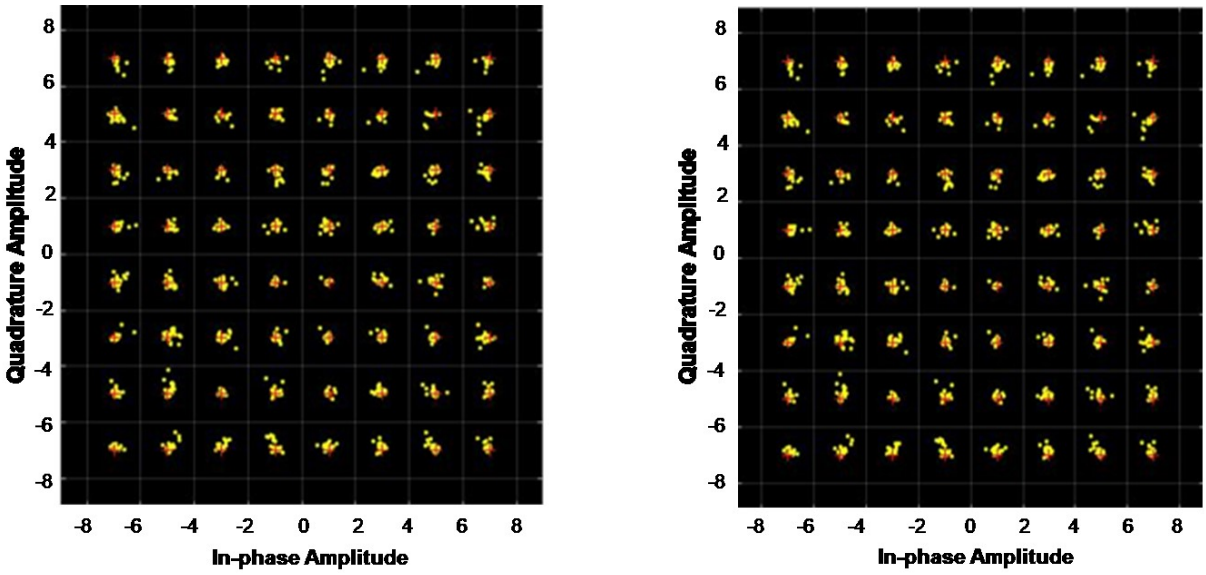

a) b)

Figure 4-17: Constellation Diagram plots for 6th order EDSM with 2.112 GHz LTE signal – a) after EDSM and b) after transmission

Compared to the 2nd and 4th order results, the 6th order plots have the least amount of error. Figure 4-17 a) has the recovered points closer to the positions of the original 64-QAM. The EVM change between Figure 4-17 a) and b) is 0.0958%.

Next, another single carrier LTE signal is used, but at 2.64 GHz. The EVM is measured at two points: after the EDSM and after the transmission. Table 4-6 summarizes the EVMs for each order.

Table 4-6: EVM Results for 2.64 GHz LTE signal with EDSM

Order	EVM after EDSM	EVM after transmission
2	4.1751	4.2907
4	3.5592	3.8824
6	3.4384	3.5014

In comparison to the single carrier 2.112 GHz signal, the EVMs for the second and fourth order EDSM are higher for the 2.64 GHz signal. For the sixth order EDSM, the EVMs of Table 4-6 are lower than the values in Table 4-5. Like the previous case, the sixth order produces the loweset EVMs at both evaluation points.

The constellation diagrams for each order observed a slight change in error. The following Figure 4-18 through Figure 4-20 display the constellation after the EDSM and after transmission. The second order EDSM constellation diagrams are observed in Figure 4-18 a) and b).

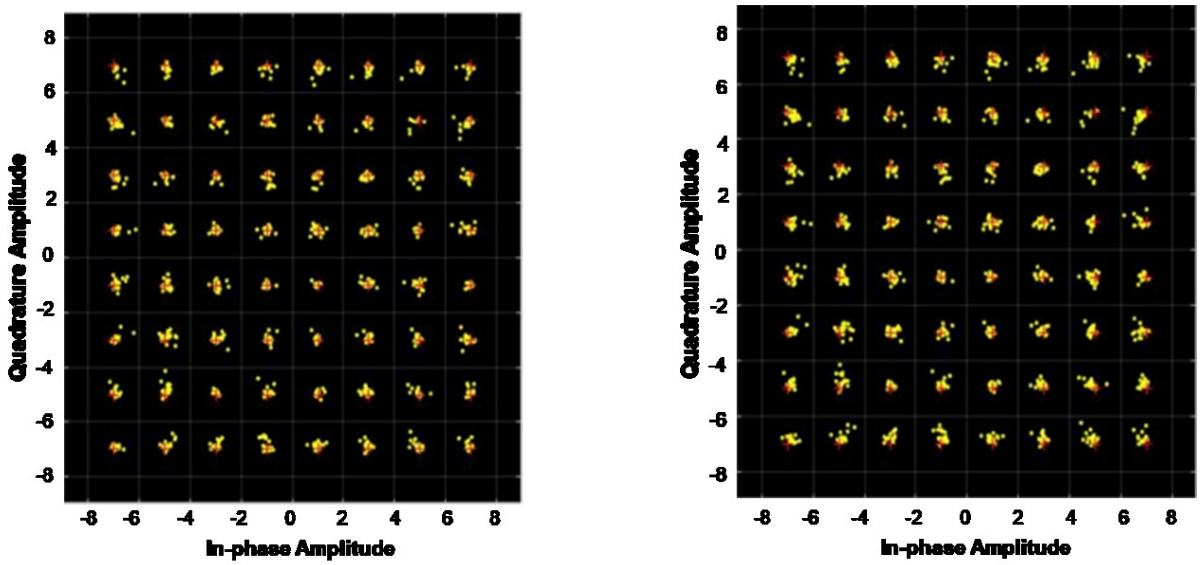

a) b)

Figure 4-18: Constellation diagram plots for 2nd order EDSM with 2.64 GHz LTE signal – a) after EDSM and b) after transmission

The difference between after the EDSM and after transmission is small. Some of the constellation points have larger distances from the main point. The exact change in error is 0.1156%. Compared to the fourth order results in Figure 4-19 for 2.64 GHz, the optical components have less impact on the signal with 2nd order EDSM.

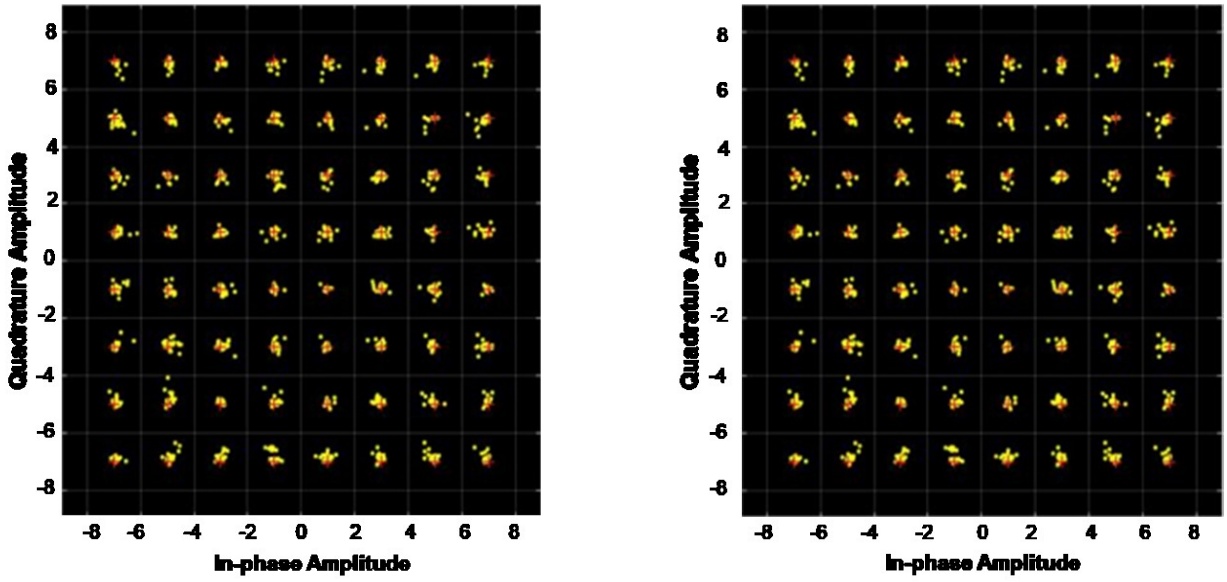

a) b)

Figure 4-19: Constellation diagram plots for 4th order EDSM with 2.64 GHz LTE signal – a) after EDSM and b) after transmission

Despite the visual similarities between Figure 4-19 a) and b), a high difference in error exists. The EVM increases 0.3232% after transmission. Despite this increase, the final EVM is still less than the second order EDSM, but higher than the sixth order EDSM. Figure 4-20 a) and b) show the improved constellation diagrams.

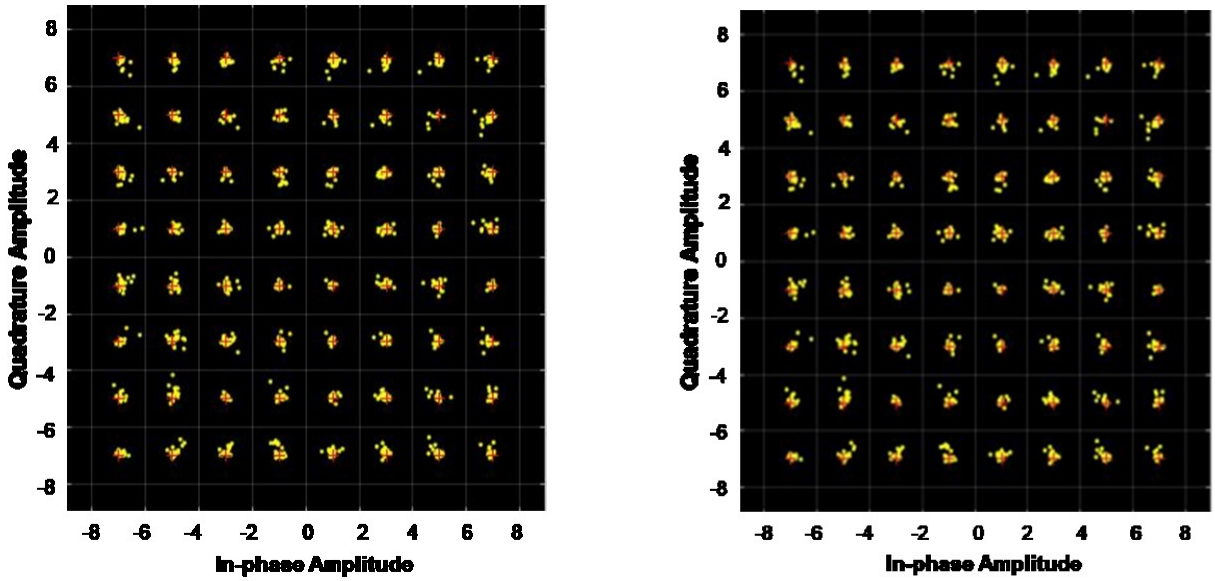

a) b)

Figure 4-20: Constellation diagram plots for 6th order EDSM with 2.64 GHz LTE signal – a) after EDSM and b) after transmission

The sixth order EDSM has very little change between Figure 4-20 a) and b). The optical transmission introduces 0.063% error keeping the two different constellation diagram outputs nearly identical.

Finally, the concurrent dual band LTE signal is tested with different ordered EDSMs. The two carrier frequencies used are 2.112 GHz and 2.64 GHz. When evaluating the dual bands, the individual frequency is examined. Similar to the other signals, the EVM is measured at two points: after the EDSM and after transmission. Table 4-7 presents the EVMs for each order and the first band, 2.112 GHz, when sent as a dual band signal.

Table 4-7: EVM Results for Dual Band LTE signal with EDSM – Band 1

	Band 1: 2.112 GHz	
Order	EVM after EDSM	EVM after transmission
2	4.5097	4.7846
4	4.3358	4.3928
6	4.233	4.2966

When evaluating the EVMs, the values rise for all orders and reading points during the dual band case. The second order EDSM has the largest susceptibility to error compared to the fourth and sixth order models. Figure 4-21 a) and b) show the constellation diagrams for EVMs of 4.5097% and 4.7846%.

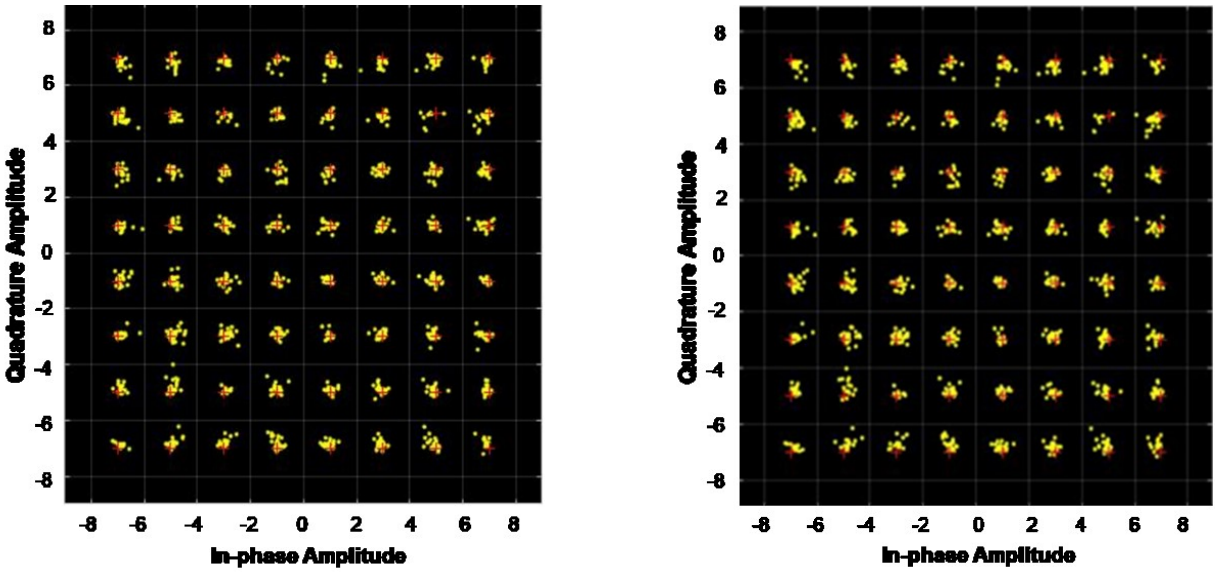

a) b)

Figure 4-21: Constellation diagram plots for 2nd order EDSM with dual carrier LTE signal: Band 1 – 2.112 GHz – a) after EDSM and b) after transmission

The recovered points in Figure 4-21 a) and b) are more scattered than the points in Figure 4-15 a) and b). This indicates the 2.112 GHz carrier frequency incurred higher amounts of distortion as a dual band rather than a single band. The same pattern is observed for Figure 4-22 a) and b).

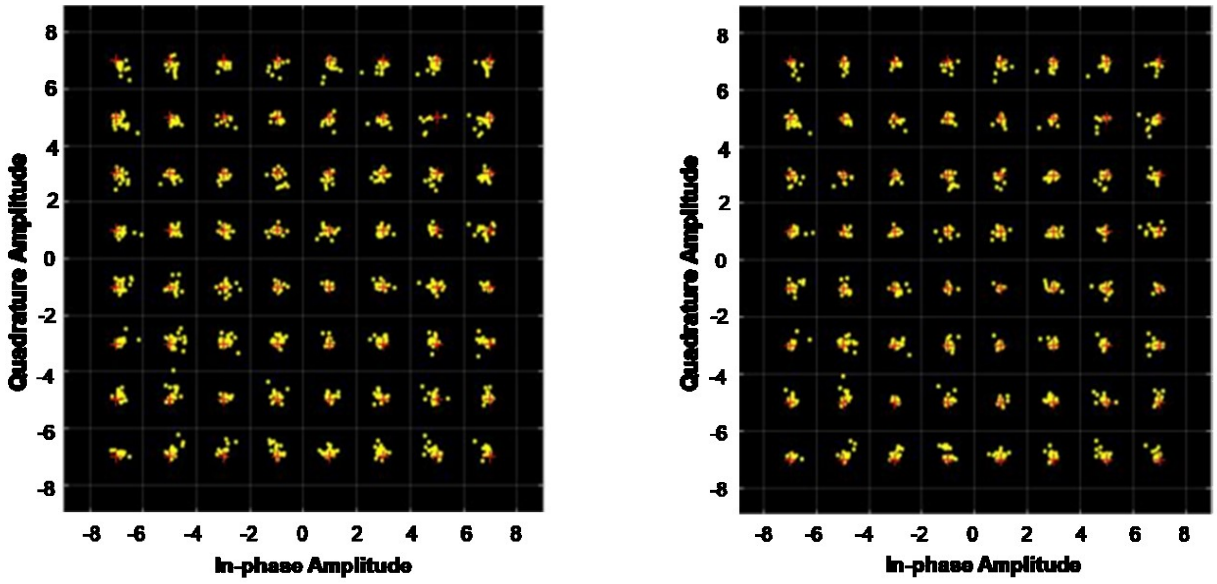

a) b)

Figure 4-22: Constellation diagram plots for 4th order EDSM with dual carrier LTE signal: Band 1 – 2.112 GHz – a) after EDSM and b) after transmission

Despite the fourth order EDSM producing lower EVMs than the second order EDSM in the dual band case for band 1, the results are still high. This is reflected in Figure 4-22 a) and b). Figure 4-22 b) in particular is has its points closer to the 64-QAM marking than Figure 4-21 b). Also, the transmission impact on the EVM is at a low of 0.057%. Still, the individual best results for this case are produced by the 6th order model. Figure 4-23 show these sixth order constellation diagrams.

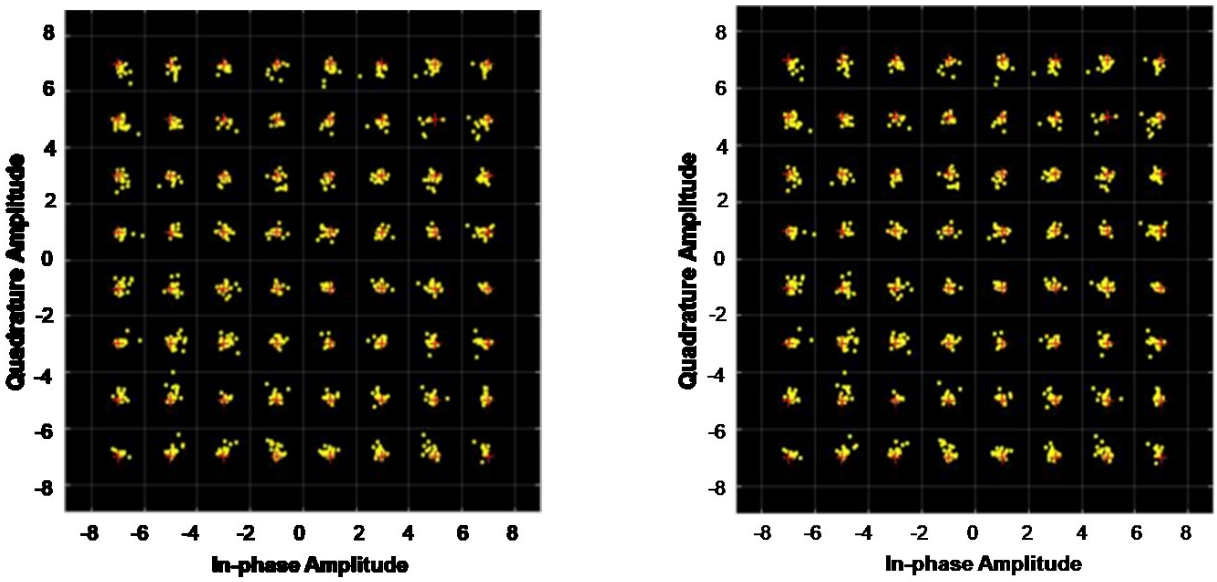

a) b)

Figure 4-23: Constellation diagram plots for 6th order EDSM with dual carrier LTE signal: Band 1 – 2.112 GHz – a) after EDSM and b) after transmission

The EVM change between Figure 4-23 a) and b) is minimal at 0.0636% making the difference between the plots difficult to visualize.

For band 2 of the dual band case, the results are identical to band 1. Table 4-8 displays the same EVM values as Table 4-7.

Table 4-8: EVM Results for Dual Band LTE signal with EDSM – Band 2

	Band 2: 2.64 GHz	
Order	EVM after EDSM	EVM after transmission
2	4.5097	4.7846
4	4.3358	4.3928
6	4.233	4.2966

With 2.64 GHz having the same outputs as 2.112 GHz, the constellation diagrams in Figure 4-24 through Figure 4-26 match the previous figures.

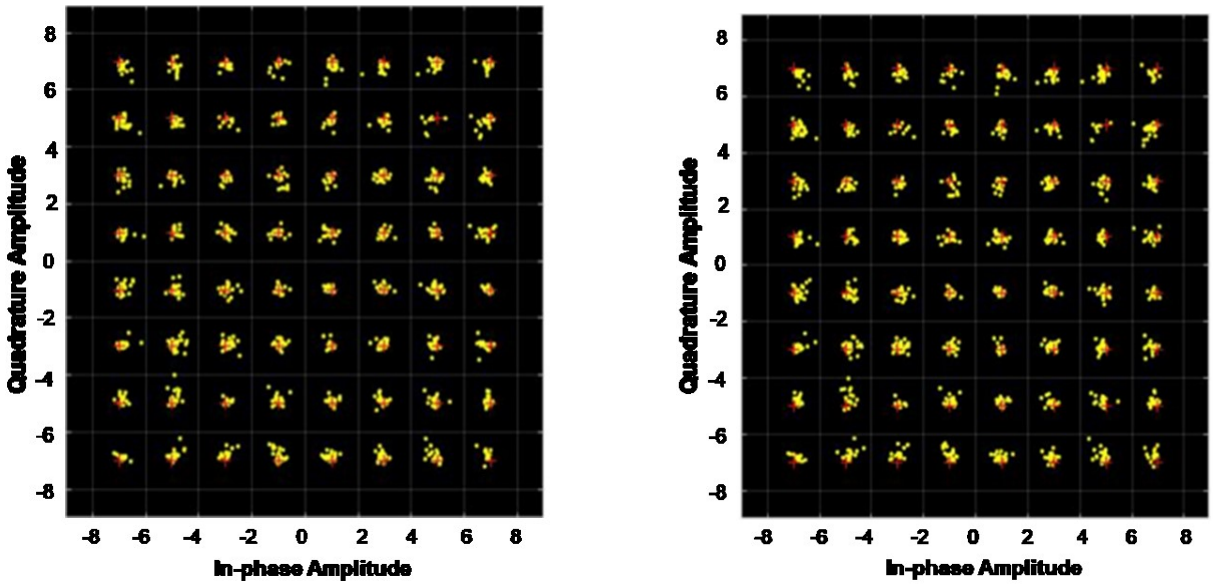

a) b)

Figure 4-24: Constellation diagram plots for 2nd order EDSM with dual carrier LTE signal: Band 2 – 2.64 GHz – a) after EDSM and b) after transmission

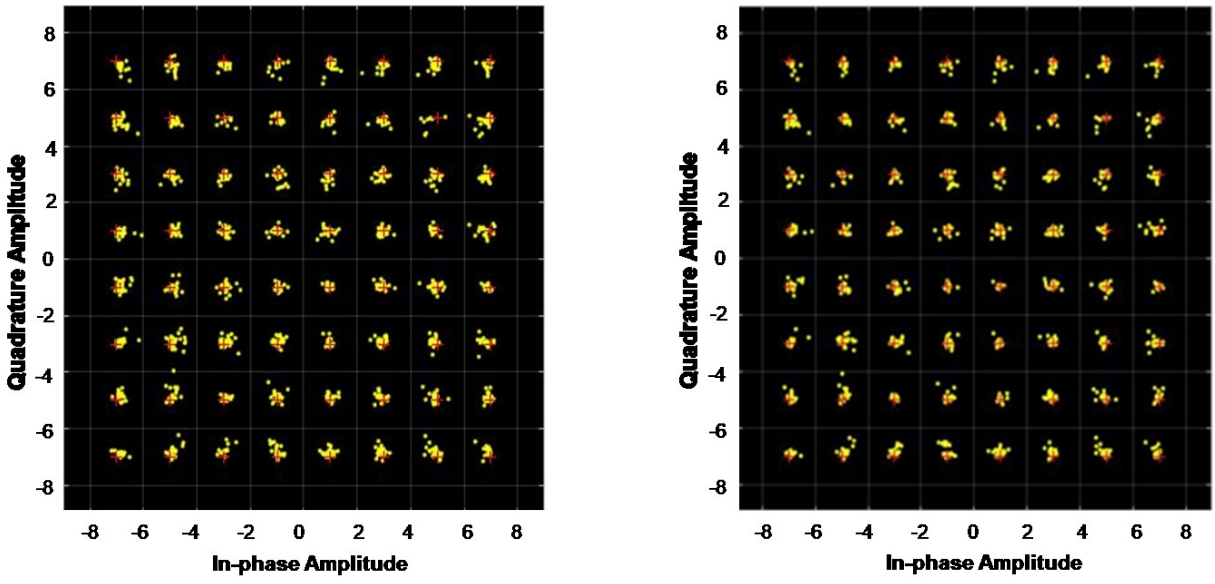

a) b)

Figure 4-25: Constellation diagram plots for 4th order EDSM with dual carrier LTE signal: Band 2 – 2.64 GHz – a) after EDSM and b) after transmission

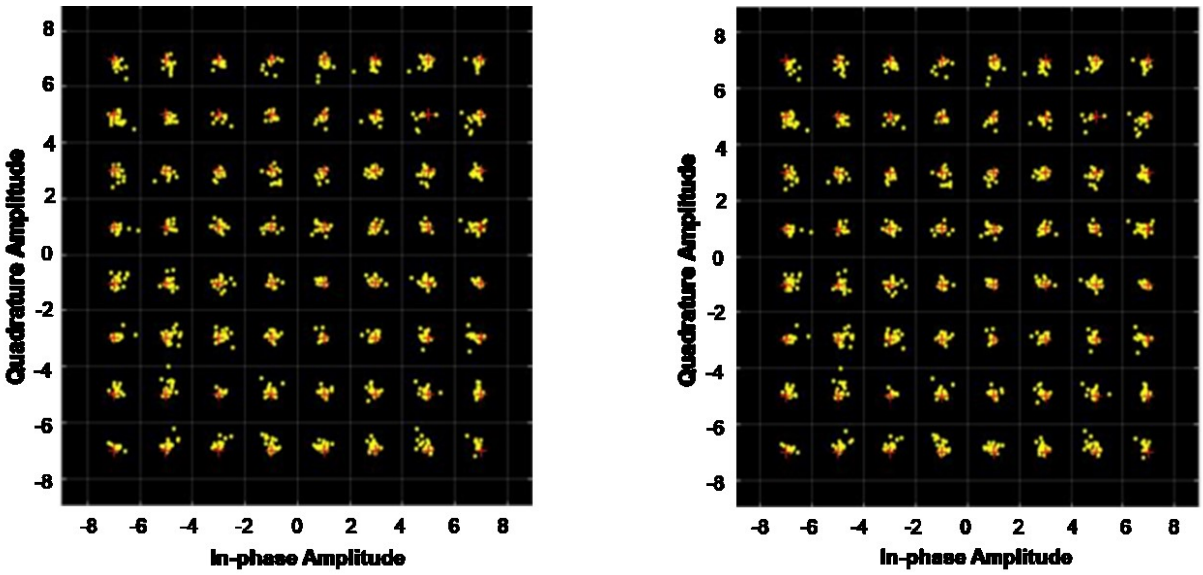

a) b)

Figure 4-26: Constellation diagram plots for 6th order EDSM with dual carrier LTE signal: Band 2 – 2.64 GHz – a) after EDSM and b) after transmission

Charting the results nicely illustrates the impact of DSM order on EVM. The graphs are shown in Figure 4-27 and Figure 4-28. Figure 4-27 compiles the first column of EVMs to demonstrate the effect of the DSM order after EDSM modulation.

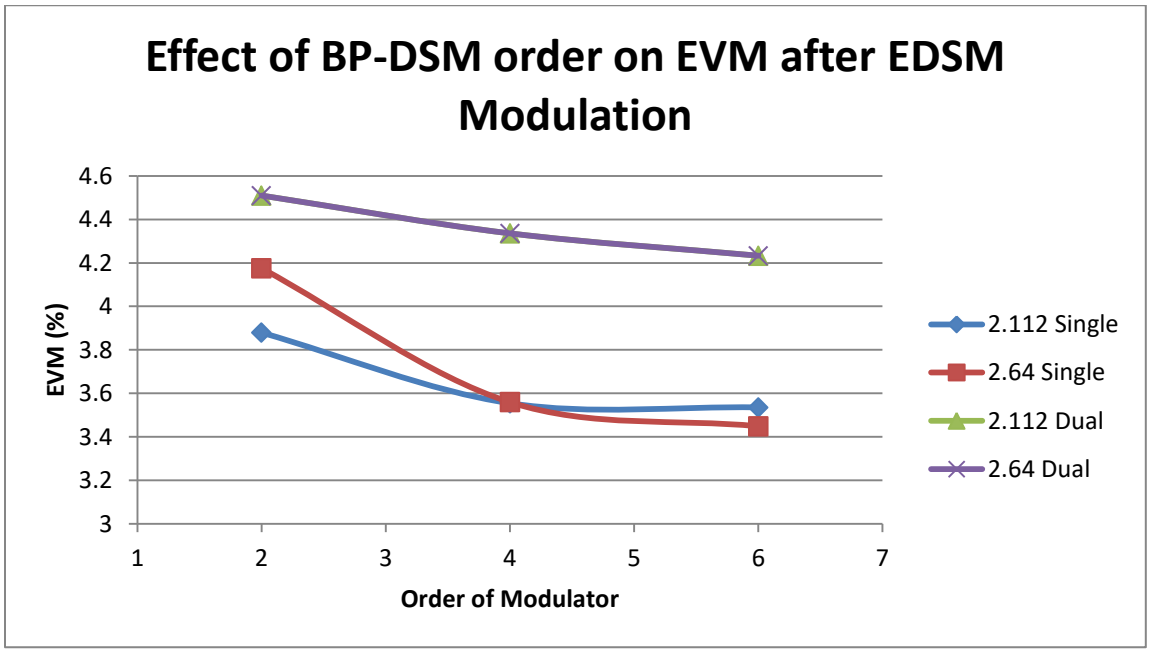

Figure 4-27: Graph of the EVMs changing as the BP-DSM of the EDSM is increased – After EDSM

As the order of the BP-DSM increases, the EVM decreases after the envelope delta-sigma modulator. The single carrier frequency signals have lower EVMs than the dual case, but follow

the same pattern. The change is more significant from orders 2 to 4 than from 4 to 6. Also, the single carrier case is more affected by the order than the dual band case. The same pattern can be observed when the optical link is included.

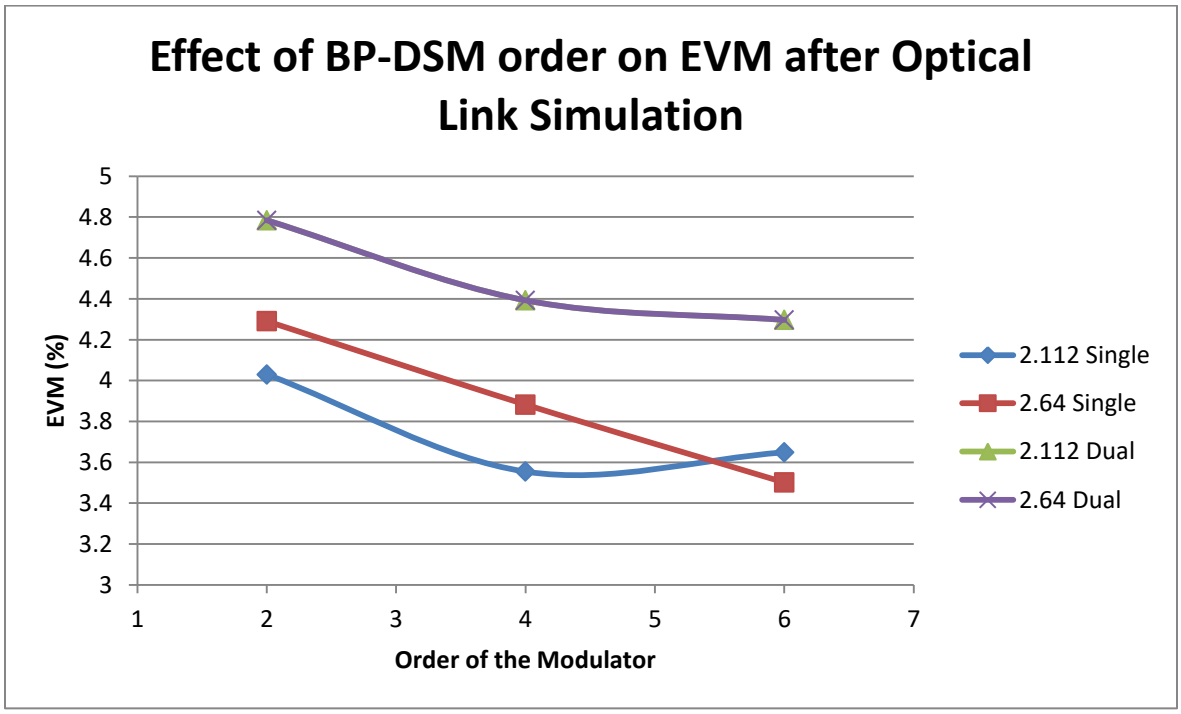

Figure 4-28: Graph of the EVMs changing as the BP-DSM of the EDSM is increased – After transmission

Figure 4-28 shows the decreasing EVM as the order increases like Figure 4-27. Here, the EVM changes between the orders are larger than in Figure 4-27. In the 2.112 GHz single carrier case, the change from 2nd to 4th order is 0.44756% while the 2.64 GHz single carrier change is 0.4083%. However, the change is not as significant from 4th to 6th order DSM. The error actually rises 0.0943% for the 2.112 GHz carrier. The 2.64 GHz carrier follows the same pattern in the 2nd to 4th order case for 4th to 6th by decreasing the error of 0.381%. As for the dual band case, the EVM lowers by 0.0962% when increasing the order from fourth to sixth. With the exception of the 2.64 GHz single carrier, all signals saw the most impact when switching from the 2nd to 4th order models. Overall, the analysis of the EVMs after the EDSM demonstrates the improvement in the EVM with a higher order than 2. Despite the 6th order model producing the best results for all scenarios except one, the 4th order BP-DSM is selected as it has lower complexity and can provide EVM improvements.

4.3. Single Carrier Bandpass Delta-Sigma Modulation Radio-over-Fiber

To compare the changes among the single and dual case and the BP-DSM versus EDSM, the single carrier BP-DSM RoF is simulated. Figure 4-29 shows the general layout.

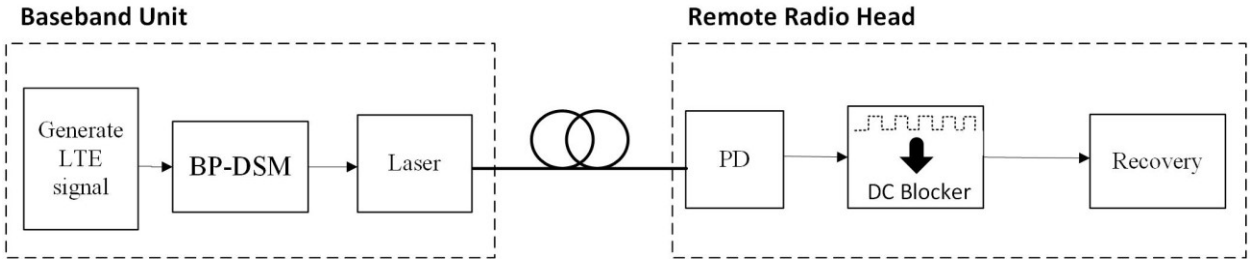

Figure 4-29: Single Carrier BP-DSM RoF Setup

First, a single carrier LTE signal is generated in MATLAB at either 2.112 GHz or 2.64 GHz using the parameters from Table 4-1. Since BP-DSM is being used, the signal is upconverted before entering the DSM. The 4^{th} order CRFB BP-DSM in Figure 3-2 modulates the signal before sending to the laser. It is centered at the specified center frequency for ideal noise shaping. The output from the DSM is a digital signal with the quantized noise shifted away from the carrier of interest. Running the VPIphotonics simulation in Figure 4-10, MATLAB is initiated to design the signal. When the signal is setup, it is sent directly to the direct feedback laser module. The laser creates an optical signal to be sent along the 2 km standard single mode fiber. At the base station, a photodiode block receives the signal and changes it back to an electrical signal. Afterwards, the signal passes through a DC blocker to negate the current. Finally, the signal returns to MATLAB for recovery as described in Chapter 4.1.

The next two sections examine the results of the 2.112 GHz signal and 2.64 GHz signal when combined with the DSM RoF. The signals are measured in terms of error vector magnitude and illustrated using constellation diagrams. For 64-QAM LTE signals, the EVM needs to be less than 8%.

4.3.1. 2.112 GHz LTE Bandpass Delta-Sigma Modulation in Radio-over-Fiber

This section evaluates the first LTE signal band, 2.112 GHz, with BP-DSM RoF. To test the DSM with the single carrier, the signal constellation diagram of the modulated signal is compared with its input. The signal is evaluated at two reading points: after the BP-DSM and after transmission. The constellation diagram for the signal after the BP-DSM is shown in Figure 4-30.

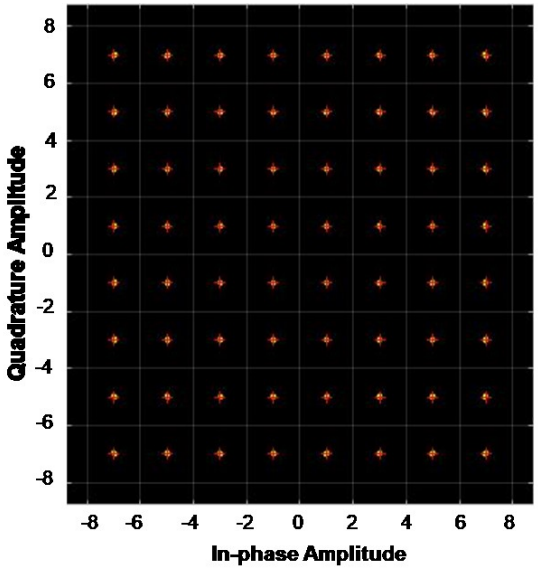

Figure 4-30: Constellation diagram of 2.112 GHz signal after BP-DSM

The constellation points for the recovered signal in yellow are almost identical to the original 64-QAM layout in red. The corresponding EVM is calculated as 0.4680%. The impact of the BP-DSM is small. After the optical link, the error only slightly increases as seen in Figure 4-31.

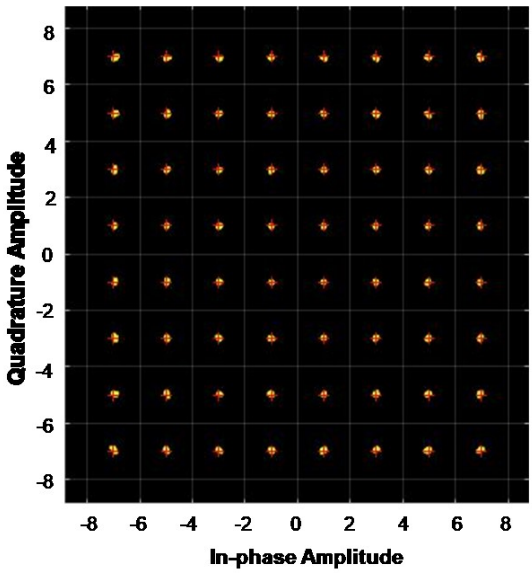

Figure 4-31: Constellation diagram of 2.112 GHz signal after transmission

The yellow points of Figure 4-31 are more than in Figure 4-30. The corresponding EVM is 1.0171% indicating the error rose 0.5491% from the optical components. Since the error is lower than 8%, the signal setup satisfies the LTE conditions.

4.3.2. 2.64 GHz LTE Bandpass Delta-Sigma Modulation in Radio-over-Fiber

This section evaluates second band, 2.64 GHz, with BP-DSM RoF. The BP-DSM in this case is centered for 2.64 GHz. Similar to the Chapter 4.3.1, the signal constellation diagram of the modulated signal is compared with its input at the two evaluation marks. Figure 4-32 illustrates the constellation diagram after the BP-DSM.

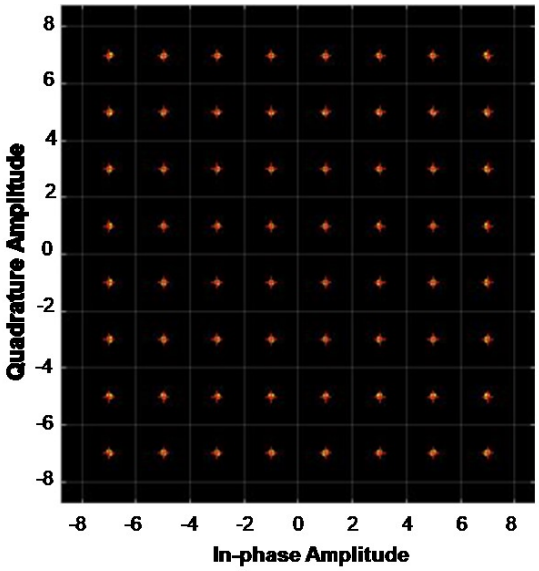

Figure 4-32: Constellation diagram of 2.64 GHz signal after BP-DSM

The recovered constellation for the 2.64 GHz signal nearly matches the original. The EVM is calculated as 0.4680% like the previous signal. However, the optical link has slightly a larger impact with the second band. Figure 4-33 shows the constellation diagram for after transmission.

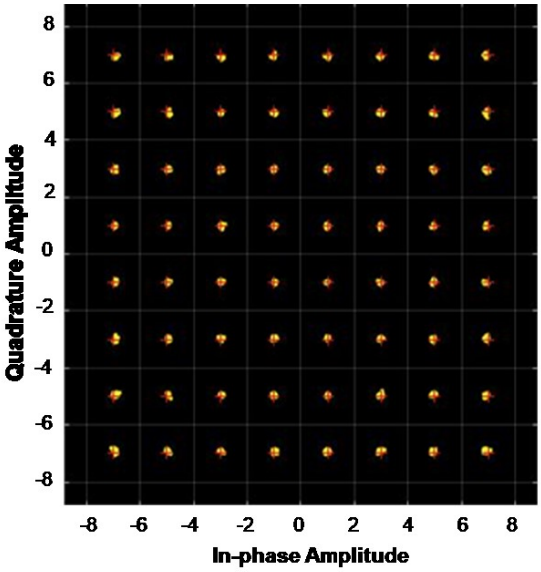

Figure 4-33: Constellation diagram of 2.64 GHz signal after transmission

Figure 4-33 has more defined yellow error points than Figure 4-32. The corresponding EVM is 1.4583%. The EVM increases 0.9903% after the BP-DSM, but it still keeps well below the LTE standard.

4.4. Dual Carrier Bandpass Delta-Sigma Modulation in Radio-over-Fiber

In this part, the two bands, 2.112 GHz and 2.64 GHz, are combined into a concurrent setup. Figure 4-34 displays the dual carrier BP-DSM RoF layout.

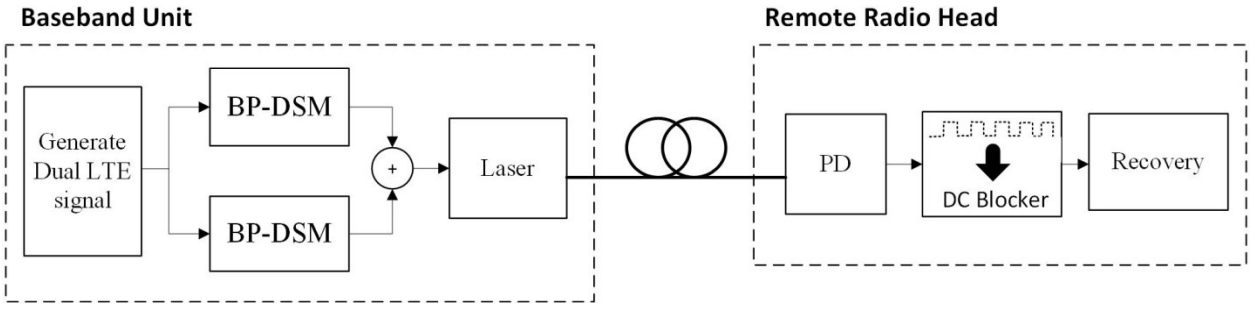

Figure 4-34: Dual Carrier BP-DSM RoF Setup

In the dual band setup, two BP-DSMs are employed in parallel for each carrier. The signal is designed by first creating each individual band. The steps are highlighted in Chapter 4.1. Once each signal is built, it passes through the corresponding BP delta-sigma modulator. The same BP-DSMs are implemented for the single carrier cases in Chapter 4.3. The signal becomes a digital output with noise shaping from the DSM. Afterwards, the two modulated signals are added together to create the concurrent LTE signal.

To simulate the RoF portion of Figure 4-34, VPIphotonics is implemented. The same schematic in Figure 4-10 is applied. Here, the MATLAB code is initiated from the VPI environment and VPI uses the output from MATLAB as the incoming signal. The signal directly modulates the laser and becomes an optical signal. It travels 2 km along a standard mode fiber before being received by a photodiode. Afterwards, a DC blocker removes the current from the signal. Finally, the recovery is performed in MATLAB to examine the state of the transmitted signal.

For evaluation, the signal constellation diagram of the modulated signal is compared with its input. The constellation diagrams for each band after the BP-DSM are shown Figure 4-35.

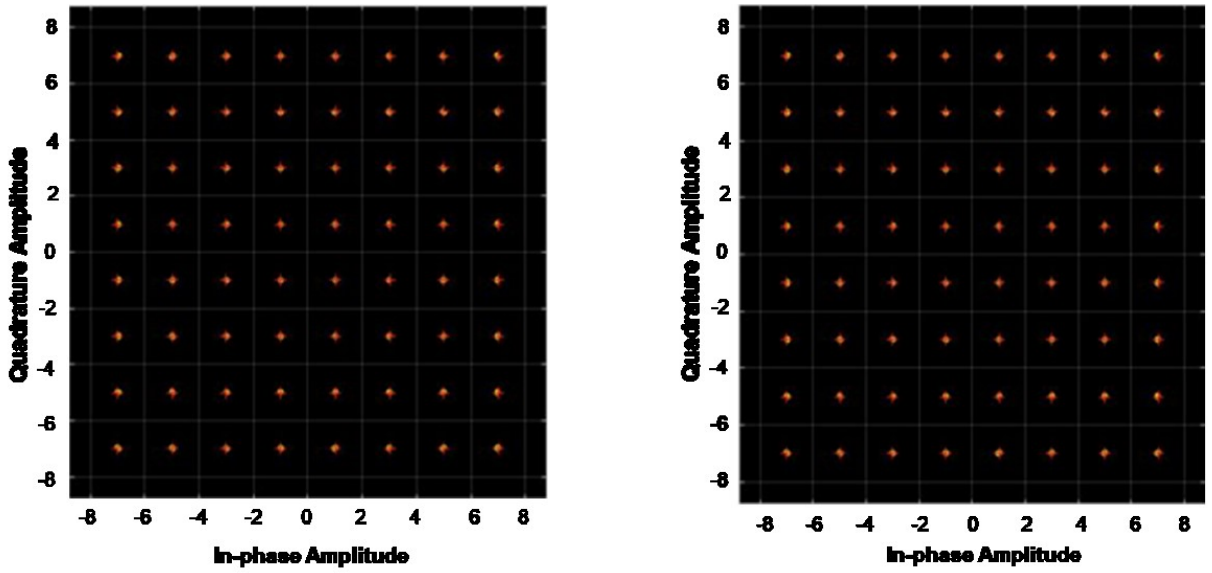

a) b)

Figure 4-35: Constellation diagram of a) 2.112 and b) 2.64 GHz signals after BP-DSM

The recovered constellation after the BP-DSM has low error for each band. The EVMs calculated are a) 0.5146% and b) 0.4563%. As a concurrent signal, the EVM after the BP-DSM for 2.112 GHz is higher than when as single carrier. Yet, when the 2.64 GHz carrier is sent in a dual band setup, the EVM after the BP-DSM is lower. After the optical link, the error increases much more than the single band case. Figure 4-36 shows the constellation outputs for the dual band case.

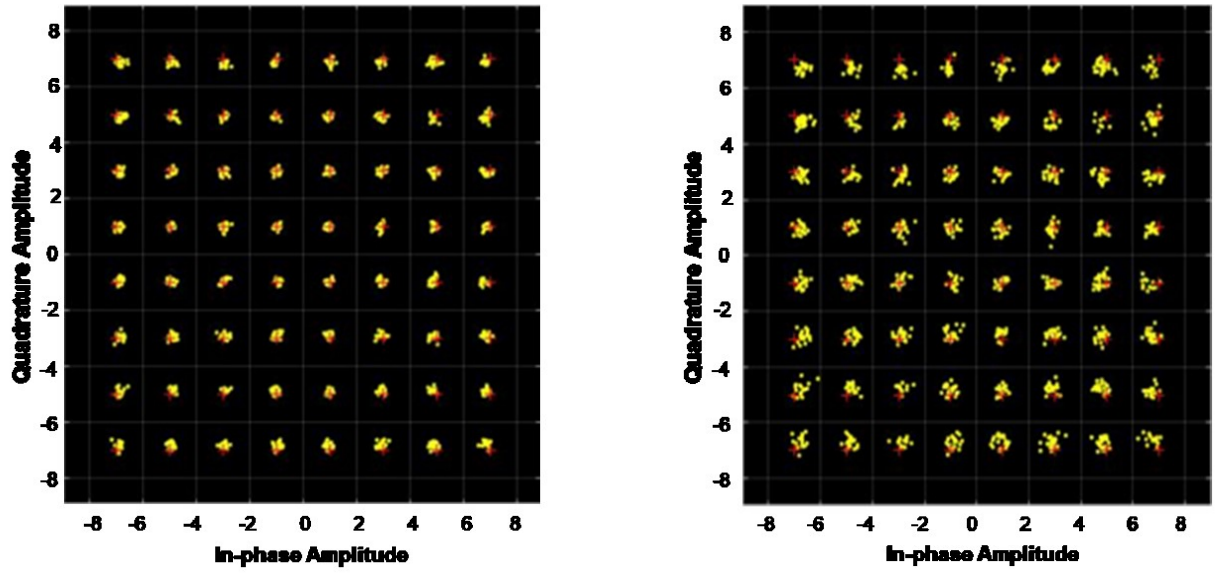

a) b)

Figure 4-36: Constellation diagram of a) 2.112 and b) 2.64 GHz signals after transmission

The error in the constellation diagrams is well defined in Figure 4-36 a) and b). For the first band, 2.112 GHz, the EVM rises to 3.0404% and for the second band, 2.64 GHz, it rises 5.3965%. The high degradation of the second band is likely from alignment issues and timing jitter. The error change is very significant compared to the signal band case. It rises 2.5258% for band 1 and 4.9402% for band 2. Despite being high values, the EVMs satisfy the LTE requirement for 64-QAM LTE signals.

4.5. Single Carrier Envelope Delta-Sigma Modulation in Radio-over-Fiber

In contrast to setups in Chapter 4.3 and 4.4, envelope delta-sigma modulation is used in place of BP-DSM for the simulation. Specifically, this section examines the single carrier LTE signals with EDSM RoF. Figure 4-36 shows a block diagram of the implemented setup.

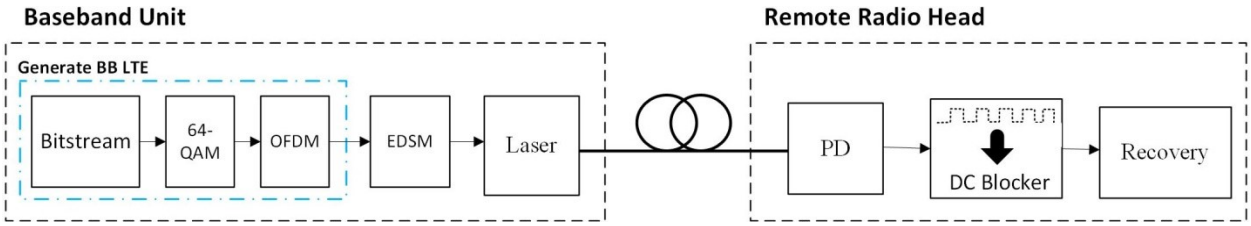

Figure 4-37: Block diagram of Single Carrier EDSM RoF

As discussed in Chapter 4.1, the baseband LTE signal is generated first for EDSM. In MATLAB, the bitstream is generated using the stages of Figure 4-2 and the parameters in Table 4-1. Once generated, the signal is converted to its polar coordinates to follow the Figure 3-5 block diagram in Chapter 3.2. The envelope is upsampled to match the digital upconversion of the phase. Next, it travels through the 4^{th} order BP-DSM in Figure 3-2 for noise shaping specified at the carrier frequency. Meanwhile, the phase undergoes digital upconversion as explained in Figure 4-3 to Figure 4-5. After the vector is designed, the phase signal is quantized to values of 1 and -1. The two parts are multiplied together to create an RF LTE signal.

Like the previous test cases, VPIphotonics controls the RoF portion of the setup. The output of the EDSM is obtained by the co-simulation module in MATLAB running the

corresponding code and extracting the final output. The RF EDSM LTE signal directly modulates the laser instance which produces an optical signal. This signal travels along the 2 km single mode fiber to a photodiode where the signal reverts back to an electrical signal. The recovered electrical signal passes through a DC blocker module before returning to MATLAB for recovery and evaluation.

The following two subsections discuss the results of single carrier signals with EDSM RoF. Two carriers are evaluated: 2.112 GHz from LTE band 1 and 2.64 GHz from LTE band 7. Error vector magnitudes are used to measure the signals at two stages. First, the signal after the EDSM is compared with the original and afterwards, the signal after transmission is compared. Constellation diagrams for each stage are also presented. Like the DSM cases, the EVM must be below 8%.

4.5.1. 2.112 GHz LTE Envelope Delta-Sigma Modulation in Radio-over-Fiber

The first scenario evaluates how a single carrier, 2.112 GHz, signal functions with an EDSM RoF. To test the functionality of the EDSM, the signal constellation diagram of the modulated signal is compared with its input. The signal is measured at two points: after the EDSM and after transmission. Figure 4-38 shows the constellation diagram of the signal after the EDSM.

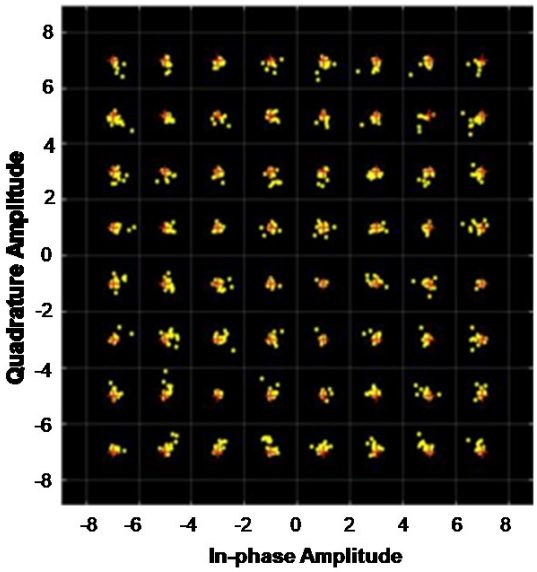

Figure 4-38: Constellation diagram of 2.112 GHz signal after the EDSM

Unlike the constellation diagrams after the BP-DSM, the recovered constellation in Figure 4-38 depicts more defined error. The corresponding EVM is calculated as 3.5543 %. This is over 3% more compared to the BP-DSM test in Chapter 4.3.1. After the optical link, the error only slightly increases as seen in Figure 4-39.

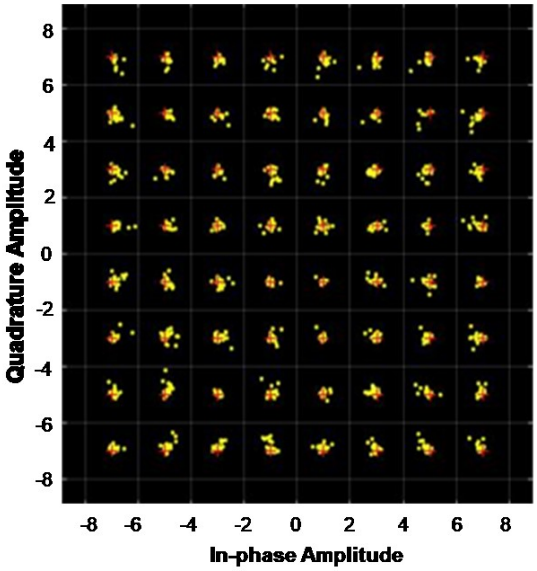

Figure 4-39: Constellation diagram of 2.112 GHz signal after transmission

Figure 4-39 is not much different from Figure 4-38. The optical components do not have the same impact as the previous signal setups. The corresponding EVM for the recovery after

transmission is 3.5545%. The change between the two EVMs is 0.0002%. Despite being higher, the EVM still is below the LTE cut-off of 8%.

4.5.2. 2.64 GHz LTE Envelope Delta-Sigma Modulation in Radio-over-Fiber

The second case evaluates how a single carrier, 2.64 GHz, signal works with EDSM RoF. The functionality of the setup is assessed by comparing the constellation diagram of the modulated signal with its input. The signal is examined after the EDSM and after transmission. Figure 4-40 provides the constellation diagram of the signal after the EDSM.

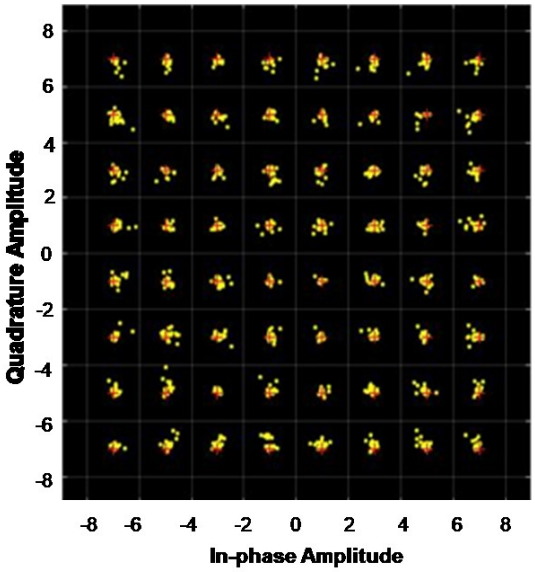

Figure 4-40: Constellation diagram of 2.64 GHz signal after EDSM

Similar to the previous single carrier case, the scattering of the modulated signal's constellation is visually apparent in Figure 4-40. Using the recovered signal, the EVM is determined as 3.5592%. The error is slightly higher than the 2.112 GHz signal. After the optical link, the error increases a little more than the previous case. The corresponding constellation diagram can be seen in Figure 4-41.

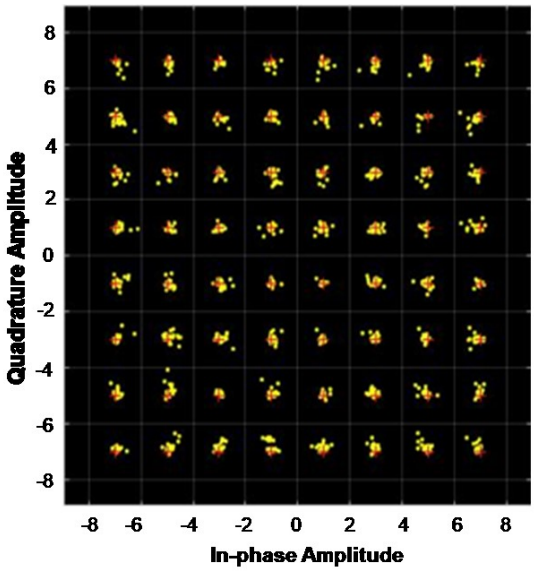

Figure 4-41: Constellation diagram of 2.64 GHz signal after transmission

The difference between Figure 4-40 and Figure 4-41 is difficult to identify. Comparing the two figures, the recovered constellation in Figure 4-41 has nearly identical positioning. Nevertheless, the corresponding EVM is 3.8824% indicating a change of 0.3232%. The 2.64 GHz carrier suffers more from the Radio-over-Fiber parts than the 2.112 GHz carrier. Yet, it still has better resistance to the optical link than single carrier BP-DSM RoF where the EVM increased 0.9903%. The final EVM meets the 8% cut-off.

4.6. Dual Carrier Envelope Delta-Sigma Modulation in Radio-over-Fiber

The final simulation evaluation is testing dual bands of the previously used signal carriers. 2.112 GHz and 2.64 GHz are combined into a concurrent signal after individual EDSM processing. Figure 4-42 shows the block diagram of the dual carrier EDSM RoF.

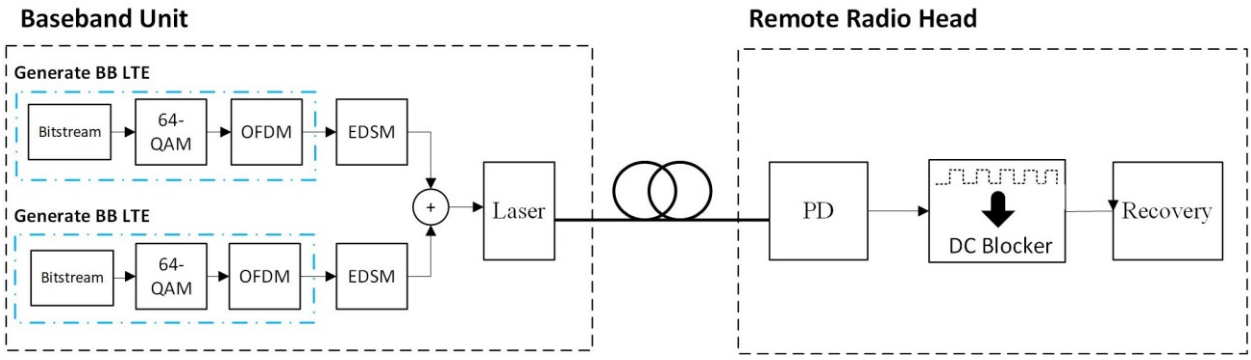

Figure 4-42: Dual Carrier EDSM RoF block diagram

The dual band EDSM setup is an extension of Figure 4-37. An extra BB LTE generation path is included in the setup for the second carrier. The same steps in Chapter 4.5 are used except for the addition of the two signals before directly modulated the laser. The RoF path from the laser to the recovery is identical to Chapter 4.5, but now with dual carriers.

Measuring the EVM of the recovered signal after the EDSM and after transmission provides an overall evaluation of the performance of the setup. The two carriers following inter-band CA are 2.112 GHz and 2.64 GHz. Figure 4-43 provides the constellation diagram for both carriers after the EDSM.

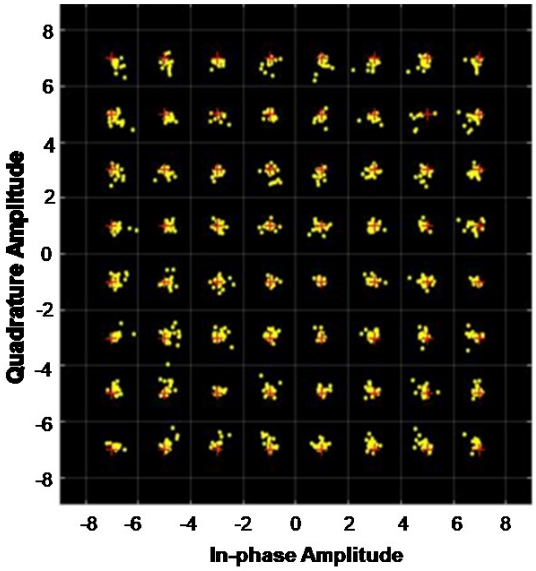

Figure 4-43: Constellation diagram of the 2.112GHz and 2.64 GHz signal after EDSM

The yellow points are spread out from the main 64-QAM (red) in Figure 4-43. The EVM for each carrier after the EDSM is the same at 4.3358%. This EVM is the highest value among

all the simulated results. Fortunately, like the other EDSM cases, the error only slightly increases after the optical link as seen in Figure 4-44.

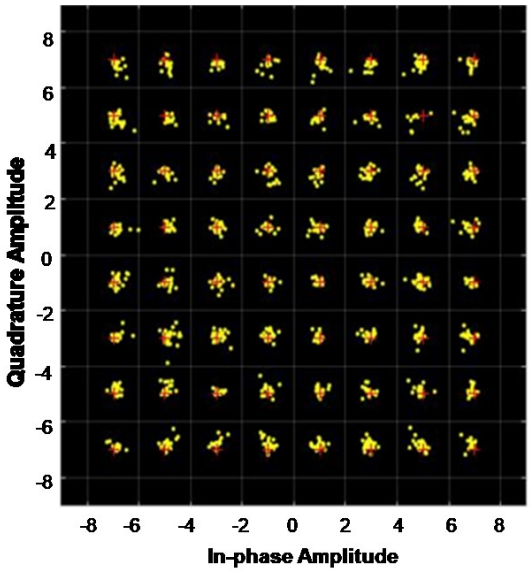

Figure 4-44: Constellation diagram of the 2.112GHz and 2.64 GHz signal after transmission

The constellation for the recovered signal in Figure 4-44 does not change much from Figure 4-43. The EVM for both bands after transmission is calculated as 4.3928%. The difference between the two checkpoints is 0.057%. This value is much lower than the 2-4% change observed in Chapter 4.4 with dual carrier BP-DSM RoF. The 2.112 GHz carrier in the dual carrier BP-DSM has a lower EVM than the EDSM scenario after transmission. Conversely, the 2.64 GHz carrier has a higher EVM than the EDSM setup after transmission. Overall, the dual band EDSM RoF provides more resistance to the inclusion of the optical link than dual band BP-DSM RoF.

4.7. Observations

Based on the simulated results, the EVM values satisfy the LTE requirement of less than 8% for 64-QAM with 20 MHz BW. Nonetheless, some perform better than others. When looking at the error after the modulation, the BP-DSM has better EVMs than the EDSM setup. Table 4-9 shows the comparisons of the EVMs after the delta-sigma modulation.

Table 4-9: Summary of EVMs measured after BP-DSM or EDSM

Type of Signal	After BP-DSM	After EDSM
2.112 GHz LTE signal	0.4680%	3.5543 %
2.64 GHz LTE signal	0.4680%	3.5592%
Dual band LTE Signal: Band 1 – 2.112 GHz	0.5146%	4.3358%
Dual band LTE Signal: Band 2 – 2.64 GHz	0.4563%	4.3358%

The EDSM adds considerable error to the signal for all signals simulated. When examining the transmitter side only, the BP-DSM outperforms the EDSM setup in terms of EVM. However, it does not take into account the other benefits the EDSM setup brings.

After the optical link or RoF addition, the performance results become more complicated. In the single carrier cases, the BP-DSM outperforms the EDSM with EVMs. In the dual band case, the EDSM setup responds better than the standalone BP-DSM for transmission. The results are summarized in Table 4-10.

Table 4-10: Summary of EVMs measured after transmission

Type of Signal	With BP-DSM	With EDSM
2.112 GHz LTE signal	1.0171%	3.5545%
2.64 GHz LTE signal	1.4583%	3.8824%
Dual band LTE Signal: Band 1 – 2.112 GHz	3.0404%	4.3928%
Dual band LTE Signal: Band 2 – 2.64 GHz	5.3965%	4.3928%

At first glance, the signals in Table 4-10 generally produce lower EVMs with a standalone BP-DSM than EDSM. Yet, it is important to note the influence of the RoF components on the EVM after the DSM. In the standalone BP-DSM dual band case, the error rises to 3.04% and 5.39% for band 1 and band 2, respectively. Band 2 suffers more due to alignment problems. In the EDSM dual band case, the EVM only increases from 4.3358% to 4.3928%. This corresponds to a change of 0.057% instead of 2.5% and 4.8%. This is a significant addition of error from transmission. Also, the single band cases for BP-DSM have larger changes in EVM over their EDSM counterparts. For the BP-DSM, the 2.112 GHz carrier EVM increases by 0.5491% and the 2.64 GHz carrier rises by 0.9903%. Contrarily, for the EDSM, the 2.112 GHz carrier EVM increases 0.0002% and the 2.64 GHz carrier EVM increases

0.3232%. The higher 2.64 GHz EVM may be from the use of a higher frequency. In general, the adaptation of the EDSM in the simulations provides stronger resistance against the RoF elements and produces more stable results for the dual band case.

4.7.1. Fiber Length Impact

In the MATLAB and VPI simulations, it is found that altering the fiber length in the VPI module led to an increased error vector magnitude (EVM) in all scenarios. This is due to the dispersion parameters set for a standard single mode fiber. In addition, the nonlinear index parameter of the fiber played a minor role. The values are summarized in Table 4-4. By turning on and off these parameters, the EVM would either increase or stay the same based on the distance.

To test the impact of the dispersion parameters and nonlinear index, a single band LTE signal with BP-DSM RoF is used. The setup and parameters discussed in Chapter 4.1 are kept for the testing. The variables adjusted are the dispersion (D) and nonlinear index (NL) values. The dispersion is either zero or its pre-set value. The nonlinear index follows the same options. This produces four different cases: dispersion and nonlinear index at zero, dispersion and nonlinear index with original parameters, dispersion equal to zero and nonlinear index at pre-set and dispersion at pre-set and nonlinear equal to zero. Table 4-11 summarizes the EVM outcomes for each scenario at a variety of fiber distances.

Table 4-11: Dispersion (D) and Nonlinear (NL) Effects on EVM with varying fiber distances

	EVM (%)			
Distance	D = 0 NL = 0	D, NL – pre-set	D = 0, NL pre-set	D pre-set, NL = 0
2 km	0.945	1.4583	0.945	1.4502
6 km	0.9455	3.3958	0.9455	3.326
10 km	0.946	5.4714	0.946	5.2992
15 km	0.9467	8.0884	0.9467	7.7574
20 km	0.9476	10.6387	0.9476	10.1356
25 km	0.9485	13.0668	0.9485	12.3916

The EVMs in Table 4-11 are measured after transmission for a 2.64 GHz LTE signal. When the dispersion and nonlinear index are zero, the fiber distance has minimal impact on the EVM. Conversely, when both parameters have their given values, the EVM rises significantly for larger distances. When the dispersion is zero, but the nonlinear index has a value, the effects on the EVM are tiny. Alternatively, when the dispersion is on and the nonlinear index is zero, the EVMs rise as the fiber distance increases. The EVMs are slightly lower for this case than when both D and NL are set, but the change is not as significant. These patterns can be observed in Figure 4-45. Note: ON in Figure 4-45 refers to the parameter having its pre-set value.

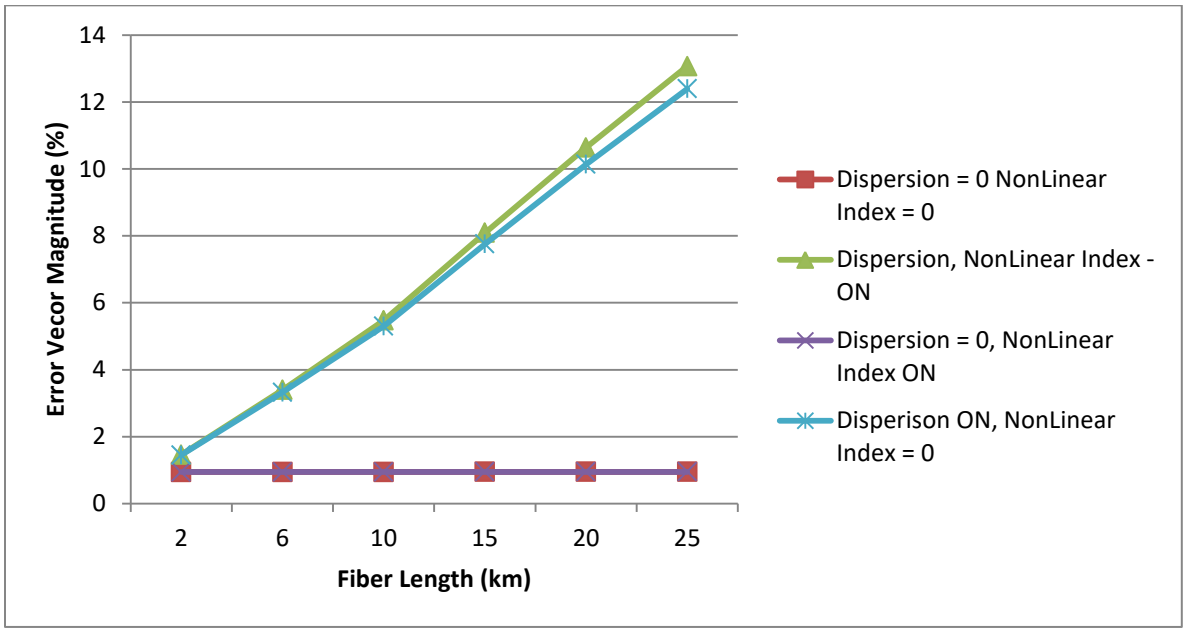

Figure 4-45: Simulated results of the effects of fiber dispersion on EVM

Using the graph in Figure 4-45, it is evident that the dispersion parameters have a strong impact. The EVM discrepancies observed are significant when the fiber length increases. The dispersion has the most effect on the EVM while the nonlinear index does not show much impact on the EVM as the distance increased. As a consequence, after interpreting the data, in order for dispersion to have less of an effect, the fiber length is kept to 2 km for both simulation and experimentation.

4.7.2. Analysis of Fiber Properties

Additional simulations are conducted to understand the impact of fiber properties on the change of EVM due to RoF transmission. Four cases are examined: attenuation only, attenuation and group velocity dispersion (GVD), attenuation and the Kerr effect, and attenuation, GVD and Kerr effect. The analysis is performed for all the discussed signals. The bands 2.112 GHz and 2.64 GHz are studied.

First, the BP-DSM signals are evaluated with the four cases. Figure 4-46 to Figure 4-49 depict the results.

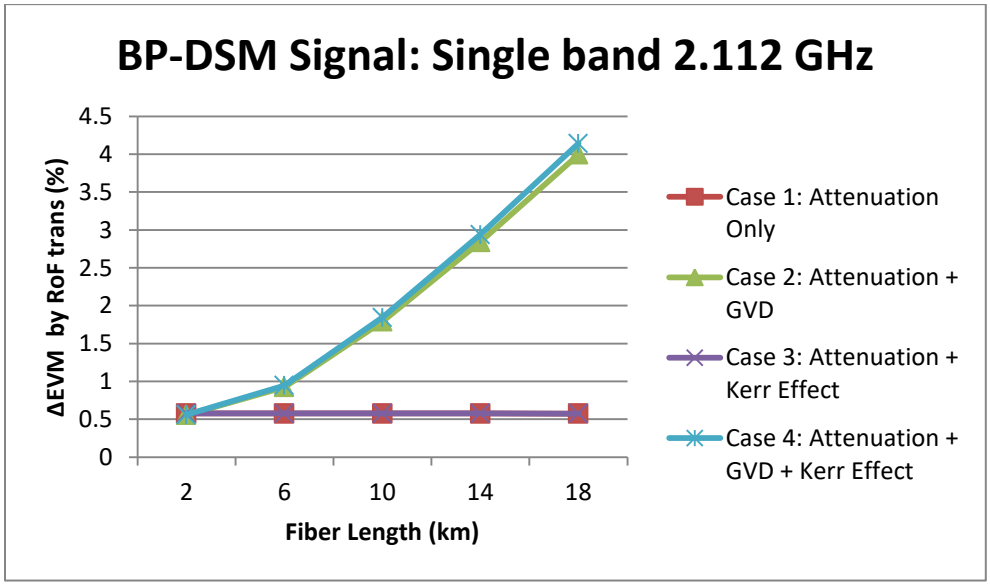

Figure 4-46: Change of EVM by RoF transmission for BP-DSM single band 2.112 GHz

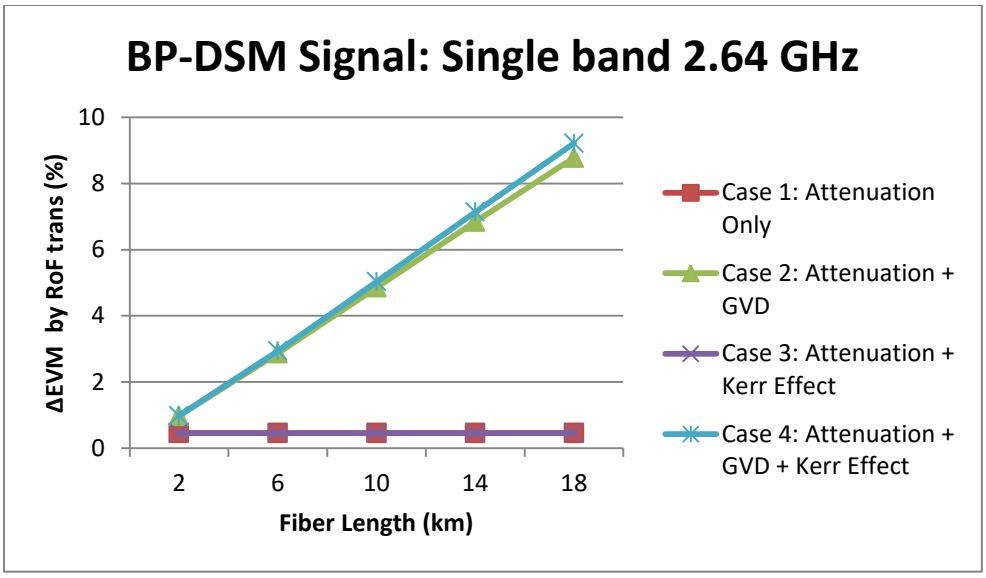

Figure 4-47: Change of EVM by RoF transmission for BP-DSM single band 2.64 GHz

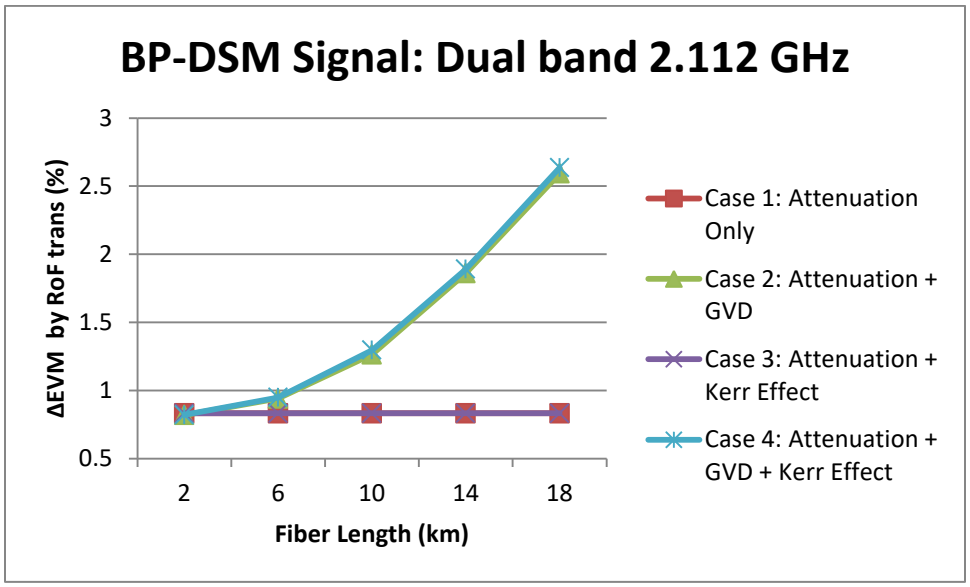

Figure 4-48: Change of EVM by RoF transmission for BP-DSM dual band 2.112 GHz

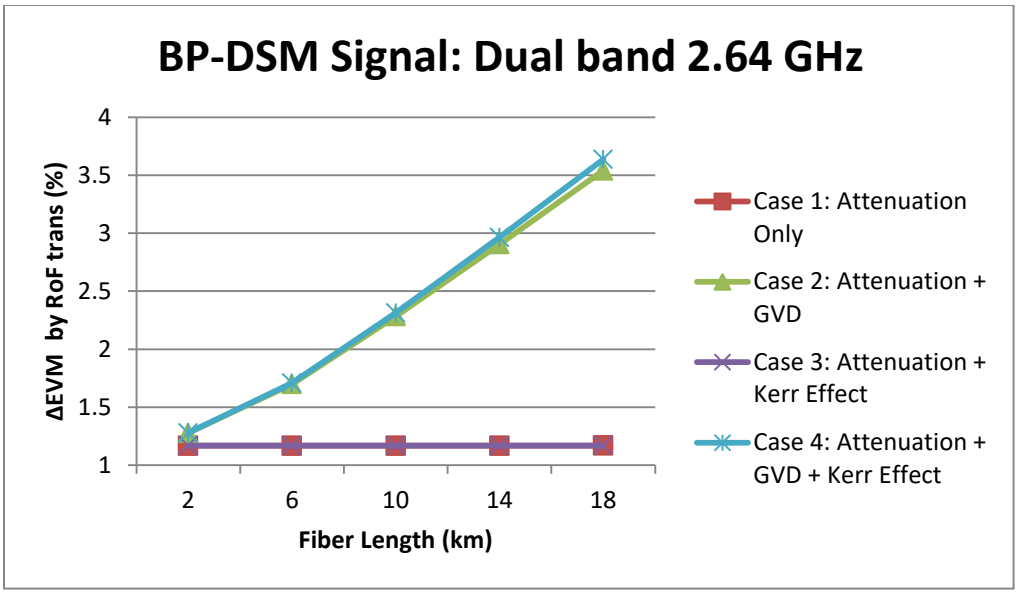

Figure 4-49 Change of EVM by RoF transmission for BP-DSM dual band 2.64 GHz

The BP-DSM signals all follow similar patterns for the conducted fiber cases. The attenuation and Kerr effect have no significant impact on the EVM as the fiber length increases. The GVD displays the greatest influence on the EVM for each BP-DSM signal. In Figure 4-47, the EVM results are significantly higher when distortion is included than the other cases. This is likely due to the center frequency of 2.64 GHz. When the frequency is higher, it is known to have a higher error rate [52]. Also, the spacing of 20 MHz has shown to have more error at higher frequencies [52].

Next, the same calculations are done for the EDSM signals. Figure 4-50 through Figure 4-53 illustrate the effects.

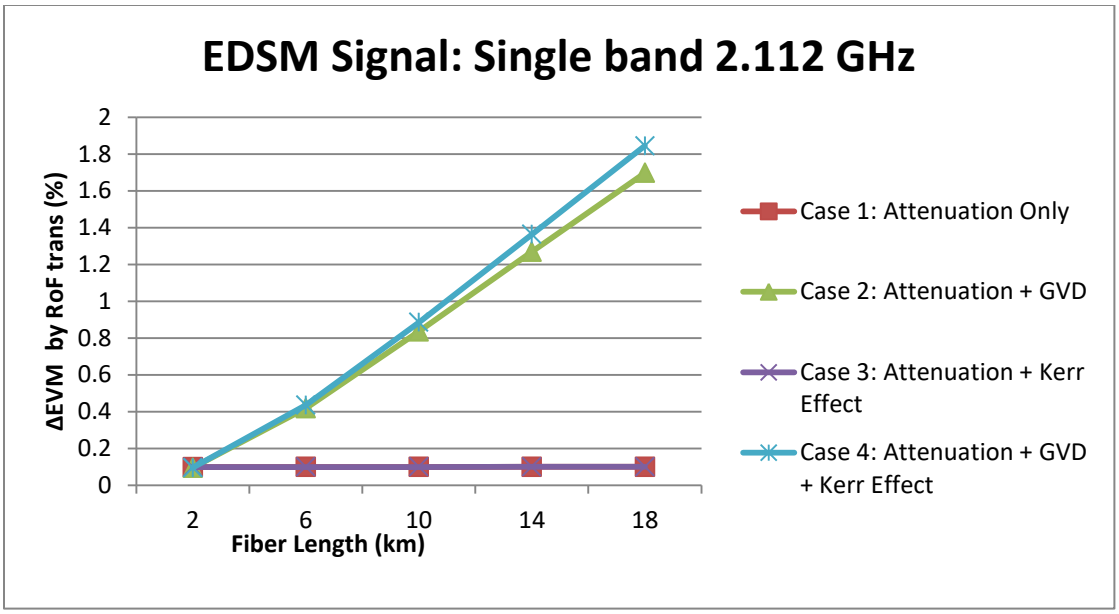

Figure 4-50: Change of EVM by RoF transmission for EDSM single band 2.112 GHz

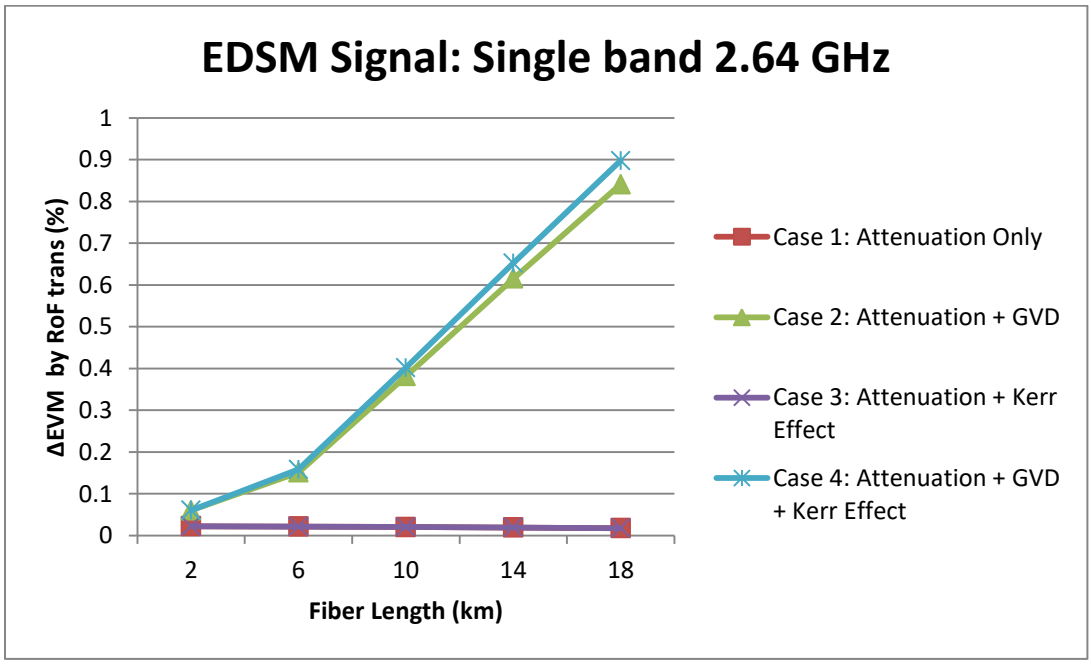

Figure 4-51: Change of EVM by RoF transmission for EDSM single band 2.64 GHz

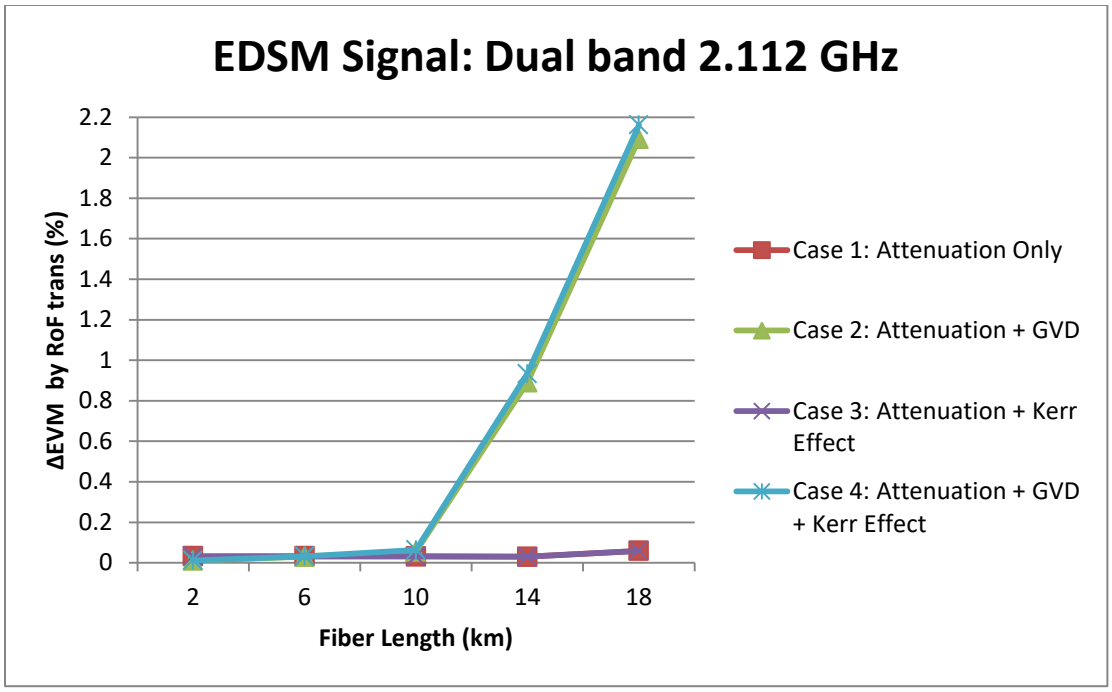

Figure 4-52: Change of EVM by RoF transmission for EDSM dual band 2.112 GHz

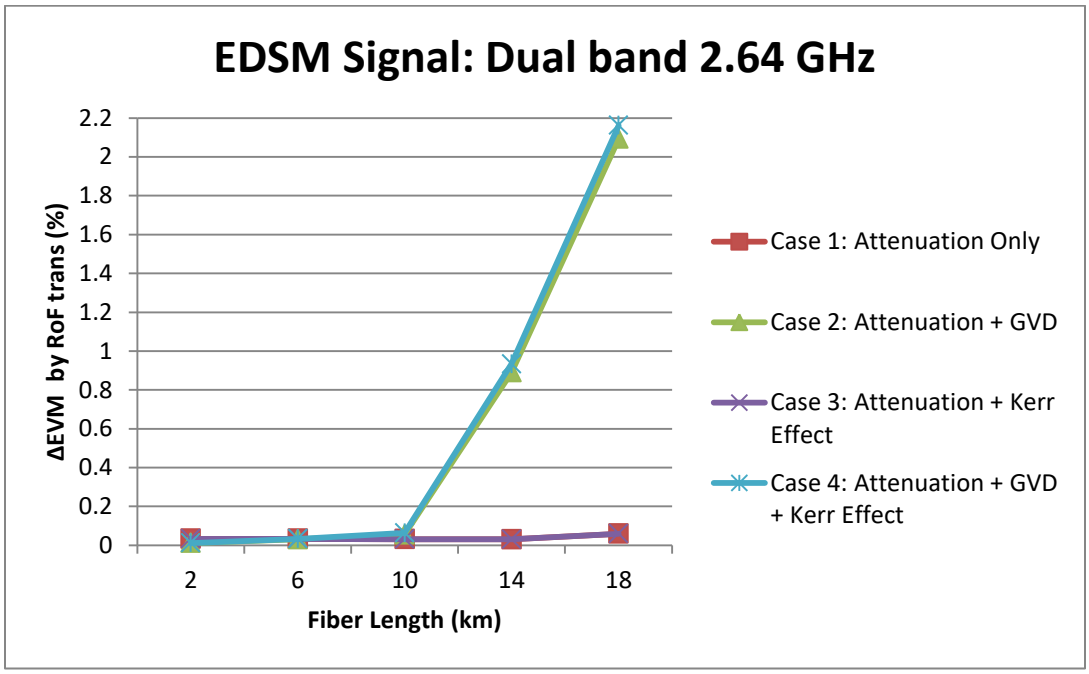

Figure 4-53: Change of EVM by RoF transmission for EDSM dual band 2.64 GHz

In all the presented EDSM signal figures, the greatest influence on the change of EVM is caused by the inclusion of the GVD. As the distance increases, the error rises. In the dual band EDSM signal, both bands observed a sudden spike in EVM after 10km.

Overall, the BP-DSM signals observe the largest increase in the change of EVM by RoF transmission while the EDSM signals do not see a serious impact in comparison. The GVD is the main fiber property that causes the dramatic change in EVM for all signals. For all signals, the graphs follow the same pattern where any case with GVD has a steady error rise. Yet, the cases without GVD are generally flat.

Chapter 5. Experimental Verification of Concurrent Dual Band Envelope Delta-Sigma Modulation in Radio-over-Fiber

To test the modulated signals and proposed setup, experimental verification is conducted. For extended comparison purposes, the single and dual BP-DSM cases are tested to understand how they stood up to the EDSM variants. Like the simulated work, the transmission is examined as proof of concept.

5.1. Experimental Setup

Using a combination of MATLAB and lab equipment, the experiment setup is constructed. Figure 5-1 depicts the general flowchart of the experiment.

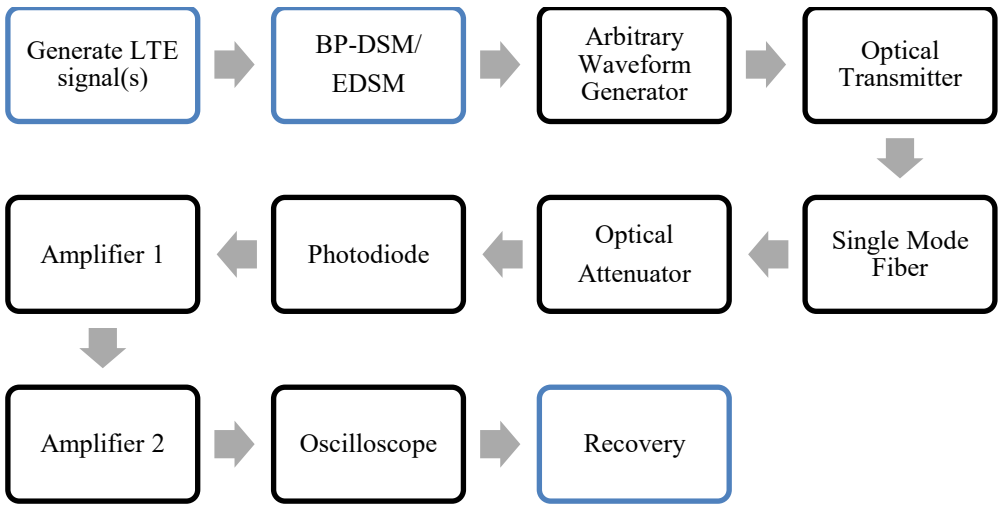

Figure 5-1: Experimental Setup Flowchart

Blocks in with blue borders represent the steps performed in MATLAB. The remaining blocks are specific lab equipment used.

The single or dual band 64-QAM 20MHz LTE signal is created and undergoes BP-DSM or EDSM in MATLAB. The process follows the same setups outlined in Chapter 4.1. For lab accommodation, the sampling rate needs to be 10.32192 GHz instead of 6 GHz used in the

simulated work. Consequently, the vector for the RF signal needs to be a 10.32192 GHz signal and be divided into 30 kHz sized subcarriers instead of the 6 GHz and 15 kHz, respectively. Figure 5-2 shows the updated empty RF vector for the signal upconversion.

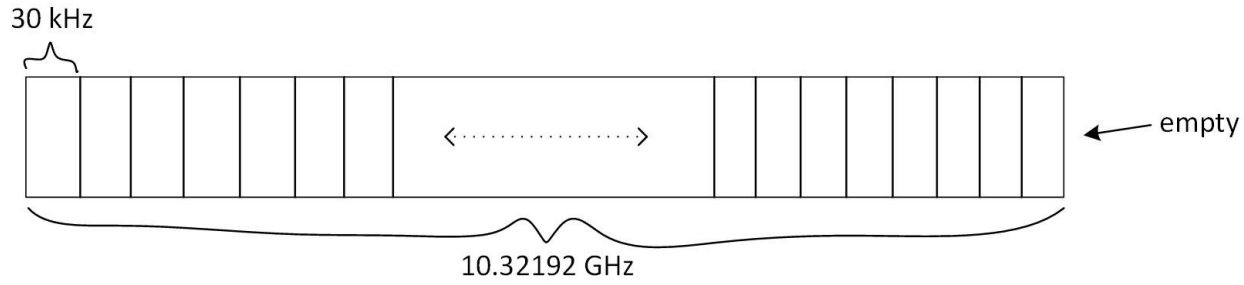

Figure 5-2: Updated RF Vector for experiment LTE signals

The empty vector only changes in size of subcarriers and the overall length. The array of Figure 5-2 is divided into 344064 sections. The center frequencies remain unadjusted for the experiment. The intersecting point to place the ODFM signal into the newly designed RF array follows the same method as the simulation, but at a different subcarrier size. Now, the starting subcarrier for the BB LTE signal is:

$$starting\ subcarrier = \frac{f_c}{30e3} - \frac{NFFT}{2} \qquad 21$$

where NFFT is the size of the FFT. Additionally, with the doubling of the subcarrier size, the sampling rate of the LTE vector doubles to 61.44 MHz. The inserting of the FFT vector is shown in Figure 5-3.

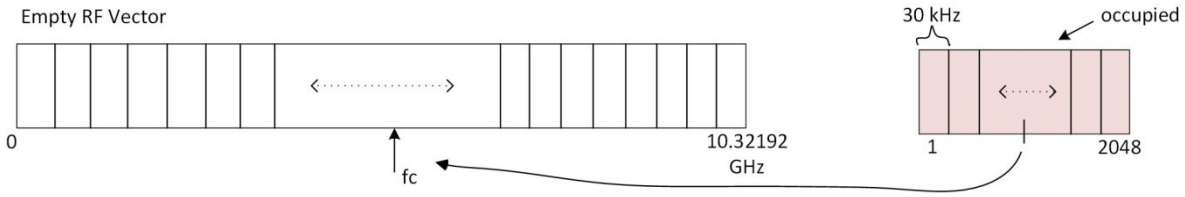

Figure 5-3: Empty RF Vector for experiment with fc point marked and FFT vector

Identical to the steps shown in Figure 4-5, Figure 5-3 demonstrates the insertion step, but with the experiment parameters. Depending on the DSM applied, the upconversion happens either with an FFT vector of the BB LTE signal or the phase component. Once the fc starting point is

determined, the FFT vector is placed into the RF vector, subcarrier by subcarrier. Figure 5-4 shows the updated finished RF vector.

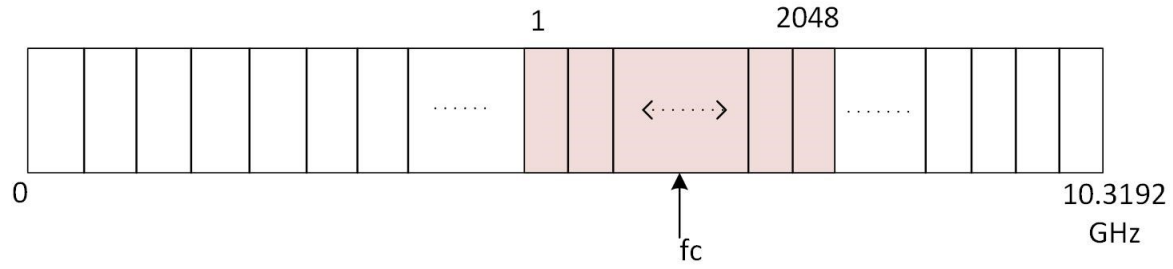

Figure 5-4: Finished RF Vector – FFT vector inserted into RF vector – experiment accommodation

The finished RF vector of Figure 5-4 will either be a new RF LTE signal for the BP-DSM case or it will be the RF phase component ready to be multiplied with the RF envelope for the EDSM case.

The DSM steps for each case do not change from Chapter 4.1 nor does the BP-DSM structure in Figure 3-2. The only parameter that changes is the sampling rate of the BP-DSM due to the increased rate from the lab equipment. Subsequently, the OSR changes to 258 and the center frequency ratio changes to fc/10.32182 GHz. With these updates, the noise transfer functions are recalculated through the DSM toolbox [12] in MATLAB. The coefficients for the CRFB are also recalculated and populated into a new Simulink model. A higher DSM rate is not particularly desired, but no difference to the performance is noticed. After the desired DSM, the RF signals are collected for use in the laboratory.

In the lab, a Tektronix AWG7122B arbitrary waveform generator (AWG) downloads the variety of signals for transmission at 10.32192 Giga samples per second (GS/s). The AWG is capable of transmitting signals up to 12 GS/s and possesses two arbitrary waveform outputs [53]. Using a coaxial cable, the AWG transmits the desired 20 MHz LTE signal into the transmitter side of a MITEQ 6GHz SCM fiber optic link [54]. The average input power from the AWG into the transmitter is ~ -22dBm. The optical transmitter is a direct modulated laser where the received RF signals directly modulate the laser current. Figure 5-5 shows the detailed layout of the optical transmitter.

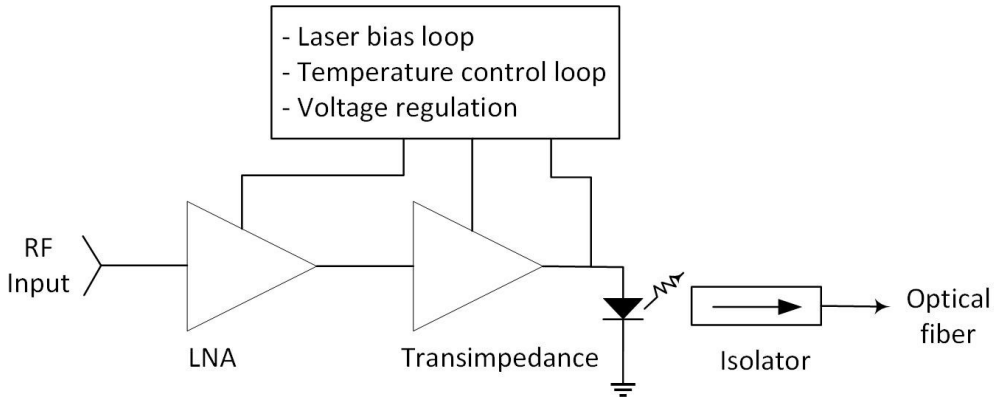

Figure 5-5: Block diagram of optical transmitter (from [54])

In Figure 5-5, The RF LTE signal enters the LNA first to keep the noise low [54]. Afterwards, the signal passes through a transimpedance amplifier to change the current to voltage [54]. Next, the signal passes through a laser diode coupled with an optical isolator to become an optical signal. Table 5-1 summarizes the main characteristics of the optical transmitter.

Table 5-1: Characteristics of the MITEQ 6GHz SCM fiber optic link transmitter (from [54])

Parameters	
Maximum Operating Frequency	6 GHz
Gain	14 dB
Laser and Amplifier Bias	+12 VDC
Laser Diode Cooler	-12 VDC
Laser Diode Heater	+4 VDC
Maximum Input Power	10 dBm

The transmitter is powered using two BK Precision 1672 triple power supplies by connecting +4V, +12V and -12V. Once receiving the power, the signal can directly drive the laser current. The bias current from the laser is ~160mA.

From the output of the transmitter, the signal travels along a 2-kilometer standard single mode fiber (SMF). The optical power entering the fiber is 6.76 dBm. A Corning SMF-28 optical fiber is used with an attenuation of 0.2 dB/km [55]. This translates to a loss of 0.4 dB. The measured optical power from the fiber is 5.65 dBm equating to a drop of 1.11 dB. As a

safety precaution, a tunable optical attenuator is included before the PD to ensure the incoming power is not too high. The receiver, a Discovery Semiconductors balanced photodiode with a BW up to 40 GHz, receives the transmitted signal [56]. This DSC740 model transforms the signal back to its electrical form. It features a push-pull InGaAs PD in a "Lab Buddy" to simplify the biasing and power setup [56]. Table 5-2 highlights characteristics of the optical receiver.

Table 5-2: Characteristics of Discovery Semiconductors balanced photodiode in Lab Buddy (from [56])

Parameter	
Maximum Input Power	10 dBm
Responsivity	0.60 A/W
- 3 dB Bandwidth	30 GHz
Minimum Optical Return Loss	25 dB
Bias	+/- 5V
Lab Buddy Plug-in	110/220V

Based on the parameters presented in Table 5-2, the PD used is more than adequate for the proposed work. The incoming power to the Lab Buddy unit is 0 dBm due to the influence of the optical attenuator. Once converted back to electrical form, two 26 dB power amplifiers in series are connected. During initial trial runs, the signal could not be detected by the oscilloscope. After debugging the setup, it was discovered the output power from the PD was too low. As a result, two Super Ultra Wideband amplifiers (ZVA-213+) [57] are included to boost the signal power post optical link. The amplifiers are powered using additional BK Precision 1672 triple power supplies with +12V. The signals boost the signal to around -20 ≈ -30 dBm.

The output is received by an Agilent DSO81204B oscilloscope. It samples the modulated signal at the same transmitted sample rate of 10.32192 GHz and displays the time domain and frequency domain of the signal [58]. Table 5-3 summarizes the characteristics of the oscilloscope.

Table 5-3: Characteristics of Agilent DSO81204B oscilloscope (from [58])

Parameters	
Bandwidth	12 GHz
Sample Rate	40 Giga Samples per second (2 channels) 20 Giga Samples per second (4 channels)
Number of Channels	4

One channel is used to receive the signal from the second power amplifier. Therefore, according to Table 5-3, the maximum sample rate is 40 GS/s. The received signal is saved in a text file and processed in MATLAB offline for comparisons. Chapter 4.1 explains the recovery steps.

Figure 5-6 shows the overall setup from the lab.

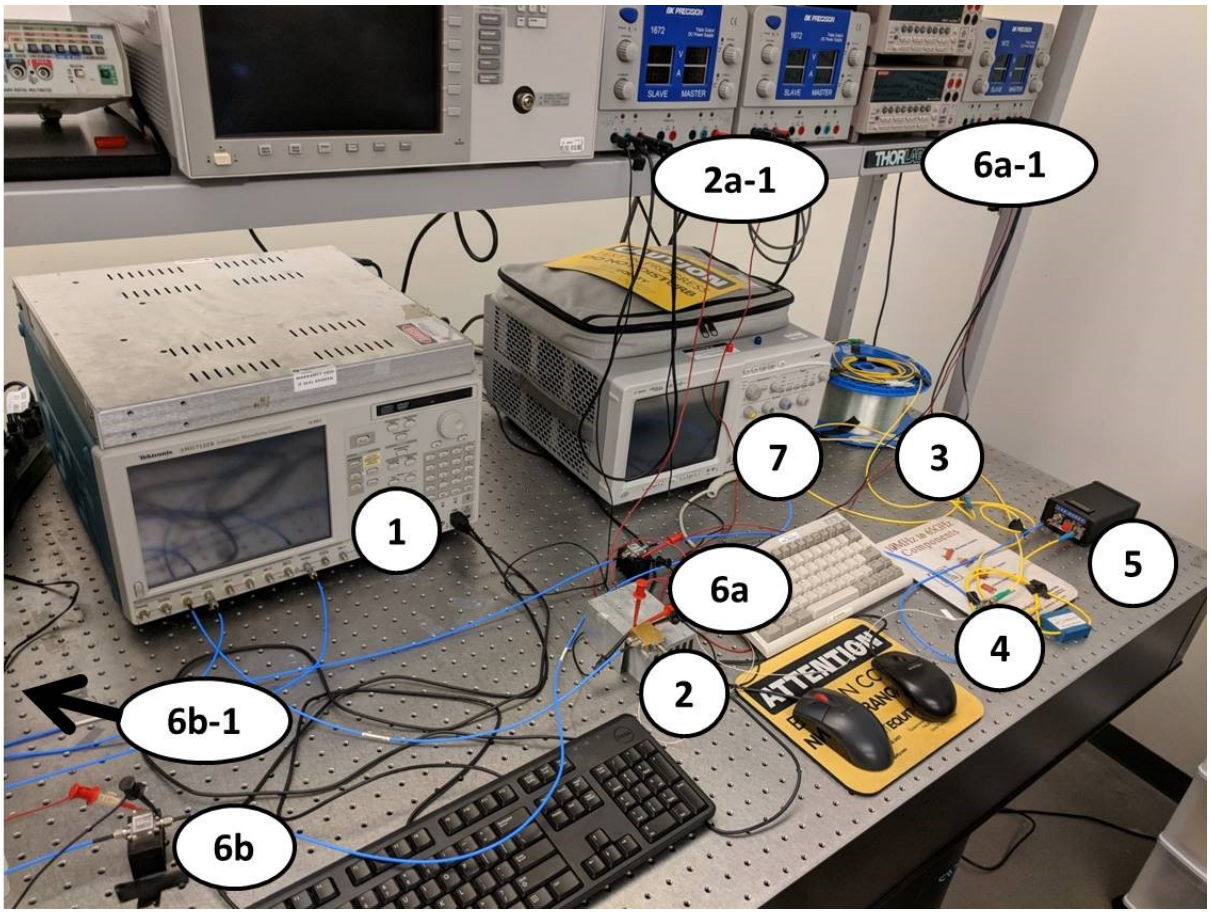

Figure 5-6: Lab Setup

The components of the lab setup are numbered in Figure 5-6. Table 5-4 specifies each part.

Table 5-4: Equipment Used in the Experimental Setup referencing Figure 5-6

Number	Equipment
1	Tektronix AWG7122B Arbitrary Waveform Generator
2	MITEQ 6GHz SCM fiber optic link – Transmitter
3	Corning SMF-28 Optical Fiber – 2km
4	Optical Attenuator
5	Discovery Semiconductors balanced photodiode – DSC740
6a	Super Ultra Wideband Amplifier 1
6b	Super Ultra Wideband Amplifier 2
7	Agilent DSO81204B Oscilloscope
2a-1, 6a-1, 6b-1	BK Precision 1672 triple power supplies

Using the setup in Figure 5-6, all the different cases performed in the simulations could be tested experimentally. The experiments are performed to demonstrate the effects of EDSM in a dual band RoF system. For the following scenarios, the dual bands of the RF LTE signal are 2.112 GHz and 2.64 GHz.

5.2. Bandpass Delta-Sigma Modulation in Radio-over-Fiber Transmission

For comparison purposes, single and dual band 20 MHz LTE signals with BP-DSM are tested in the lab. The following experiments subject the signals to the 1-bit BP sigma-delta modulator that runs at 10.32192 GHz. Figure 5-7 shows the experimental setup for the BP-DSM RoF transmission link.

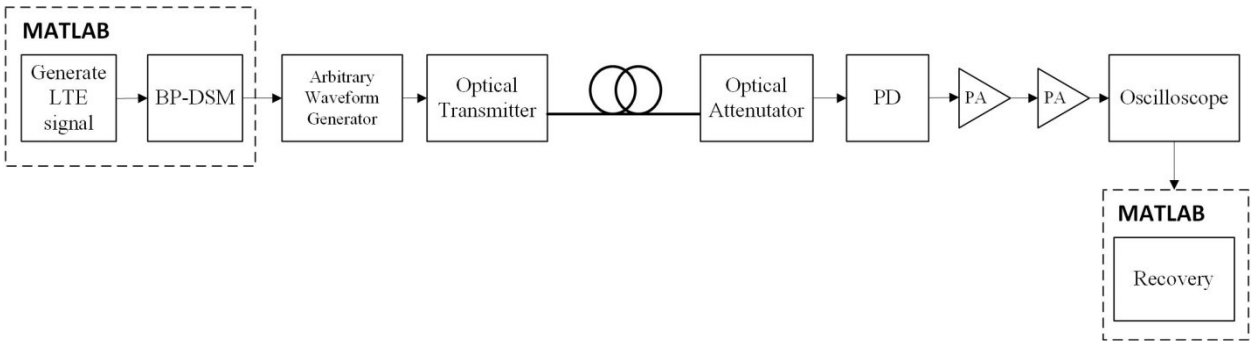

Figure 5-7: Block diagram of experimental setup with BP-DSM RoF transmission

Once the modulated LTE signal is created in MATLAB, it is directly transmitted using the AWG to the optical transmitter. The optical transmitter is the same as described in Figure 5-5. The SMF carries the signal to an optical attenuator. Afterwards, the PD receives the signal and the recovered electrical signal travels through two amplifiers. Once boosted, the oscilloscope receives the signal. For evaluation, the data are saved for MATLAB where the EVM is calculated and the constellations are designed.

5.2.1. Single Carrier Bandpass Delta-Sigma Modulation in Radio-over-Fiber Transmission

In the single carrier cases, LTE signals are generated in MATLAB for each carrier frequency. The signal is sent through the 1-bit BP-DSM for modulation. Figure 5-8 shows the specific MATLAB setup for the transmitter.

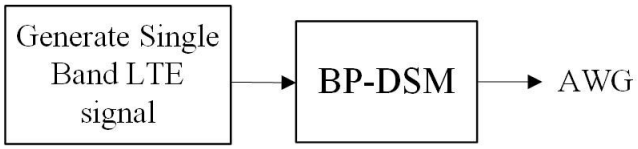

Figure 5-8: MATLAB setup for single band LTE signal with BP-DSM

The carrier generated is 2.112 GHz from the LTE band 1 or 2.64 GHz from the LTE band 7. Once created, the signal is sent to the AWG where it is transferred to the rest of the experimental RoF setup as seen in Figure 5-7. Figure 5-9 shows the time domain and frequency spectrum of the received signals collected from the vector spectrum analyzer.

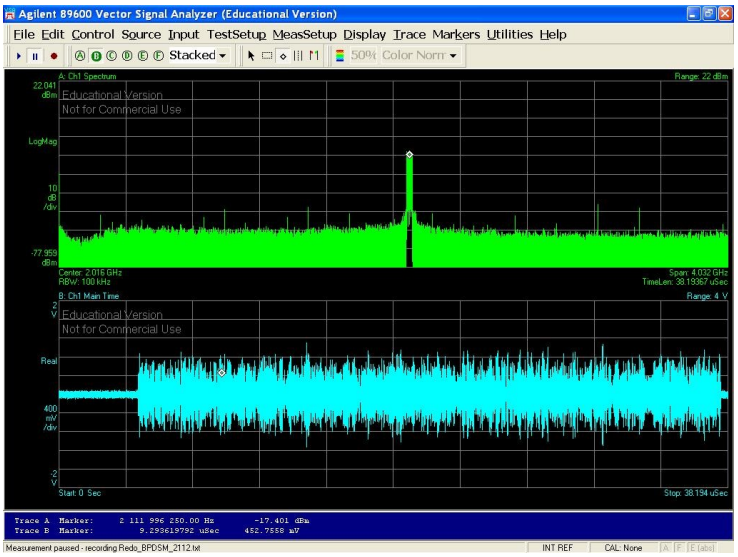

a)

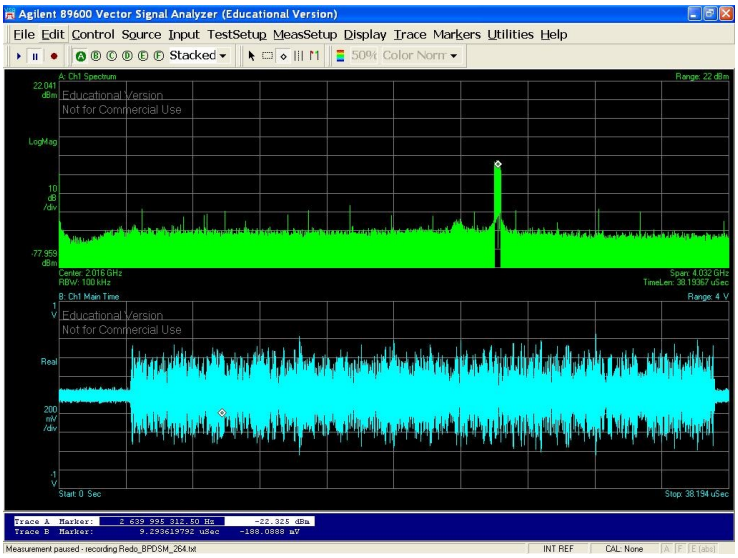

b)

Figure 5-9: Time domain and frequency spectrum of BP-DSM signal after RoF transmission – a) 2.112 GHz and b) 2.64 GHz

The signals in Figure 5-9 are the expected outputs. Both single carriers resemble the signal before the transmission. After extracting this time domain signal, the signal is recovered and has the EVM calculated. Table 5-5 summarizes the EVM results for both carriers at two reading points: after the BP-DSM and the oscilloscope.

Table 5-5: EVMs of single carrier LTE signals

	Single Carrier	
	2.112 GHz	**2.64 GHz**
After BP-DSM	0.5434%	0.5435%
From Oscilloscope	4.5237%	4.9168%

The signals in Table 5-5 are designed using the lab sampling rate and subcarrier spacing presented in Chapter 5.1. Compared to the simulated results in Chapter 4.3, the EVMs in at both evaluation marks have increased from the adjusted parameters. Using the recorded data from the oscilloscope, the EVMs for each carrier are much higher post BP-DSM. For the 2.112 GHz carrier frequency, the error rises to 3.9803% while the 2.64 GHz carrier frequency observes an increase of 4.3733%.

When calculating the EVMs, the corresponding constellations are designed for comparison with the original 64-QAM. Figure 5-10 displays the constellations for each tested single carrier recovered from the oscilloscope.

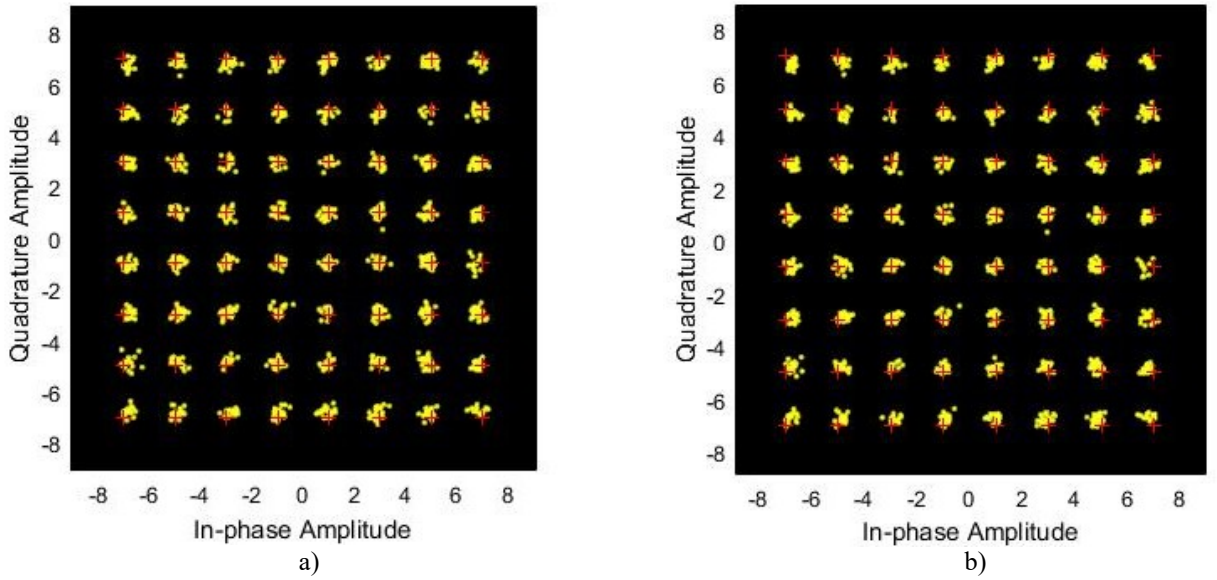

Figure 5-10: Constellations of recovered single carrier signals with BP-DSM from oscilloscope – a) 2.112 GHz and b) 2.64 GHz

The error increase is quite apparent when observing the constellations in Figure 5-10. The yellow points are not as concentrated on the original layout. This clearly demonstrates the

negative impact of the optical interface on the single carrier signals with BP-DSM. Despite the error, the overall results are still below the LTE standard of 8%.

5.2.2. Dual Carrier Bandpass Delta-Sigma Modulation in Radio-over-Fiber Transmission

In dual carrier case, two LTE signals are generated in MATLAB where they are individually upconverted to the two aforementioned center frequencies. Afterwards, they are subjected to the 1-bit BP-DSM and adder together ready for the lab. Figure 5-11 shows the described setup.

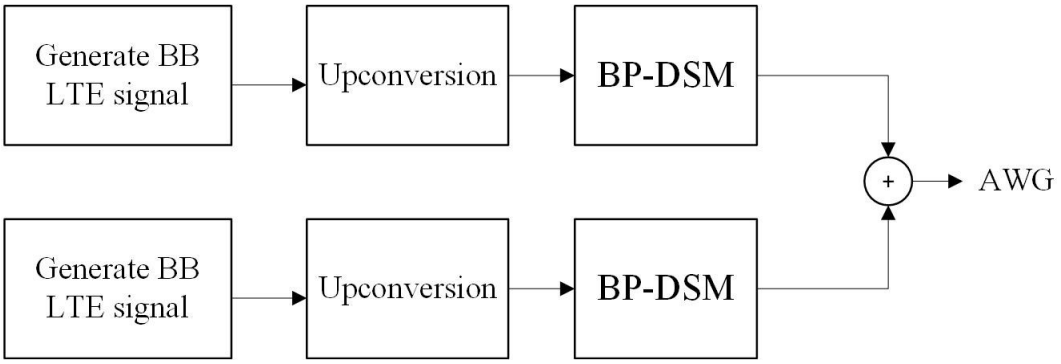

Figure 5-11: MATLAB setup for dual band LTE signal with BP-DSM

After the RF signal is designed, it is sent to the AWG for use in the lab experiment. The signal proceeds to follow the block diagram from AWG in Figure 5-7 and the details in Chapter 5.1. The corresponding time domain and frequency spectrum plots in Figure 5-12 are collected.

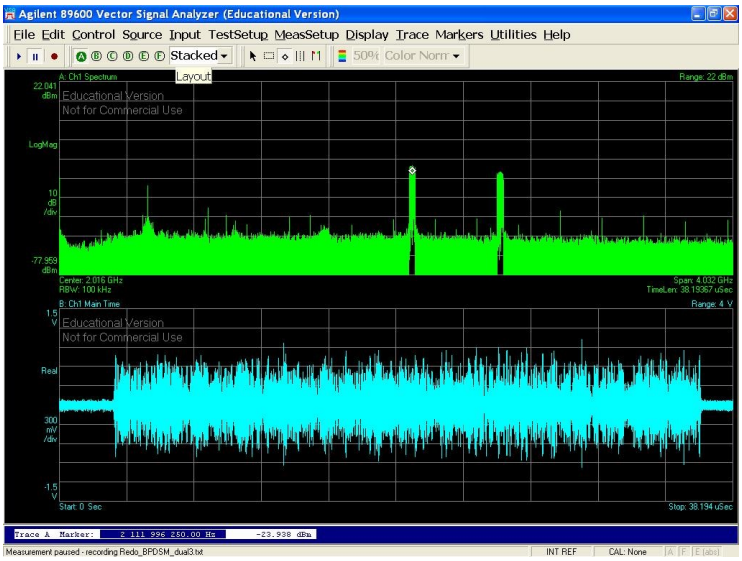

Figure 5-12: Time domain and frequency spectrum of BP-DSM dual band signal after RoF transmission

The frequency spectrum in the dual band case is like single band, but with less power at the bands. Using the time domain signal in Figure 5-12, the EVMs are calculated from the recovered signal. Table 5-6 show the EVMs from the post DSM to post power amplifiers.

Table 5-6: EVMs of dual carrier LTE signal

	2.112 GHz	**2.64 GHz**
After BP-DSM	0.5376%	0.5592%
From Oscilloscope	5.2307%	5.4673%

Similar to the single band case, the dual band carriers produce higher EVM percentages in Table 5-6 after the BP-DSM than the simulations due to the larger sampling rate and subcarrier spacing. The EVMs after the BP-DSM for dual band are a bit more than the single carrier experimental values. The recovered dual band signal from the oscilloscope has worse EVMs for each carrier than the results in Table 5-5. The 2.112 GHz carrier has a 4.6931% increase in EVM and the 2.64 GHz carrier has a 4.9081% increase. These changes in EVM for the dual band case are higher than the single band case.

After calculating the EVMs for the recovered signal in MATLAB, the corresponding constellations are designed to compare to the original 64-QAM. Figure 5-13 shows the constellation diagrams for each carrier in the dual band signal.

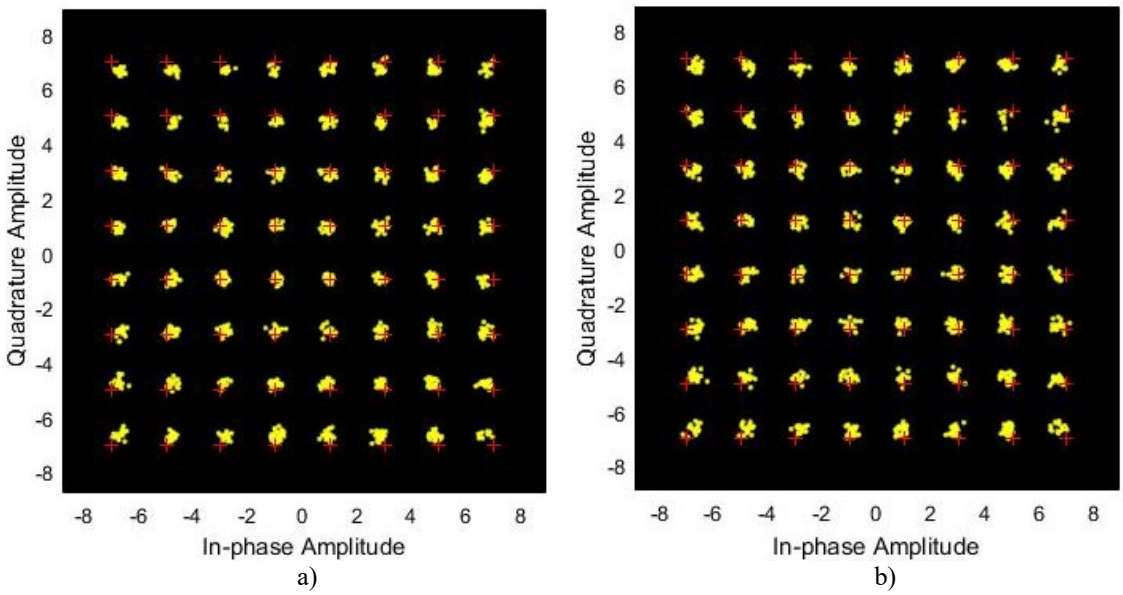

Figure 5-13: Constellations of recovered dual band signals with BP-DSM from oscilloscope – a) 2.112 GHz and b) 2.64 GHz

Despite the recovered points being prominent in Figure 5-13, the constellations are relatively neat. Compared to Figure 5-10, the error is more for each carrier and the points are further away from the original 64-QAM constellation. The diagrams support the EVMs from the oscilloscope in Table 5-6. Overall, the single band case performs better in the BP-DSM RoF transmission in the experiments than in dual band case.

5.3. Envelope Delta-Sigma Modulation in Radio-over-Fiber Transmission

After the BP-DSM RoF transmission experiments, EDSM RoF transmission is tested. Envelope delta-sigma modulation is applied in place of standalone BP-DSM. The EDSM has its 1-bit BP-DSM running at 10.32192 GHz to meet the lab requirements. Figure 5-14 shows the experimental setup for the EDSM RoF transmission link.

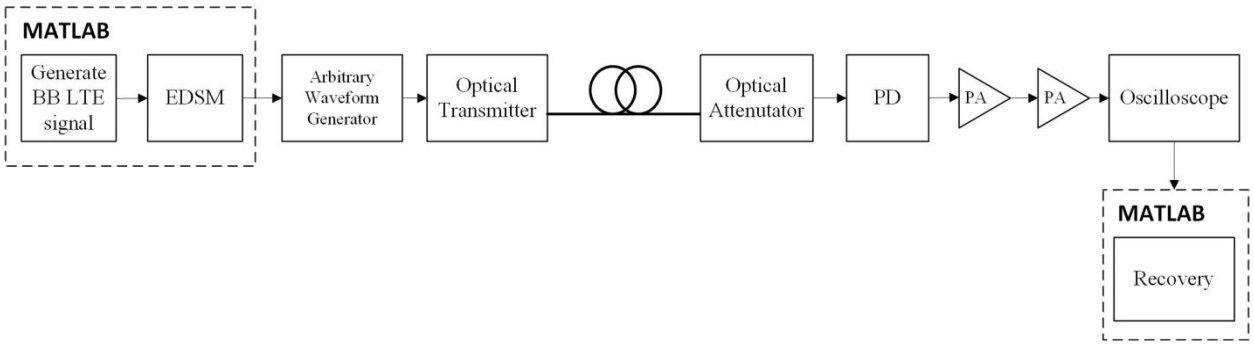

Figure 5-14: Block diagram of experimental setup with EDSM RoF transmission

After the BB LTE signal has been processed by the EDSM in MATLAB, the signal is directly transmitted using the AWG to the optical transmitter. The optical transmitter is the same as described in Figure 5-5. The SMF carries the signal to an optical attenuator. Afterwards, the PD receives the signal and the recovered electrical signal travels through two power amplifiers. Once boosted, the oscilloscope receives the signal. For evaluation, the data are saved for MATLAB where the EVM is calculated and the constellations are designed.

5.3.1. Single Carrier Envelope Delta-Sigma Modulation in Radio-over-Fiber Transmission

For the single carrier case, a baseband LTE signals is created in MATLAB. Each signal is subjected to the 1-bit envelope delta-sigma modulator running at 10.32192 GHz in MATLAB. Figure 5-15 shows the specific MATLAB setup for the transmitter.

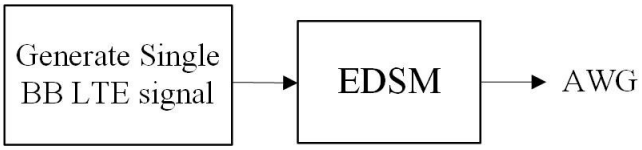

Figure 5-15: MATLAB setup for single carrier baseband LTE signal with EDSM

The EDSM setup is described in Chapter 3.2 and presented in Figure 3-5. Inside the EDSM, the signal is upconverted to 2.112 GHz of the LTE band 1 or 2.64 GHz of the LTE band 7. Afterwards, the processed signal is uploaded to the AWG to be transmitted to the remainder of the RoF setup shown in Figure 5-14. At the oscilloscope, Figure 5-16 illustrates the received single carrier signals.

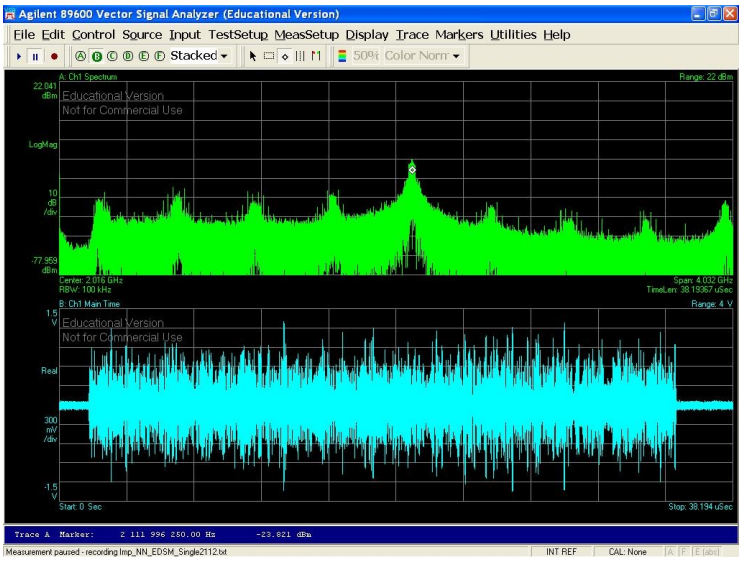

a)

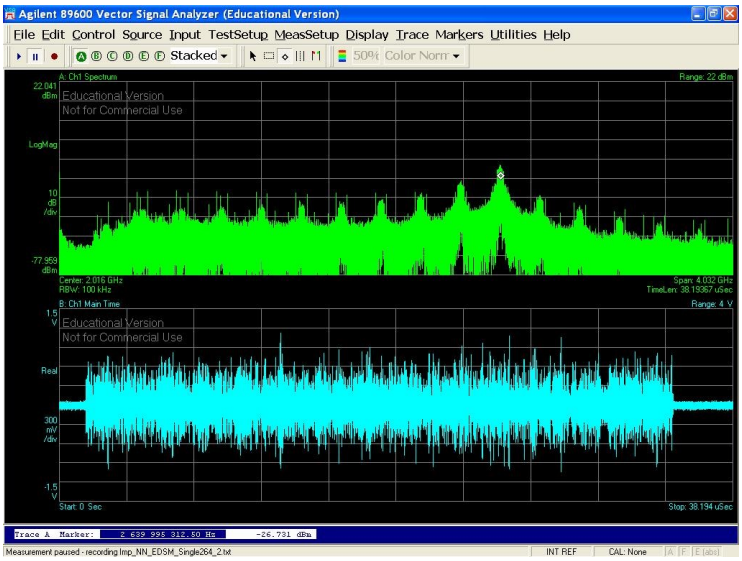

b)

Figure 5-16: Time domain and frequency spectrum of EDSM signal after RoF transmission – a) 2.112 GHz and b) 2.64 GHz

From the oscilloscope outputs in Figure 5-16, the signal is saved for evaluation in MATLAB. Unlike the BP-DSM cases, the EDSM frequency spectrums have additional components from quantization. Table 5-7 shows the EVM results for each single carrier at two evaluation points: after EDSM and at the oscilloscope.

Table 5-7: EVMs of single carrier LTE signals

	Single Carrier	
	2.112 GHz	**2.64 GHz**
After EDSM	3.5993	3.5967
From Oscilloscope	5.2195	6.1114

The errors after the EDSM from Table 5-7 for each carrier are slightly more than the simulated results presented in Chapter 4.5 due to the lab parameter accommodation. The EVMs of the recovered signal from the oscilloscope are high. The change from the EDSM to the oscilloscope is much larger than the error increase observed in the simulations. The 2.112 GHz carrier frequency has the EVM increase 1.6202% and the 2.64 GHz carrier frequency has the EVM increase 2.5147%. Compared to the BP-DSM single carrier RoF transmission results in Chapter 5.2.1, the individual EVMs are higher. However, the EVM change from the RoF influence is much less.

When recovering the signals from the oscilloscope, the corresponding constellation diagrams were created in MATLAB. Figure 5-17 show the recovered single carrier signal compared to the original 64-QAM constellation.

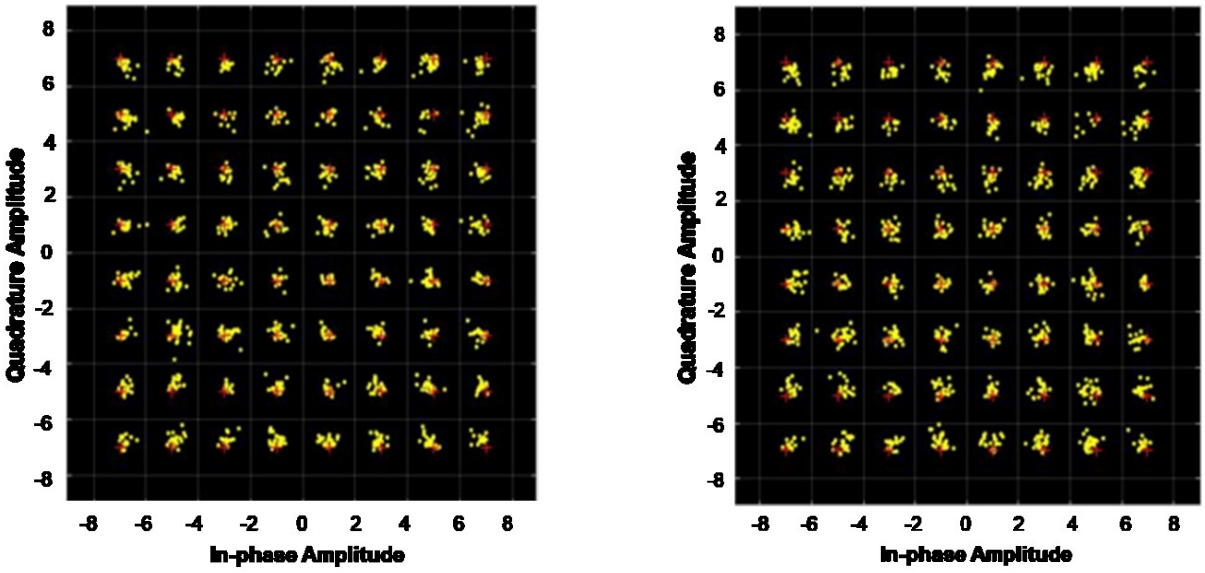

a) b)

Figure 5-17: Constellations of recovered single carrier signals with EDSM from oscilloscope – a) 2.112 GHz and b) 2.64 GHz

The scattered constellations of the recovered single carrier signals are apparent. Figure 5-17 b) clearly is more spread out than Figure 5-17 a). This matches the EVM results from Table 19 for the oscilloscope evaluation point. In comparison to the BP-DSM constellations in Figure 5-10, the Figure 5-17 results are similar. Yet, the simulated results in Chapter 4.5 produced more concentrated constellations. Overall, the recovered signals have EVMs in line with the LTE standard.

5.3.2. Dual Carrier Envelope Delta-Sigma Modulation in Radio-over-Fiber Transmission

For the dual carrier case, two baseband LTE signals are generated and subjected to the 1-bit envelope delta-sigma modulator running at 10.32192GHz in MATLAB. Figure 5-18 shows the implemented setup.

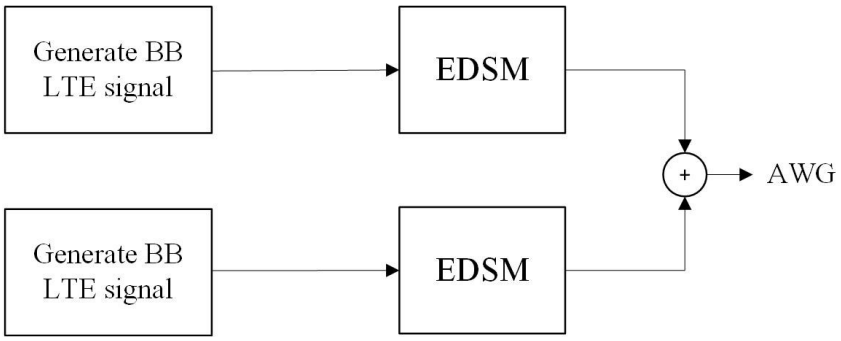

Figure 5-18: MATLAB setup for dual band LTE signal with EDSM

Inside the EDSM, the signal is upconverted to 2.112 GHz of the LTE band 1. Simultaneously, another baseband LTE signal is generated. This time the EDSM is configured to upconvert the signal to 2.64 GHz of the LTE band 7. An adder combines the two RF LTE signals and the processed signal transferred to the AWG. A detailed block diagram of the setup is shown in Figure 3-7 from Chapter 3.3. The signal proceeds from the AWG to the remaining components in the lab as shown in Figure 5-14. Figure 5-19 shows the time domain and frequency spectrum of the dual band signal at the oscilloscope.

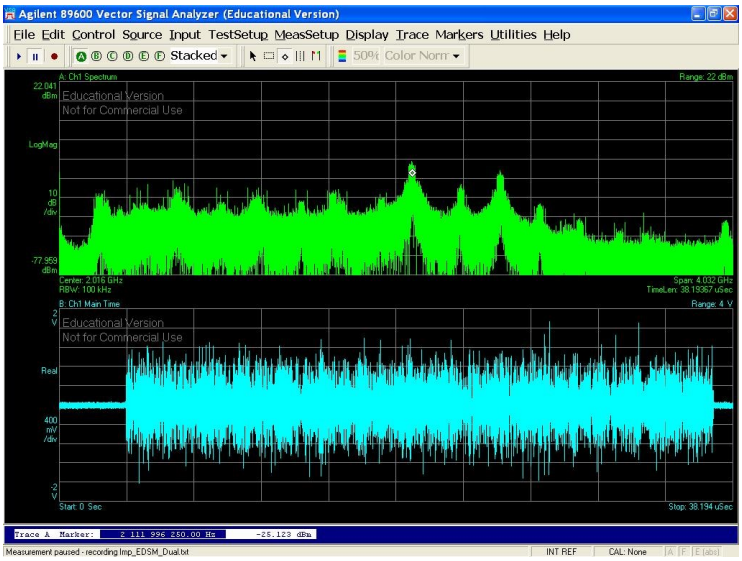

Figure 5-19: Time domain and frequency spectrum of EDSM dual band signal after RoF transmission

Like Figure 5-16, Figure 5-19 has stronger additional components from the EDSM quantizers. However, the main bands are still visible in the frequency spectrum. The extracted signal is able to be recovered and produces the following EVM values in Table 5-8.

Table 5-8: EVMs of dual carrier LTE signals

	2.112 GHz	**2.64 GHz**
After EDSM	4.3358%	4.3358%
From Oscilloscope	6.509%	6.509%

The errors presented in Table 5-8 after the EDSM and at the oscilloscope are the highest of all the presented scenarios. Still, compared to the dual band BP-DSM case, the dual carrier signal with EDSM inherits less error from the RoF transmission. The change for both carriers is 2.1732%.

After calculating the EVMs, the constellation diagram for each carrier in the dual band signal from the oscilloscope is developed. Figure 5-20 shows the recovered lab signal and the original 64-QAM constellation.

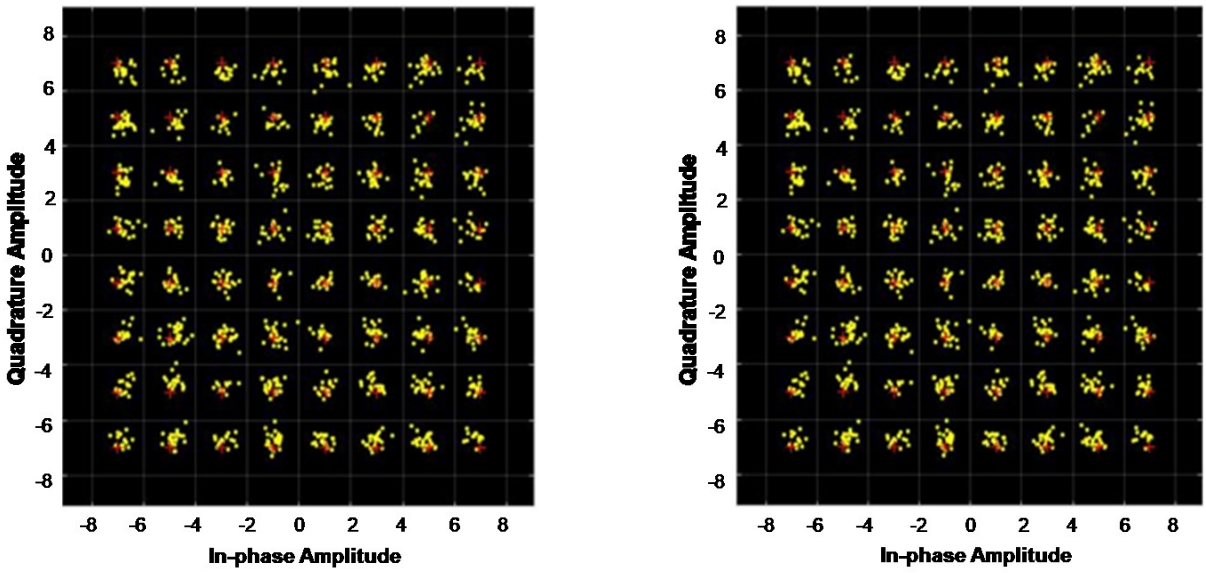

a) b)

Figure 5-20: Constellations of recovered dual band signals with EDSM from oscilloscope – a) 2.112 GHz and b) 2.64 GHz

The recovered constellations in Figure 5-20 are not as clean as the previous cases. The 6.509% error for both carriers is evident. The dual band BP-DSM RoF transmission constellations in Figure 5-13 are better with EVMs of 5.2-5.5%. Overall, the proposed EDSM case is still below the 8% LTE requirement.

5.4. Envelope Delta-Sigma Modulation in Radio-over-Fiber Transmission Comparison

A comparison of the proposed EDSM work with similar published papers is conducted. Table 5-9 summarizes the acquired error vector magnitudes of single and dual-band EDSM RoF transmission setups. EDSM out refers to the EVM being calculated before transmission and EDSM distance corresponds to the EVM reading after the optical link.

Table 5-9: EVMs of proposed EDSM setups

Carrier frequency	**EVMs of EDSM single (%)**		**EVMs of EDSM dual (%)**	
fc (GHz)	EDSM out	EDSM distance	EDSM out	EDSM distance
2.112	3.5993	5.2195	4.3358	6.509
2.64	3.5967	6.1114	4.3358	6.509

The EVMs for the single band EDSM case are lower than the dual band EDSM case. The change due to the RoF transmission is around 1.6 – 2.5 % when using EDSM. The EVMs in Table 5-9 are compared with the work from two comparable sources. In the first comparison, the researchers use 20 MHz LTE signal with a range of frequencies. Table 5-10 shows the results of the single carrier EDSM with tri-level quantization from Cho et al [37].

Table 5-10: EVMs from Cho et al. [37]

	EVMs of EDSM single (%)	
fc (GHz)	RF modulator	Transmitter output
2.13	3.7	7.5
2.6	3.2	7.2

For a better comparison, only the similar carrier frequencies are shown in Table 5-10. Also, their work does not feature RoF transmission so only the EDSM out values from the EDSM single case in Table 5-9 are compared. After the RF modulator, Cho et al. have similar EVM results. The EVM at the RF modulator for 2.13 GHz is 3.7% [37] while the proposed work at 2.112 GHz is 3.5993%. Their 2.6 GHz at the modulator has a better EVM of 3.2% [37] compared to the 2.64 GHz with 3.5967%. Both transmitter output EVMs are much worse than the acquired values for the given work.

The second compared research results come from a propose downlink EDSM RoF transmission with 5 MHz LTE signals. Table 5-11 shows the EVM results of carrier frequencies similar to those used in the proposed work.

Table 5-11: EVMs from Hori et al. [8]

	EVMs of EDSM single (%)	
fc (GHz)	EDSM out	After 18km SMF
2.14	7.6	7.5
2.64	7.4	7.5

After the EDSM, the EVMs from Hori et al. are much higher than those of the proposed work. Nevertheless, after radio transmission, their EVMs do not change like the proposed work. While around a 2% increase is observed for 2 km in this work, Hori et al. had 0.1% for 18km [8].

Despite this change in the proposed work, the EVMs are still lower than the Hori et al results. This may be due to the differences in the EDSM setup and recovery process.

Overall, the proposed EDSM setup has better EVMs than current publications. For 20 MHz LTE signals, the error vector magnitude should be < 8%. In the EDSM single band case, the EVMs from the proposed work are similar or better when comparing the EDSM outputs of the other works. The only result of 3.2% at a carrier frequency of 2.6 GHz [37] performed better than the ~3.6% error found. The dual case is expected have a higher EVM before transmission, but it is much better than Hori et al in the single case. With the proposed work, the results differ significantly when the RoF is introduced in regardless of single or dual band. The error increases by almost 1.6-2.5% unlike the second research [8] where little or no change occurs.

5.5. Experimental Error

As discussed in Chapter 4.7, possible fiber impact is strong candidate for the discrepancies observed in the results. Another possible source of error is the environmental noise. The experiment setup is not in a controlled environment and with the equipment being subjected to temperature fluctuations and the external noise of the loud scopes, signal degradation becomes noticeable. Acquiring repeatable results was a challenge and the influences for one signal could vary between runs. Figure 5-21 shows the variations in signal changes.

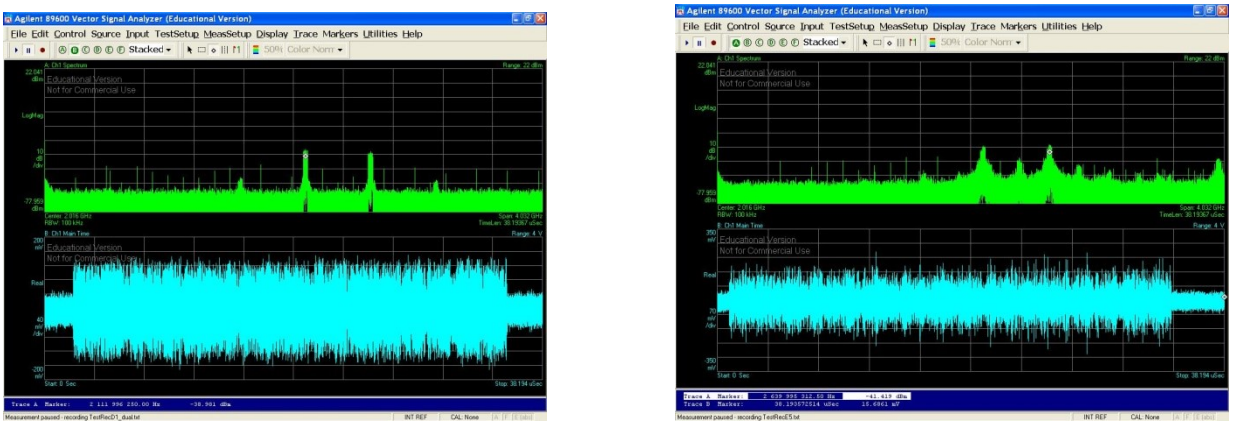

Figure 5-21: Oscilloscope outputs - frequency domain (green) and time domain (blue) of dual band LTE signals

Despite being the same input signal, the two recorded instances of the spectrum are different. In the time domains of Figure 5-21, it is evident that the noise influence is present in the signal. This type of change is not observed in the simulation spectrums. Despite knowing simulations are ideal controlled tests, the change is significant in certain situations. For instance, the single band DSM test observe the EVM change from 1% to 5% while other cases only see increases of ~2%. Using the outputs from the simulations as guidelines, extensive test runs were conducted before the final results were collected.

5.6. Experimental Results Summary

Overall, the experimental outcomes agree with the simulated counterparts and meet the 20 MHz LTE criteria of below 8%. The recovered single carrier LTE signals with EDSM from the oscilloscope have worse EVMs than the recovered single carrier LTE signals with BP-DSM. The 2.112 GHz carrier degrades the EVM by ~0.7% while the 2.64 GHz carrier degrades by ~0.2%. In the dual band case, the EVMs with the BP-DSM are much lower than the EVMs with EDSM. However, the EDSM dual band case observes a lower change post EDSM than the standalone BP-DSM.

Chapter 6. Conclusion

6.1. Thesis Conclusion

RoF is optimal for transferring high frequency or RF signals of mobile communications with minimal loss. Partnering it with delta-sigma modulation allows for less complex systems, minimal cost and more bandwidth. This has prompted the simplification of D-RoF and various developments into the RoF transmitter. One change involves lowering the quantization bits to a single bit in the DSM permitting less processing bandwidth. Additionally, the use of high order DSMs permit improved noise shaping at the band of interest. High order structures can be integrated into any main topology: LP, HP or BP. BP-DSM is a good choice of DSM due to being custom for the carrier frequency. They allow the noise to be shifted away from the band of interest. Still, high order setups suffer from linearity issues due to clock jitter introduced from the feedback loops. Integrating the high order BP-DSM into an EDSM setup counters this impact of clock jitter from the DSM. Besides providing linearity, EDSM is an attractive option due to easy integration to switch mode power amplifiers. Chapter 2 highlighted the different EDSM models being developed and how they work with PAs. Researchers have studied quantization levels, DSM vs EDSM and DSM/EDSM RoF integration, but none have examined carrier aggregation with EDSM RoF. Carrier aggregation involves combining two or more carriers and transmitting them as a single instance. In this work, a concurrent dual band 64-QAM 20MHz LTE Radio-over-Fiber transmission using 1 bit 4^{th} order EDSM was proposed. The DSM in the EDSM was custom tailored for the carrier frequency and uses 4^{th} order BP-DSM CRFB design. Two bands are included in the setup to demonstrate the interband compatibility from LTE-Advanced.

Through MATLAB, Simulink and VPIphotonics simulations, the proposed system demonstrated functionality in-line with LTE standards (EVM < 8%). First, the DSM order tests showed the 4^{th} order BP-DSM as the best choice for the design. They produced EVMs around 3.5-4% and had the best improvement with increased complexity. For the single band case, the BP-DSM setup performed better than the EDSM setup with and without the RoF addition.

Before transmission, the EVM was 0.468% for the BP-DSM and 3.5% for the EDSM. After transmission, the EVM rose to 1% and 3.5/3.8%, respectively. The EVM change due to the optical link was minimal for the single band cases. Contrarily, in the dual band case, the EDSM setup responded better to optical transmission than the standalone BP-DSM. After the BP-DSM, the dual case had error around 0.5% while after the EDSM, the EVM was at 4.3358%. When the RoF was introduced, the standalone BP-DSM dual band case saw its error rise to 3.04% and 5.39%. The EDSM dual band case only changed to 4.3928%. This corresponds to a change of 0.057% instead of 2.5% and 4.8%. For dual band simulation, the EDSM RoF was less sensitive than the BP-DSM RoF. Overall, BP-DSM is a better choice for single bands while EDSM is better for dual band cases when examining RoF transmission resistance.

In the experimental work, the result patterns matched the simulated results. When using BP-DSM only, the dual band case produced more error than the single carrier case. The recovered 2.112 GHz signal in the single band had an EVM of 4.5237% and the recovered 2.64 GHz signal was 4.9168%. This was different than the simulated work where the single band BP-DSM case saw minimal change from the optical link. The EVMs for the 2.112 GHz and 2.64 GHz dual band case were 5.2307% and 5.4673%, respectively. The difference between the two BP-DSM cases is ~0.6%. When comparing the single carrier cases, the experimental BP-DSM and EDSM RoF performed differently. For the 2.112 GHz signal, the EDSM setup had a higher EVM at 5.22% than the BP-DSM with 4.52%. Similarly, the 2.64 GHz signal performed better with the standalone BP-DSM at 4.92% than the EDSM with 6.11%. Finally, in the dual band carrier signal cases, the BP-DSM performed better than the EDSM. The BP-DSM EVMs were 5.2307% and 5.4673% for the 2.112 GHz and 2.64 GHz carriers, respectively. The EVMs rose to 6.509% for both carriers in the EDSM RoF. Input power levels may have played a role in the discrepancies as the standalone BP-DSM cases sometimes had higher amplitudes than their EDSM counterparts. From the experimental EVM results, the BP-DSM would be a better choice than an integrated EDSM for carrier aggregation.

6.2. Future Work

Due to the observations fiber impact had in the simulated work, future experimental tests with varying fiber lengths would be beneficial to uncover the true influence of dispersion. These tests would help understand if the error impact was only from fiber or other components in the lab. Based on the results, dispersion compensation techniques and nonlinearity measures could be determined and added.

With multiple standards in the communication industry, compatibly systems are highly important. Expanding the transmitter to work with additional standards would be a main extension of the presented thesis. In particular, research had been started into the adaptation for WLAN signals. WLAN is a key type of signal that is becoming incorporated into RoF systems despite being primarily used for wireless transmission. This is due to the setup of the network where part of the system would use fiber to deliver the signal from the main source to substations. At the substation, the signal would be sent wirelessly. Figure 6-1 shows the potential setup of the WLAN EDSM RoF transmission.

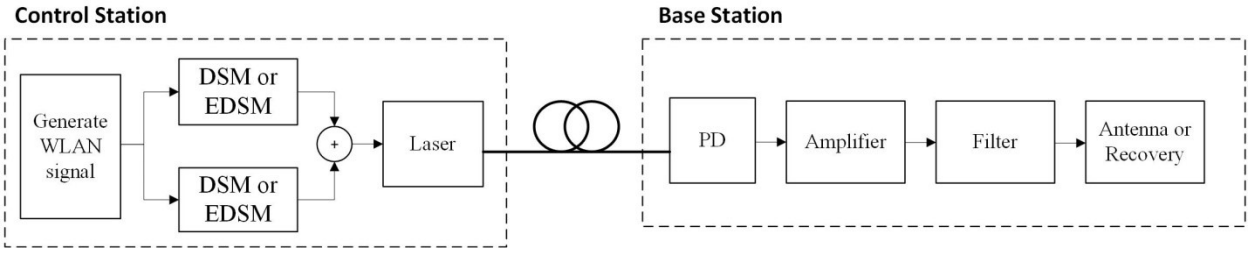

Figure 6-1: Potential WLAN dual band RoF transmission setup using DSM or EDSM

The design of the WLAN signal in Figure 6-1 will be crucial to the performance and recovery of the signal. Attempts were made using the MATLAB WLAN toolbox, but the constraints of the program made upsampling not possible. Additionally, using this toolbox made it difficult to perform the recovery of the signal due to the pre-set rules. It would be highly recommended the WLAN signal be created from scratch or with another program.

Another area for expansion is the types of DSM used in the EDSM. This thesis only covered one particular type of DSM in comparison to the other models using a LP-DSM or alternative BP-DSM. As the BP-DSM topology has other implementations like a tuning method

[20] or notches [42], a review of the different BP-DSMs would be beneficial. The top 3 alternative BP-DSMs would be compared with the basic BP-DSM used in the EDSM setup. Furthermore, they would be tested with the different signals to learn if the bandwidth or frequency band were dependent on the DSM setup.

Finally, a large investigation into a receiver setup for this RoF transmission is necessary for a full system structure. Currently, the receiver is assumed to know the exact details of the transmitted signals for recovery. However, in a real world scenario this would not case and the receiver would need specific components like bandpass filters, amplifiers and integrated logic.

References

[1] X. Zhang, “Broadband linearization for 5G fronthaul transmission,” *Front. Optoelectron.*, vol. 11, no. 2, pp. 107–115, Jun. 2018.

[2] L. M. Pessoa, D. Coelho and H. M. Salgado, “Experimental evaluation of a digitized fiber-wireless system employing sigma delta modulation,” *Opt. Express*, vol. 22, no. 14, pp. 17508–17523, 2014.

[3] Techplayon (2017, July 14). *What is RRH (Remote Radio Head), How it is connected to BBU (Base Band Unit) ?*. [Online]. Available: http://www.techplayon.com/rrh-remote-radio-head-connected-bbu-base-band-unit/ [Accessed 10 Jun. 2018].

[4] M. DeGrasse. (2015, Dec. 22). *What is C-RAN?*. [Online]. RCR Wireless News. Available at: https://www.rcrwireless.com/20151222/featured/what-is-c-ran-tag4 [Accessed 10 Jun. 2018].

[5] D. Wake, M. Webster, G. Wimpenny, K. Beacham, and L. Crawford, “Radio over fiber for mobile communications,” in *Microwave Photonics, 2004. MWP’04. 2004 IEEE International Topical Meeting on*, 2004, pp. 157–160.

[6] C. Mateo, P. L. Carro, P. Garcia-Ducar, J. de Mingo, and J. R. Perez-Cisneros, “Modeling and Digital Predistortion based on Zernike polynomial functions for LTE-RoF system,” in *2016 IEEE MTT-S International Microwave Symposium (IMS)*, 2016, pp. 1–4.

[7] L. C. Vieira and N. J. Gomes, “Clipping and predistortion for compensation of OFDM-radio over Fiber link distortion,” in *2015 IEEE International Conference on Signal Processing for Communications (ICC)*, 2015, pp. 977–981.

[8] S. Hori, T. Yamase, M. Tanio, T. Kaneko, N. Tawa, K. Motoi, and K. Kunihiro, “A digital radio-over-fiber downlink system based on envelope delta-sigma modulation for multi-band/mode operation,” in *2016 IEEE MTT-S International Microwave Symposium (IMS)*, 2016, pp. 1–4.

[9] R. Zhu, X. Zhang and D. Shen, “Linearization of radio-over-fiber systems using directly modulated and electro-absorption modulator integrated lasers,” in *2016 IEEE MTT-S International Microwave Symposium (IMS)*, 2016, pp. 1–3.

[10] H.-D. Jung, K. W. Lee, J.-H. Kim, Y.-H. Kwon, and J. H. Park, “Performance Comparison of Analog and Digitized RoF Systems with Nonlinear Channel Condition,” *IEEE Photonics Technol. Lett.*, vol. 28, no. 6, pp. 661–664, 2016.

[11] E. Janssen and A. van Roermund, “Basics of Sigma-Delta Modulation,” in *Look-Ahead Based Sigma-Delta Modulation*, Dordrecht: Springer Netherlands, 2011, pp. 5–28.

[12] R. Schreier and G. C. Temes, *Understanding Delta-Sigma Data Converters*. New Jersey: Wiley-IEEE Press, 2004.

[13] M. M. Ebrahimi, M. Helaoui and F. M. Ghannouchi, “Delta-sigma-based transmitters: Advantages and disadvantages,” *IEEE Microw. Mag.*, vol. 14, no. 1, pp. 68–78, 2013.

[14] K. K. Parhi, *VLSI Digital Signal Processing Systems: Design and Implementation*. New York: John Wiley & Sons, 1999.

[15] R. Khoini-Poorfard, L. B. Lim and D. A. Johns, “Time-interleaved oversampling A/D converters: theory and practice,” *IEEE Trans. Circuits Syst. II Analog Digit. Signal Process.*, vol. 44, no. 8, pp. 634–645, 1997.

[16] M. Tanio, S. Hori, N. Tawa, and K. Kunihiro, “An FPGA-based all-digital transmitter with 9.6-GHz 2nd order time-interleaved delta-sigma modulation for 500-MHz bandwidth,” in *2017 IEEE/MTT-S International Microwave Symposium - IMS 2017*, 2017, pp. 149–152.

[17] J. P. A. V. and B. R. Jose, “Low-Power Reconfigurable Cross-Coupled ∑Δ Modulator for Multi-standard Wireless Applications,” in *2014 Fourth International Conference on Advances in Computing and Communications*, 2014, pp. 130–133.

[18] R. F. Cordeiro, A. S. R. Oliveira, J. Vieira, and T. O. e Silva, “Wideband all-digital transmitter based on multicore DSM,” in *2016 IEEE MTT-S International Microwave Symposium (IMS)*, 2016, pp. 1–4.

[19] A. Frappe, A. Flament, A. Kaiser, B. Stefanelli, A. Cathelin, and R. Daouphars, “Design techniques for very high speed digital delta-sigma modulators aimed at all-digital RF transmitters,” in *ICECS 2006 - 13th IEEE International Conference on Electronics, Circuits and Systems, December 10, 2006 - December 13*, 2006, pp. 1113–1116.

[20] D. C. Dinis, R. F. Cordeiro, A. S. R. Oliveira, and J. Vieira, “Tunable delta-sigma modulator for agile all-digital transmitters,” in *2016 IEEE MTT-S International Microwave Symposium (IMS)*, 2016, pp. 1–4.

[21] L. Ding, R. Hezar and S. Erez, “Modeling and predistortion for digital transmitters based on delta-sigma and pulse-width modulation,” in *2016 IEEE MTT-S International Microwave Symposium (IMS)*, 2016, pp. 1–4.

[22] F. Elsayed, M. Ibrahimi, M. Helaoui, and F. Ghannouchi, “Performance enhancement of first order three-level envelope delta sigma modulator based transmitter,” in *2014 IEEE 27th Canadian Conference on Electrical and Computer Engineering (CCECE)*, 2014, pp. 1–5.

[23] T. Halsig, L. Landau and G. Fettweis, “Spectral Efficient Communications Employing 1-Bit Quantization and Oversampling at the Receiver,” in *2014 IEEE 80th Vehicular Technology Conference (VTC Fall)*, 2014, pp. 1–5.

[24] Q. Ling, “Using a single bit to stabilise an n-dimensional quantised non-linear feedforward system,” *IET Control Theory Appl.*, vol. 6, no. 12, pp. 1778–1786, 2012.

[25] S. Hatami, M. Helaoui, F. M. Ghannouchi, and M. Pedram, “Single-bit Pseudoparallel Processing Low-oversampling Delta-sigma Modulator Suitable for SDR Wireless Transmitters,” *IEEE Trans. Very Large Scale Integr. Syst.*, vol. 22, no. 4, pp. 922–931, 2014.

[26] W. V. Kuang and J. Wight, “1-bit digital tuning of continuous-time filter by the use of unstable sigma-delta modulation,” in *2009 IEEE International Symposium on Circuits and Systems - ISCAS 2009*, 2009, pp. 41–44.

[27] T. Maehata, S. Kameda and N. Suematsu, “1-bit feedforward distortion compensation technology for bandpass delta-sigma modulation,” *IEICE Trans. Commun.*, vol. E99B, no. 5, pp. 1087–1092, 2016.

[28] S. Z. Reyhani and O. Hashemipour, “SAR-based delta-sigma modulator using single-bit shared-DAC,” *Electron. Lett.*, vol. 50, no. 3, pp. 156–158, 2014.

[29] T. Memon, P. Beckett and A. Z. Sadik, “Sigma-Delta Modulation Based Digital Filter Design Techniques in FPGA,” *ISRN Electron.*, p. 538597 (10 pp.), 2012.

[30] Y. Wang, “An improved Kahn transmitter architecture based on delta-sigma modulation,” in *IEEE MTT-S International Microwave Symposium - IMS 2003*, 2003, vol. 2, pp. 1327–1330.

[31] A. Dupuy and Y. E. Wang, “A practical scheme for envelope delta-sigma modulated (EDSM) microwave power amplifier,” *Microw. Opt. Technol. Lett.*, vol. 43, no. 6, pp. 491–495, 2004.

[32] B. Zhou and S. Liu, “Polar transmitter with differential DSM phase and digital PWM envelope,” *J. Semicond. Technol. Sci.*, vol. 14, no. 3, pp. 313–321, 2014.

[33] J. Choi, J. Yim, J. Yang, J. Kim, J. Cha, D. Kang, D. Kim, and B. Kim, “A $\Delta\sum$-digitized polar RF transmitter,” *IEEE Trans. Microw. Theory Tech.*, vol. 55, no. 12, pp. 2679–2690, 2007.

[34] R. Singh, G. C. Tripathi and M. Rawat, “Performance analysis of multilevel delta sigma modulators for 3G/4G communication,” in *2015 IEEE UP Section Conference on Electrical Computer and Electronics (UPCON)*, 2015, pp. 1–5.

[35] Y. K. Cho, S. J. Lee, S. H. Jang, B. H. Park, J. H. Jung, and K. C. Lee, “A CMOS advanced class-S transmitter architecture based on tri-level envelope encoding,” in *2014 44th European Microwave Conference*, 2014, pp. 600–603.

[36] S. Hori, K. Kunihiro, K. Takahashi, and M. Fukaishi, “A 0.7-3GHz envelope ∑Δ modulator using phase modulated carrier clock for multi-mode/band switching amplifiers,” in *2011 IEEE Radio Frequency Integrated Circuits Symposium*, 2011, pp. 1–4.

[37] Y.-K. Cho, B. H. Park, and C.-Y. Kim, “Wideband and multiband long-term evolution transmitter using envelope delta-sigma modulation technique,” *Analog Integr. Circuits Signal Process.*, vol. 91, no. 1, pp. 155–162, 2017.

[38] T. Maehata, K. Totani, S. Kameda, and N. Suematsu, “Concurrent dual-band 1-bit digital transmitter using band-pass delta-sigma modulator,” in *2013 European Microwave Conference*, 2013, pp. 1523–1526.

[39] J. Wannstrom. (June 2013). *Carrier Aggregation explained*. [Online] 3gpp.org. Available at: http://www.3gpp.org/technologies/keywords-acronyms/101-carrier-aggregation-explained [Accessed 21 Mar. 2018].

[40] Niviuk.free.fr. (2017). *LTE Carrier Aggregation*. [Online] Available at: http://niviuk.free.fr/lte_ca_band.php [Accessed 21 Mar. 2018].

[41] L. Miller, *Carrier Aggregation Fundamentals for Dummies, Qorvo Special Edition*. New Jersey: John Wiley & Sons, Inc., 2016.

[42] S. A. Rahman, “Delta-Sigma Modulator for Wideband and Multi-Band Radio Systems,” M.S. thesis, Dept. Elect. and Comput. Eng., Univ. Calgary, Calgary, Canada, 2014.

[43] J. He, W. Ren, D. Shen, J. Zeng, X. Zhang, and H. Yuan, “Dual-band transmitters based on Lowpass and Bandpass delta-sigma modulators,” in *2016 IEEE International Conference on Microwave and Millimeter Wave Technology (ICMMT)*, 2016, vol. 2, pp. 590–592.

[44] T. Maehata, S. Kameda and N. Suematsu, “A novel channel coding scheme for digital RF transmitter comprising a 1-bit band-pass delta-sigma modulator,” in *2014 Asia-Pacific Microwave Conference*, 2014, pp. 932–934.

[45] T. Maehata, S. Kameda and N. Suematsu, "1-bit band-pass delta-sigma modulator with parallel IIR form for concurrent multiband digital transmitter," *IEICE Trans. Commun.*, vol. E100B, no. 7, pp. 1152–1159, 2017.

[46] J. Wang, Z. Yu, K. Ying, J. Zhang, F. Lu, M. Xu, L. Cheng, X. Ma, and G.-K. Chang, "Digital mobile fronthaul based on delta-sigma modulation for 32 LTE carrier aggregation and FBMC signals," *J. Opt. Commun. Netw.*, vol. 9, no. 2, pp. A233–A244, 2017.

[47] Anonymous. 3rd Generation Partnership Project; Technical Specification Group Radio Access Network; Evolved Universal Terrestrial Radio Access (E-UTRA); User Equipment (UE) radio transmission and reception (Release 14). *3GPP TS 36.101 V14.2.1 (2017-01),* pp. 1-1200, 2017.

[48] Keysight Technologies (2018). *Concepts of Orthogonal Frequency Division Multiplexing (OFDM) and 802.11 WLAN*. [Online]. Available: http://rfmw.em.keysight.com/wireless/helpfiles/89600b/webhelp/subsystems/wlan-ofdm/content/ofdm_basicprinciplesoverview.htm [Accessed 10 Apr. 2018].

[49] MathWorks (2018). *16-QAM with MATLAB Functions.* [Online]. Available: https://www.mathworks.com/help/comm/gs/compute-ber-for-a-qam-system-with-awgn-using-matlab.html [Accessed 10 Apr. 2018].

[50] MathWorks (2018). *comm.OFDMModulator System object.* [Online]. Available: https://www.mathworks.com/help/comm/ref/comm.ofdmmodulator-system-object.html [Accessed 10 Apr. 2018].

[51] H. Kim, *Wireless Communications Systems Design.* West Sussex: John Wiley & Sons, 2015.

[52] P. A. J. Nuyts, P. Singerl, F. Dielacher, P. Reynaert, and W. Dehaene, "A Fully Digital Delay Line Based GHz Range Multimode Transmitter Front-End in 65-nm CMOS," *IEEE J. Solid-State Circuits*, vol. 47, no. 7, pp. 1681–1692, 2012.

[53] Tektronix, "Arbitrary Waveform Generators AWG7000B Series Data Sheet," 76W-22259-4 datasheet, Sept. 2009.

[54] MITEQ, “6 GHz SCM Fiber Optic Link,” D-286 datasheet, May 2003.

[55] Corning, “Corning® SMF-28™ Optical Fiber Product Information,” PI1036 datasheet, Dec. 2001 [Revised April 2002].

[56] Discovery Semiconductors, Inc., “Balanced Photodiodes to 40 GHz Bandwidth,” F720-48 datasheet, Sept. 2009.

[57] Mini-Circuits, “Super Ultra Wideband Amplifier ZVA-213+,” M157938 datasheet, Dec. 2008.

[58] Agilent Technologies, “Infiniium DSO80000B Series Oscilloscope and InfiniiMax Series Probes: 2 GHz to 13 GHz Real-time Oscilloscope Measurement Systems,” 5989-4604EN datasheet, Dec. 2007.